Promotors:

    Prof. dr. ir. Jo Dewulf
    Department of Organic Chemistry
    Environmental Organic Chemistry and Technology Research Group (EnVOC)
    Ghent University

    Prof. dr. ir. Christophe Leys
    Department of Applied Physics
    Plasma technology
    Ghent University

Dean:

    Prof. dr. ir. Herman Van Langenhove

Rector:

    Prof. dr. Paul Van Cauwenberge

ir. Jim Van Durme

Development of heterogeneous plasma catalysis for the abatement of health damaging organic micropollutants in indoor environments

Thesis submitted in fulfillment of the requirements for the degree of Doctor (Ph.D) in

Bioscience engineering: Environmental Technology

Dutch translation of the title:

Ontwikkeling van heterogene plasmakatalyse voor de verwijdering van gezondheidsbelastende organische micropolluenten in binnenlucht

Cover illustration: Picture of DC positive corona discharge (own picture)

Ghent, May 2008

The author,   The promotors,

ir. Jim VAN DURME   Prof. dr. ir. Jo DEWULF   Prof. dr. ir. Christophe LEYS

Dankwoord

Het is beschamend dat enkel mijn naam op dit proefschrift te lezen staat. Zoveel mensen hebben mij op elk hun manier geholpen, het lijkt me bijna onmogelijk jullie mijn dank enkel op deze bladzijde te betuigen.

Eerst en vooral wil ik mijn promotor prof. Jo Dewulf bedanken voor de aangename samenwerking. Jo, uw expertise en enthousiasme werkten zeer inspirerend, dit werk was er niet gekomen zonder jou. Ook mijn co-promotor, prof. Christophe Leys, wil ik bedanken voor de suggesties, de steun en de hulp van uw medewerkers. Prof. Herman Van Langenhove, veel dank voor de opbouwende en kritische discussies tijdens mijn doctoraat.

Het feit dat ik 's morgens meestal met een lach naar het labo vertrok, heb ik te danken aan mijn collega's bij EnVOC. Amit, Bram, Christophe, Eva, Evelien, Geert, Karlien, Kristof, Lore, Maarten, Moogi, Olga, Patrick, Theo, Wouter en ook Bavo, het was leuk samenwerken met jullie. Daarnaast zal ik nooit vergeten hoeveel steun en vriendschap ik kreeg tijdens persoonlijk moeilijkere tijden. Ik hoop dat we samen nog vele pintjes mogen pakken en wens jullie alle geluk toe...Ook de thesisstudenten wil ik graag bedanken voor de ambiance en hun inzet. Wouter, Jacub, Pieter, Olivier, Eszter, Tadesse en Eric... ik kan dit werk niet lezen, zonder aan jullie te denken.

Minstens even belangrijk was de hulp van de vrienden op het thuisfront. Mijn "Entrenadores Escondidos" wielervrienden Willem, Pieter en Nathan, maar evenzeer Christine, Lien, Chris, Dieter en de hele "Vogezen-bende", dank voor jullie steun en vriendschap.

Woorden tekort om mijn familie, mijn zus Vicky, Jurgen en vooral mijn schatten van ouders te bedanken... zonder het warme nest thuis, jullie opofferingen en steun zou ik nooit tot dit punt gekomen zijn. Last but not least, wil ik Melissa duizendmaal bedanken voor alles wat ze deed voor mij.

Word of thanks

It is shameful that only one name is to be read on this manuscript. So many people helped me each on their manner, it seems almost impossible to write my words of thank on only one page.

First, I would like to thank my promoter, prof. Jo Dewulf, for the pleasant collaboration. Jo, your knowledge and enthusiasm were very inspiring for me, this work wouldn't be here without you. Also to my co-promotor, prof. Christophe Leys, many thanks for your suggestions, support and the help of your colleagues. Prof. Herman Van Langenhove, many thanks for the constructive and critical discussions during my PhD research.

The fact that in the morning, I mostly arrived in the lab with a smile on my face, is due to my EnVOC colleagues. Amit, Bram, Christophe, Eva, Evelien, Geert, Karlien, Kristof, Lore, Maarten, Moogi, Olga, Patrick, Theo, Wouter and also Bavo, it was so nice to work together with you. Next, I will never forget which kind of support and friendship I got at personal more difficult times. I hope we will continue to have a lot "pintjes" together, I wish you all the very best. I would also like to acknowledge my thesis students for the ambiance and their effort. Wouter, Jacub, Pieter, Olivier, Eszter, Tadesse and Eric… I can not read this work, without thinking about you.

As important was the help of my friends at home. My "Entrenadores Escondidos" cycling buddies Willem, Pieter and Nathan, but also Christine, Lien, Chris, Dieter and my "Vogezen friends", thank you for your support and friendship.

Not enough words to thank my family, my sister Vicky, Jurgen and especially my beloved parents… without the warm nest at home, your sacrifices and support, I would have never come to this point. Lost but not least, I want to send thousands thanks to Melissa for all the things she did for me.

List of contents

Abbreviation index

a.u.	Arbitrary units
AOP	Advanced oxidation process
BET	Brunauer-Emmett-Teller
BTEX	Benzene, toluene, ethylbenzene, xylene
DC	Direct current
ETS	Environmental tobacco smoke
FID	Flame ionization detector
GC	Gas chromatograph
HA	Proton acceptor = electron donator
HD	Proton donor = electron acceptor
IAQ	Indoor air quality
KI	Kovàts index
LOD	Limit of detection
LOQ	Limit of quantification
MFC	Mass flow controller
MS	Mass spectrometry
N.D.	Non-detectable
NTP	Non-thermal plasma
PDMS	Polydimethylsiloxane
ppb_v	Parts per billion (volumetric) = $\mu L\ m^{-3}$
ppm_v	Parts per million (volumetric) = $mL\ m^{-3}$
SBS	Sick building syndrome
SPDE	Solid-phase dynamic extraction
SPME	Solid-phase microextraction
SVOC	Semi-volatile organic compound
UV	Ultraviolet
VB	Valence band
VdW	Van der Waals interaction ($mJ\ m^{-2}$)
VOC	Volatile organic compound
WHO	World Health Organization

Notation index

A	Surface area (m²)
C_{in}	Inlet pollutant concentration (ppm$_v$, ppb$_v$, g m^{-3})
C_{out}	Outlet pollutant concentration (ppm$_v$, ppb$_v$, g m^{-3})
D	Diffusion coefficient (m² s^{-1})
H	Henry's Law coefficient (-)
I	Electric current (ampere)
k	Reaction rate coefficient (molecules cm^{-3} s^{-1})
K	Gas/solid partitioning coefficient
k_m	Convective mass transfer coefficient (m s^{-1})
m	Number of cells in longitudinal direction
$m_{catalyst}$	Mass of heterogeneous catalyst (g)
n	Number of repetions
n'	Radial cell number in (stationary) polymeric phase (-)
n''	Radial cell number in (mobile) gas phase (-)
Nu	Nusselt number (-)
P	Power (Watt)
p	Pressure (Pa)
Pr	Prandtl number (-)
Q	Gas flow rate (m³ h^{-1})
Re	Reynolds number (-)
Sc	Schmidt number (-)
Sh	Sherwood number (-)
S_i	Radical scavenger (-)
T	Temperature (K or °C)
U	Voltage (volt)
V	Volume (m³)
v_g	Gas velocity (m s^{-1})
ΔG_{ads}	Total free energy of adsorption (J mol^{-1})

Greek symbols

μ_g	Gas viscosity (Pa s)
ξ	Constant related to system and type of AOT technology (mol s^{-1} W^{-1})
α	H-acceptor values (-)
β	H-donor values (-)
ε	Energy density = P/Q (J L^{-1})
ε_o	Charactistic energy density (J L^{-1})
λ_g	Gas thermal conductivity (W m^{-1} K^{-1})
ρ_g	Gas density (kg m^{-3})

Introductory chapter

Aim of study and overview of the different chapters

The quality of indoor air is an underestimated problem. Numerous studies report the occurrence of surprisingly high amounts of pollutants in enclosed environments. This forms a significant health risk for the inhabitants. Although people spend the largest fraction of their time indoor, current air cleaning technology and legislation has not matured yet to guarantee a healthy indoor air environment.

In **Chapter 1** an overview is given of the indoor air pollutants and their sources. The effect of a poor indoor air quality on human health is summarized and illustrated by a more detailed section on indoor smoking. Since regulatory initiatives are emerging, the available indoor air cleaning technologies are summarized in this chapter.

Chapter 2 defines non-thermal plasma technology, particularly corona discharges, as a promising advanced oxidation technology for air purification applications. Next, this chapter also described hybrid plasma-catalyst technology. Finally, environmental applications of plasma catalytic hybrid systems are discussed.

Chapter 3 focuses on solid-phase dynamic extraction as an innovative technique for VOC sampling. Although this sampling technique is very promising, today it has not matured yet. Therefore, solid-phase microextraction is mainly used as VOC sampling technique to monitor VOC degradation performance.

The main aim of this study is to develop an advanced oxidation technology capable to treat large air flows containing low concentrations of indoor VOC. Therefore a non-thermal plasma reactor has been developed, characterized and optimized (**Chapter 4** and **Chapter 5**).

Recent developments with plasma technology for air cleaning indicate an interesting synergy that occurs when plasma is combined with heterogeneous catalyst technology. This work focuses on both in-plasma and post-plasma catalysis to increase energy efficiency and decrease by-product formation during VOC abatement experiments (**Chapter 6**). For indoor air cleaning purposes, placing catalyst material down stream the plasma discharge proves to be the most promising approach. A more detailed study of post-plasma catalysis is performed by testing six different heterogeneous catalysts both for their ozone and toluene removal capabilities (**Chapter 7**).

Chapter 8 provides a general discussion of the results obtained in the framework of the research objectives. Conclusions were drawn and perspectives for future research are proposed.

Acknowledgements

Chapter 1

Indoor air pollution

1.1 Introduction

1.1.1 Indoor air quality history

The term "indoor air quality" (IAQ) refers to the air quality in enclosed environments. IAQ is affected by several physical (temperature, light, relative humidity) and chemical parameters (organic and inorganic pollutants, particulate matter, biological pollutants). Indoor air has always been more polluted than outdoor air (Sundell, 2004). Greeks and Romans already knew that polluted air had detrimental effects on human health. In the 17th century, poor indoor air quality was blamed for unpleasant sensations and the spreading of diseases. In 1853, the first professor in hygiene Pettenkofer (1818-1901) linked "bad" indoor air with a decreasing resistance against diseases. From an extensive study, professor Heyman (1829-1889) concluded that some skin and mucosal complaints are related to inadequate indoor air quality. These symptoms are very similar to today's sick building syndrome (SBS).

1.1.2 Indoor air quality today

Today, the quality of indoor air is still an underestimated issue, despite claims that on a global scale indoor air pollution causes 4000 deaths a day (Rehfuess et al., 2006). More than half the world's population still burns coals and biomass fuels (e.g. wood, dung and crop residues). Burning these solid fuels on open fires or traditional stoves results in the emission of a variety of health-damaging pollutants including particles, carbon monoxide and different carcinogens (Rehfuess et al., 2006). Even in the more developed countries, indoor air quality was not a point of concern up to the late 1960s. In that period, due to the energy crisis, regulations were made to reduce the energy consumption of buildings (Jones, 1999). Nowadays, rapid urbanization places pressure on energy resources and again increases demand on building energy conservation. Today, the main technologies used to minimize energy use include designing airtight building and using building materials with high thermal insulation

properties (Wang et al., 2004; Fanger, 2006). As a consequence, indoor air pollutant concentrations are higher than outdoor levels due to a combinatory effect of an insufficient air exchange and high levels of indoor pollutant emission sources. EPA (1991) reported that indoor air quality is 10 to 100 times worse than that of the outdoor air. Since people spend more than 85% of their time indoors, there is a significant exposure to these hazardous chemicals, negatively effecting health. Today, due to a general growing awareness, IAQ finally has acquired high priority on the scientific agenda (Sundell, 2004).

Indoor air pollutants are grouped in two subgroups; volatile organic and inorganic compounds and particulate matter (Molhave and Krzyzanowski, 2000). In this chapter both groups will be discussed, but this document will focus mainly on volatile organic compounds found in indoor air, indoor pollutant sources, and the impact of IAQ on human health. Finally, an overview of available indoor air cleaning technologies will be given.

1.2 Indoor air pollutants

1.2.1 Volatile indoor pollutants

1.2.1.1 Volatile inorganic compounds

Frequently detected inorganic compounds in indoor environments include ozone (O_3), nitrogen oxides (NO_x), sulfur dioxide (SO_2) and hydrogen sulfide (H_2S) (Schieweck et al., 2005). In the absence of ozone generating sources, indoor ozone concentrations vary from less than 10% and up to 80% of the outdoor levels. The World Health Organisation (WHO) recommends maximum ozone exposure limits of 0.1 mg m^{-3} (47 ppb$_v$) (Rakitskaya et al., 1999). Sources of NO_x are indoor fuel combustion, elevated outdoor concentrations, smoking and the use of unclean heaters (Lai et al., 2006). During smoking periods, average air

concentrations range up to 200 and 80 µg m^{-3} (376 – 150 ppb$_v$) for NO and NO$_2$, respectively (Halios et al., 2005), while during cooking with a gas range, peak levels in the kitchen for both compounds are as high as 400 – 1000 ppb$_v$ (752–1880 µg m^{-3}) (Jones, 1999). The WHO indicated an indoor air quality guideline of 40 µg m^{-3} for NO$_2$ (WHO, 2000).

Radon is an important inorganic indoor pollutant which is a naturally occurring radioactive gas with variable geographical occurrence and concentrates in the building environment. A study by Albering et al. (1996) revealed that average indoor radon concentrations in 116 houses in Visé (Belgium) were on average 116 Bq m^{-3}. High concentration of radon proved to be associated with an increased risk for lung cancer. Extrapolation from these data suggested that high indoor radon concentrations significantly increase the risk for lung cancer (Groves-Kirkby et al., 2007).

1.2.1.2   Volatile organic compounds

Problem definition

VOCs (Volatile Organic Compounds) are ubiquitous indoors. Although the indoor concentrations are below the odor threshold, they exceed outdoor levels by up to a factor of 5 (Wallace, 1997). Any chemical compound that contains at least one carbon atom in its molecular structure is referred to as an organic compound. These compounds can be further classified into VOCs, semi-volatile compounds (SVOCs) and non-volatile compounds (NVOCs). The Council of the European Community defines VOCs as 'any organic compound having a vapor pressure of 0.01 kPa or more at 293.15K or having a corresponding volatility under the particular conditions of use' (CEC, 1999).

Indoor VOC monitoring

A literature review reveals that in similar measurement campaigns, up to 900 VOCs were detected in indoor air, with more than 350 compounds having concentrations exceeding 1 ppb_v. Brown et al. (1994) summarized common trends of indoor air pollution;

i.   For all compounds, indoor concentrations were higher than outdoor concentrations by a factor of 2 to 73, indicating indoor sources were present. Mean VOC and TVOC (Total VOC) concentrations were generally higher in established residences than established public buildings.

ii.   New buildings have higher TVOC concentrations compared to older buildings.

To conclude, Table 1.1 summarizes mean and maximum concentrations of the 20 most frequently detected indoor VOCs.

Table 1.1. Top 20 indoor air pollutants based on measurements of more than 3000 indoor locations; mean and maximum concentration ($\mu g\ m^{-3}$) (AERIAS, 2008)

Rank	Chemical	Mean concentration ($\mu g\ m^{-3}$)	Max. concentration ($\mu g\ m^{-3}$)
1	Toluene (Methylbenzene)	140	36970
2	Xylene (para and/or meta)	46	6955
3	Ethanol	126	21796
4	Undecane	54	24110
5	Xylene, ortho	33	3694
6	Benzene, ethyl	28	3767
7	Benzene, 1,2,4-trimethyl	37	4931
8	Limonene	119	53235
9	Hexanal	48	46850
10	Heptane	19	2911
11	Cyclopentasiloxane, decamethyl	43	1213
12	Nonane	48	16202
13	4-Ethyltoluene	27	3568
14	Acetone	42	6606
15	Dodecane	62	50849
16	Benzene	24	5249
17	Hexane	33	5511
18	2-Propanol (Isopropanol)	132	11479
19	Decane	66	5959
20	Cyclohexane, methyl	15	3123

Table 1.1 indicates that BTEX compounds (benzene, toluene, ethylbenzene, xylene) are a major group of indoor air pollutants (Van Winkle and Scheff, 2001). Although formaldehyde is not listed in Table 1.1, this is a frequently discussed indoor VOC with irritating and carcinogenic properties. Indoor formaldehyde concentrations nearly always exceed outdoor levels and are ranked high based on cancer risk (Loh et al., 2007).

To determine the degree of indoor air pollution in Flanders, a monitoring campaign was conducted (Van Durme, 2006). Some typical indoor environments have been sampled: a new building (used as student resto), a pub and a student house. The measurements clearly proved that volatile organic compounds are abundant in indoor air environments (Figure 1.1). Detected indoor VOCs were ethylbenzene (up to 27.76 $\mu g\ m^{-3}$), α-pinene (up to 26.50 $\mu g\ m^{-3}$), hexanal (up to 12.18 $\mu g\ m^{-3}$), nonane (up to 2.16 $\mu g\ m^{-3}$), etc. Limonene concentrations up to 130 $\mu g\ m^{-3}$ were detected, while maximum concentrations of benzene, toluene and ethanol were respectively 11.47; 17.45 and 2562.00 $\mu g\ m^{-3}$. The latter three VOCs were detected at highest concentrations in the pub; Figure 1.1 shows an increasing trend towards the end of the day. This was in contrast to the more constant background levels in the new building and student home being respectively 1.52 ± 0.04 (n = 5) and 0.35 ± 0.18 (n = 5) $\mu g\ m^{-3}$ for benzene; 5.87 ± 0.40 (n = 5) and 0.72 ± 0.19 (n = 5) $\mu g\ m^{-3}$ for toluene; N.D. (non-detectable) and 44.29 ± 5.84 (n = 5) $\mu g\ m^{-3}$ for ethanol, respectively.
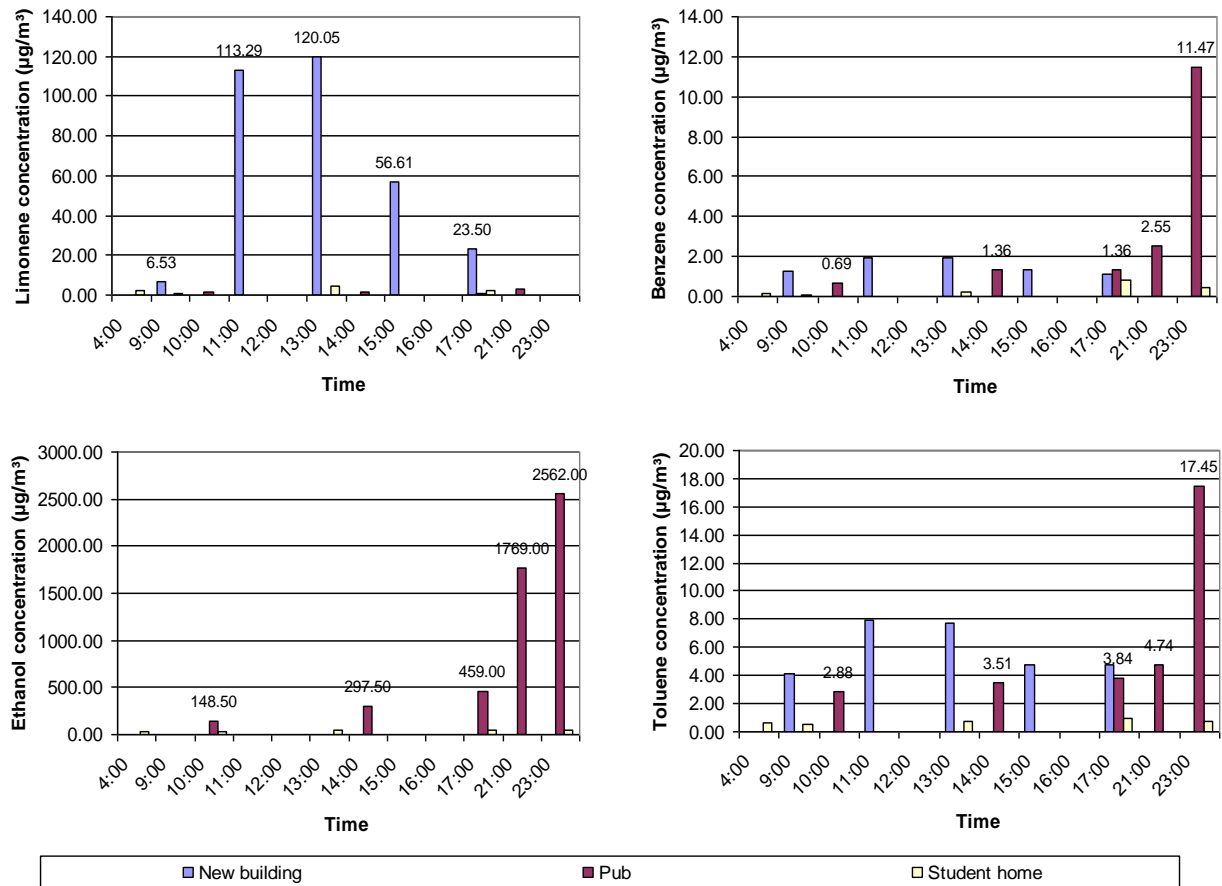
Figure 1.1. Diurnal indoor air concentration (μg m⁻³) profiles for 4 VOC pollutants (limonene, benzene, toluene, ethanol) in three typical indoor air environments (new building, pub, student home) (Sampling volume = 1 L, T= 298.15K, P=101.3 kPa) (Van Durme, 2006)

This indicates that for heavily occupied places such as a pub, not only constant indoor VOC sources (Chapter 1.3), but also human activities have a direct impact on the IAQ. Indeed, it is noteworthy to see that there is a correlation between the increasing number of people in the pub after 21h and the corresponding increase in VOC concentration (Figure 1.1). This can be explained by indoor smoking (sources of benzene and toluene) and alcohol consumption (source of ethanol).

A second proof of the strong impact of daily activities on IAQ is illustrated by monitoring results of a new building (Figure 1.1). Unlike the other sampling sites, there were cleaning

activities (at 10h) during the sampling day. Before cleaning (9 h), limonene concentrations in the indoor air amounted 6.53 µg m^{-3}. However, after cleaning (13 h), indoor limonene concentration ranged up to 120.05 µg m^{-3}. Headspace analysis of the used cleaning products revealed that they contained limonene as citrus fragrance.

1.2.2 Particulate matter (non-biological)

Particulate matter (PM) consists of airborne particles in solid or liquid form. Primary PM is emitted at the emissions source in particle form. An example of primary indoor PM emission is the burning of candles. Generally it is not known that the core of candle wicks may contain lead, which is used as a stiffening agent to keep the wick straight when submerged in the molten wax. By consequence, next to volatile organic compounds, lead is also emitted as particulate leading to indoor concentrations often exceeding 50 µg m^{-3} (EPA, 2007).

Secondary PM formation results from a series of chemical and physical reactions involving different precursor gases, such as sulphur oxides, nitrogen oxides, and ammonia, which react to form sulphate, nitrate and ammonium particulate matter respectively. Also the reaction between ozone and unsaturated compounds (e.g. terpenes) may lead to the production of semi-volatile organic compounds (SVOCs) which can further react to form aerosols or micro particles (Singer et al., 2006).

1.2.3 Biological indoor contaminants

1.2.3.1   Indoor biological allergens

The droppings of house dust mites are an important source of indoor antigens (Carrer et al., 2001). In one gram of dust, there may be up to 100,000 mite faecal particles having diameters ranging between 10 and 40 μm. Although they do not remain airborne long, in disturbed environments indoor concentrations can be high (Jones, 1999). As observed for dust mites, cockroach allergens prove to be a major indoor allergen testing positive for 60% of asthmatics.

Next, the saliva, skin and dander of domestic cats and dogs, prove to be important sources of allergens in indoor air. Allergen particles are typically smaller in particle size, and hence remain airborne for many hours with concentrations varying between 2 and 20 ng m^{-3} (Luczynska, 1994; Puerta et al., 1997).

1.2.3.2   Fungi, bacteria and viruses

A large number of species of fungi and bacteria can be found indoors; their presence is associated with the amount of organic matter in the indoor environment (IEH, 1996). Fungi produce toxic mycotoxines which induce a wide range of acute and chronic effects in occupants inhaling this 'bad' indoor air.

1.3 Indoor sources

1.3.1 Primary VOC emission

As mentioned earlier, major sources contributing to the indoor pollution are human activities, building product emissions, and infiltration of outdoor air (Table 1.2). VOC diffusion from outdoors also proves to influence indoor air quality strongly (Jaakkola et al., 1994). For new or renovated buildings, the primary emission of VOCs (e.g., solvents) from building products generally dominates for a period of up to some months. Ageing of building product, by chemical (e.g., ozone, maintenance, moisture) or physical (e.g. heat, weariness, UV-light) decomposition may result in the emission of secondary products in indoor air (Wolkoff et al., 1999).

Table 1.2. Sources of common VOCs in indoor air (Maroni et al., 1995).

Sources	Examples of typical contaminants
Consumer and commercial products	Aliphatic hydrocarbons (n-decane, branched alkanes), aromatic hydrocarbons (toluene, xylenes), halogenated hydrocarbons (methylene chloride), alcohols, ketones (acetone, methyl ethyl ketone), aldehydes (formaldehyde), esters (alkyl ethoxylate), ethers (glycol ethers), terpenes (limonene, alpha-pinene).
Paints and associated supplies	Aliphatic hydrocarbons (n-hexane, n-heptane), aromatic hydrocarbons (toluene), halogenated hydrocarbons (methylene chloride, propylene dichloride), alcohols, ketones (methyl ethyl ketone), esters (ethyl acetate), ethers (methyl ether, ethyle ether, butyl ether).
Adhesives	Aliphatic hydrocarbons (hexane, heptane), aromatic hydrocarbons, halogenated hydrocarbons, alcohols, amines, ketones (acetone, methyl ethyl ketone), esters (vinyl acetate), ethers.
Furnishings and clothing	Aromatic hydrocarbons (styrene, brominated aromatics), halogenated hydrocarbons (vinyl chloride), aldehydes (formaldehyde), ethers, esters.
Building materials	Aliphatic hydrocarbons (n-decane, n-dodecane), aromatic hydrocarbons (toluene, styrene, ethylbenzene), halogenated hydrocarbons (vinyl-chloride), aldehydes (formaldehyde), ketones (acetone, butanone), ethers, esters (urethane, ethylacetate).
Combustion appliances	Aliphatic hydrocarbons (propane, butane, isobutane), aldehydes (acetaldehyde, acrolein).
Potable water	Halogenated hydrocarbons
Tobacco smoke	Aldehydes (formaldehyde, acetaldehyde), etc.

1.3.2 Secondary VOC emission

Secondary VOC emission is the result of the reaction of primary VOCs with other indoor species such as ozone and NO_x (Pommer et al., 2004). Typically 5-10% of organic indoor pollutants contain unsaturated carbon-carbon bonds, which efficiently react with these reactive inorganic indoor pollutants. Some indoor VOCs (e.g. d-limonene) form OH radicals when reacting with ozone, again initiating a new chain of reactions. Secondary VOCs are typically aldehydes, ketones, carboxylic acids, … Weschler (2004) reported that these VOCs in the presence of ozone can react again with primary VOCs resulting in the formation of high molecular weight aldehydes (Morrison and Nazaroff, 2002). Secondary reactions can also be initiated by other inorganics; Weschler (2000) reported that NO_x react with ozone to produce nitrate radicals. These radicals react even more efficiently with indoor VOCs compared with ozone. Atkinson and Arey (2007) reported earlier that reactions between nitrate radicals and aromatics result in the production of health damaging nitro-aromatics. Indeed, reaction rate constants of toluene with ozone or nitrate radicals are of the order 10^{-21} and 10^{-17} cm^3 molecule^{-1}s^{-1} (Atkinson et al., 1988) (NIST, 2007). This indoor air chemistry leads to aldehyde and peroxynitrate formation (Nojgaard et al., 2006).

1.4 Health effects

An often used term grouping discomfort and health issues related to a bad IAQ is Sick Building Syndrome (SBS). SBS is a situation in which building occupants experience acute health effects that seem to be linked to time spent indoors. However, no specific illness or cause can be identified. Symptoms include headaches, eye, nose, and throat irritation, a dry cough, dry or itchy skin, dizziness and nausea, difficulty in concentrating, fatigue, and

sensitivity to odors (Luo et al., 1996). With SBS, no clinically defined disease or specific chemical or biological contaminant can be determined as the cause of the symptoms. Most of the complaintants feel relief soon after leaving the building. SBS reduces worker productivity and may also increase absenteeism.

More specific complaints related to indoor air pollution are the increasing incidence of allergic and asthmatic diseases which has been doubled in developed countries over the past two decades (Carrer et al., 2001; Fanger, 2006).

1.5 Indoor smoking

In Western societies with an adult smoking prevalence of 30-50%, it is estimated that over 50% of homes are occupied by at least one smoker, resulting in a high prevalence of ETS (Environmental tobacco smoke) exposure in children and other non-smokers (Hatsukami et al., 2007). ETS is composed of side-stream, emitted by the burning tip of a cigarette, and mainstream smoke, which is inhaled by and then exhaled by the smoker (Brownson et al., 2002). ETS is a dynamic, complex mixture of nearly 5000 chemical compounds found in both vapor and particle phases. Fourty-three of the chemicals found in ETS are known human or animal carcinogens (Brownson et al., 2002). The common carcinogens in ETS include arsenic, cadmium, benzopyrenes, nitrosamines and vinyl chloride. Other components that have detrimental effects on the cardio-respiratory system are carbon monoxide, which causes formation of carboxyhemoglobin, and polycyclic aromatic hydrocarbons, which increase the size of spontaneous aortic lesions. All the compounds found in mainstream smoke are also found in side-stream smoke. In addition, many of the particulate components of ETS are of a size that allows them to be drawn deeply into the lungs of non-smokers (Brownson et al., 2002) with concentrations ranging from a few $\mu g\ m^{-3}$ to over 1000 $\mu g\ m^{-3}$.

1.6 Regulation for indoor air quality

Although people are aware of problems related to poor IAQ, the number of regulatory initiatives is suprisingly low.

On the European level the first players within the European Commission working on the improvement of indoor air quality are DG (Directorate Generale) Sanco, DG Enterprise and Industry, DG Environment, DG Research and the Joint Research Centre (JRC). Initiatives from these groups resulted in the foundation of some projects such as BUMA (prioritization of building materials as indoor pollution sources), HealthyAir and CEN TC 351 (standardization approach to measure impact of building materials on indoor air, solid and (ground)water. Also some 'European expert groups' were started; their main functions are to deliver information and eduction to the public and support actions from EU member states or individual manufacturers.

On the national level, some initiatives have been taken recently to improve indoor air quality. The "prevention decreed" (Flanders, Belgium BS 03/02/2004) resulted into the realisation of a report approved by the government (11/07/2004). This document summarizes some indoor air quality standards for indoor environments in Flanders. When the IAQ does not meet these quality standards, actions have to be taken to avoid that the building will be classified as uninhabitable. Also in Poland, the Ministry of Health and Social Welfare has issued a decree determining maximum allowable concentrations of harmful substances in two categories based on exposure duration. Similar Directives on IAQ are issued in other European countries.

Despite these efforts, national legislation to control and improve indoor air quality has not matured yet today to guarantee a healthy indoor air. It can be highly expected that initiatives on European and national level will increase in near future. Overall, it can be concluded that there is an urgent need for efficient indoor air cleaning technologies (see Chapter 1.7).

1.7 Available indoor air cleaning technologies

Recent studies documented that an increase of IAQ substantially benefits human health, comfort, productivity and learning. Seppanen and Fisk (2006) reported a strong cost reduction in connection with absenteeism and medical treatment. Indeed, it was estimated that SBS decreases the productivity in offices on average of 6.5% (Fanger, 2000). Similarly, the annual 'cost of headaches' amongst the employees of the US Environmental Protection Agency was estimated as $2 million (Wallace, 1997). Consequently, there is an urgent need to develop and optimize technologies for improving the indoor air quality. To achieve this, three major strategies can be applied: source control, ventilation and air cleaning.

1.7.1 Source control - prevention

Source control was suggested as early as mid 18th century by Pettenkofer (1858), the founder of modern hygiene and environmental science, as "If there is a pile of manure in a space, do not try to remove the odor by ventilation, remove the pile of manure" (Fanger, 2006). The European Office of the World Health Organization recommended source control as the best way of reducing the concentration of VOCs indoors rather than developing guidelines (Wolkoff, 2003).

This idea is for example embodied in the development of JAS A 1901 method (January, 2003). This method is known as the standard method for the determination of volatile organic compounds and aldehydes emission from building products (small chamber method). The purpose of this method is to measure and catalogue the VOC emission factor ($\mu g\ m^{-2}\ h^{-1}$) for each building material. Based on this survey, building materials can be selected to prevent indoor air pollution (Yoshida, 2004).

1.7.2 Ventilation

Ventilation brings outdoor air indoors. It can be achieved by opening windows and doors or by using mechanical ventilation systems (preferably with heat recovery). The latter system is highly optimized, e.g. CO_2 controlled ventilation. However, there are some practical limitations to ventilation since temperature and humidity regulation of the incoming air is expensive. Next, outdoor air is often of poor quality in largely industrialized countries.

1.7.3 Indoor air cleaning – Non-destructive

Filters can effectively trap particulate contaminants and remove them from the circulating air. Filtration can be mechanical or electronical.

1.7.3.1   Mechanical filters

Mechanical filtration consists of three major types; flat, pleated or high-efficiency particulate air filters. The first two types consist out of a low packing density fibrous medium to collect particles. The third type includes HEPA (high efficiency particulate air filters) or ULPA (ultra low penetration air) filters. Their filtering media is made of submicron glass fibers having a thickness and texture very similar to blotting paper. A disadvantage of this type of filtration is the necessity of powerful fans to overcome the high pressure drop.

1.7.3.2   Electronic filters

Ionic air purifiers emit ions enhancing the agglomeration of smaller particles into larger ones, which then gravitationally settle. Ionization may also cause attraction between particles and grounded surfaces resulting in electrostatic precipitation (Grinshpun et al., 2005). One of the concerns of these filtration systems is the production of ozone. A comparison of 27 ionic air

cleaners revealed that ozone generation rates ranged from 56 to 2,757 µg h^{-1} (Berry et al., 2007).

1.7.3.3 Chemisorption

Since mechanical and electronic filters only remove particulate matter, indoor air filters are frequently equipped with a chemisorption unit which is able to remove VOCs. Chemisorption typically involves an electron transfer between sorbed VOC and sorption medium, possibly resulting in chemical reactions such as complexation or conversion of initial VOCs. Absorption is usually slower than physical adsorption, and is irreversible as the active reagent is consumed through the chemisorption process. Therefore, mainly adsorbents such as activated carbon are preferred to adsorb some gaseous indoor air pollutants (VOCs, sulphur dioxide, and ozone) but it does not efficiently adsorb volatile, low molecular weight gases such as formaldehyde and ammonia. Next, filtration technologies only transfer VOCs to another phase instead of eliminating them (Zhao and Yang, 2003). It has been proven that accumulation of pollutants, may serve as nutrient source for molds and bacteria. These organisms are able to produce VOCs such as aldehydes, ketones, alcohols, furans, esters and acids (Schleibinger and Rüden, 1999). All adsorbents have limited adsorption capacities. By consequence, there is a need for change, disposal or regeneration of filtration media (Pichat et al., 2000). The National Institute of Standards and Technology (NIST) also found that initially adsorbed toluene was slowly reemitted by the media each time the toluene concentrations decreased to lower levels. It was concluded that the amount of toluene reemitted during a 45-hour experiment, approximated the amounts that were adsorbed.

In conclusion, non-destructive techniques are not highly efficient for treating indoor air. Therefore, in recent years great attention has been given to the development of innovative destructive techniques.

1.7.4 Indoor air cleaning - destructive

Advanced oxidation processes (AOP) are receiving growing attention due to their potential for degrading a wide range of VOCs at mild conditions (ambient temperature and pressure operations). In these processes highly reactive, oxidative species such as ozone, atomic oxygen or hydroxyl radicals are produced. These species subsequently initiate the VOC degradation. Examples include ultraviolet, photolysis, direct ozonation and high-energy irradiation (He et al., 2005) and photocatalytic oxidation (PCO) (Zhao and Yang, 2003). Unlike earlier discussed control methods PCO actually oxidizes pollutants to CO_2 and H_2O, thus reducing the absolute toxicity of the treated air stream. Therefore, AOPs are referred to as "destructive technologies".

1.7.4.1   Photocatalysis

Titanium dioxide (TiO_2) is a well-known semiconductor that has been widely used as a photocatalyst for decomposing volatile organic compounds ([a]Demeestere et al., 2005; Demeestere et al., 2003). UV illumination of TiO_2 results in the production of electron-hole pairs that can induce redox reactions with adsorbed molecular oxygen, water and organic pollutants (Wittmann et al., 2005). The key oxidant in this reaction is OH$^{\cdot}$ produced from water, O_2 and electron-hole pairs on the catalyst surface (Devahasdin, 2003).

Although photocatalysis is a strong candidate for IAQ applications (modular, negligible pressure drop, room temperature conditions,…), some critical points have to be handled before this technology can be applied as efficient indoor air cleaning technology. Kim and

Hong (2002) showed that the rate of PCO decreased with decreasing pollutant concentration. In addition, at high humidity levels, water vapor competed with TiO_2 for adsorption sites which further decreased the rate of PCO (Ao et al., 2003; 2004).

1.7.4.2 Ozone generators

Ozone generators are often proposed as efficient indoor air cleaners. Indeed, ozone is highly oxidative and efficiently reacts with unsaturated indoor VOC. However ozone levels emitted by these ozone generators are frequently higher than 500 ppb_v (Hubbard et al., 2005), which is ten times higher then WHO recommended maximum ozone exposure concentrations (Rakitskaya et al., 1999). Next, scientific research has shown that these levels of ozone are too low to remove indoor VOCs (Boeniger, 1995).

1.7.4.3 Plasma technology

Non-thermal plasma (NTP) techniques are operated under atmospheric conditions. Generally, it can be postulated that plasma is a promising VOC abatement technology for flow rates smaller than 1000 $Nm^3 h^{-1}$ which are loaded with concentrations less than 10% (Lu et al., 2006). Although NTP applications as end-of-pipe technology for the removal of VOC, SO_2, H_2S and NO_x are reported (Holzer, 2005), it is seldom used due to site-specific constraints such as energy inefficiencies, poor mineralization, and by-product formation. In this work, plasma technology will be researched and optimized in order to treat polluted indoor air in an efficient manner.

Chapter 2

Non-thermal plasma and plasma-catalyst hybrid technology for air treatment: state-of-the-art

2.1 Non-thermal plasma

2.1.1 Introduction

Plasma is the fourth state of matter which can be considered as a partially ionized 'gas'. Depending on the conditions and amount of energy applied, a plasma discharge can be either thermal or non-thermal. Thermal plasmas are characterized by the fact that plasma constituents are in thermal equilibrium. This is not the case for non-equilibrium or non-thermal plasmas (NTP) since the mean electron energy, or temperature, is considerably higher than that of ions and bulk gas molecules. Indeed, a NTP typically consists of electrons which are accelerated by an electric field, gaining a typical temperature in the range of 10,000 to 250,000 K (1-25 eV), while gas molecules remain at relative low temperatures (ambient temperature). NTP techniques are economically attractive alternatives for conventional air cleaning techniques. NTP technology has potential for degrading a wide range of VOCs at mild conditions (ambient temperature and pressure). They are characterized by a potentially low energy consumption and high flexibility. The main objective of producing plasma is to produce radicals which react with pollutant molecules. The NTP process consists of many elementary processes which can be divided into primary and secondary processes (Figure 2.1). The typical time-scale of these processes are respectively in the order of $\sim 10^{-8}$ s and 10^{-3} s (Kim et al., 2002). The main primary processes are electron collisions with bulk gas molecules (N_2, O_2, H_2O) resulting in the production of ionized and excited molecules (e.g. N_2^*) or the occurrence of dissociative processes as;

$$e^- + N_2 \rightarrow e^- + N + N \tag{2.1}$$

$$e^- + N_2 \rightarrow e^- + N^+ + N \tag{2.2}$$

$$e^- + O_2 \rightarrow e^- + O(^3P) + O(^3P) \tag{2.3}$$

$$e^- + O_2 \rightarrow e^- + O(^3P) + O(^1D) \tag{2.4}$$

$$e^- + O_2 \rightarrow 2e^- + O + O^+ \tag{2.5}$$

$$e^- + H_2O \rightarrow e^- + H + OH \tag{2.6}$$

$$e^- + H_2O \rightarrow 2e^- + OH + H^+ \tag{2.7}$$
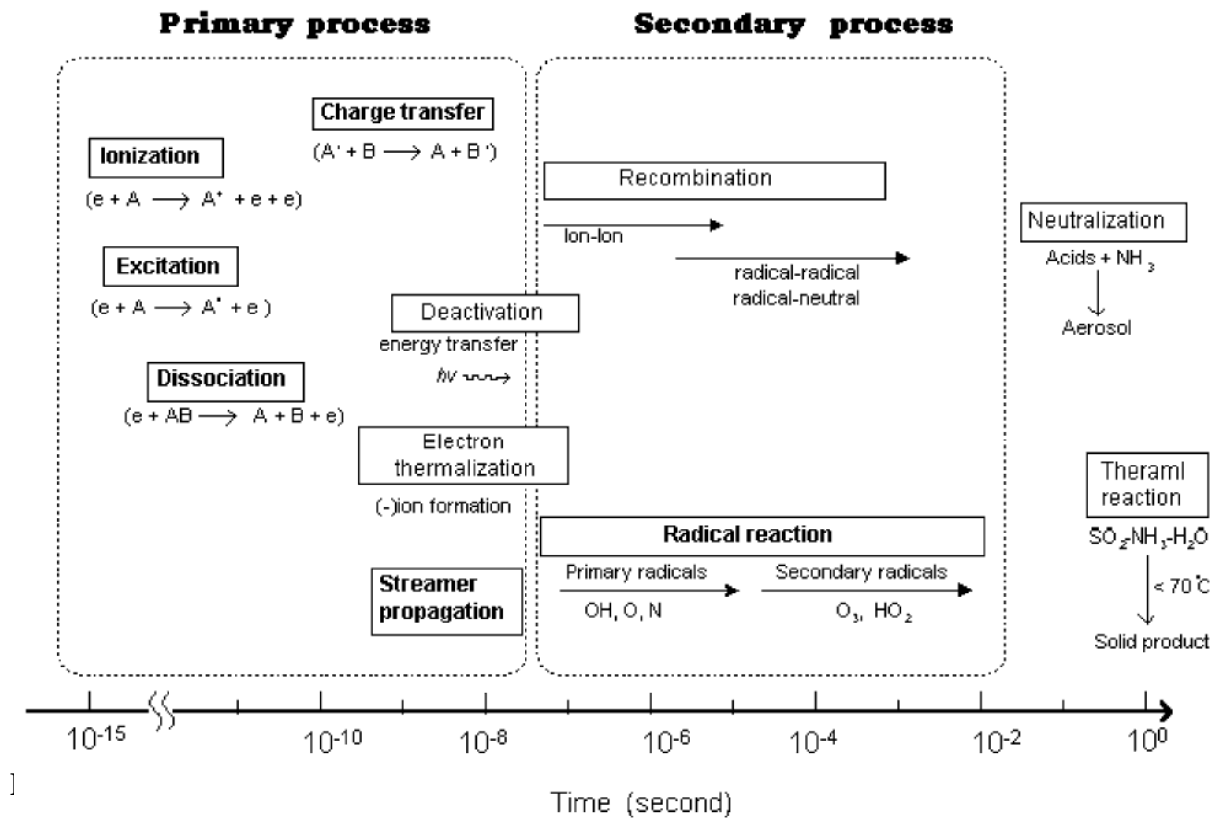
These primary processes, in combination with secondary NTP processes such as recombinations and radical reactions, result in the production of different types of reactive plasma species. Atkinson and Arey (2003) concluded that in oxygen-rich environments, primary produced H radicals are scavenged and converted into $HO_2^{\cdot}$ almost instantaneously. However, the most relevant and reactive radical in a NTP is the hydroxyl radical. This radical is formed by H_2O reaction with electrons, oxygen atoms or dissociative reaction initiated by positive ions (Penetrante et al., 1998; Hackam and Akiyama, 2000). Figure 2.2 summarizes OH radical production as function of the electric field E (kV cm^{-1}).
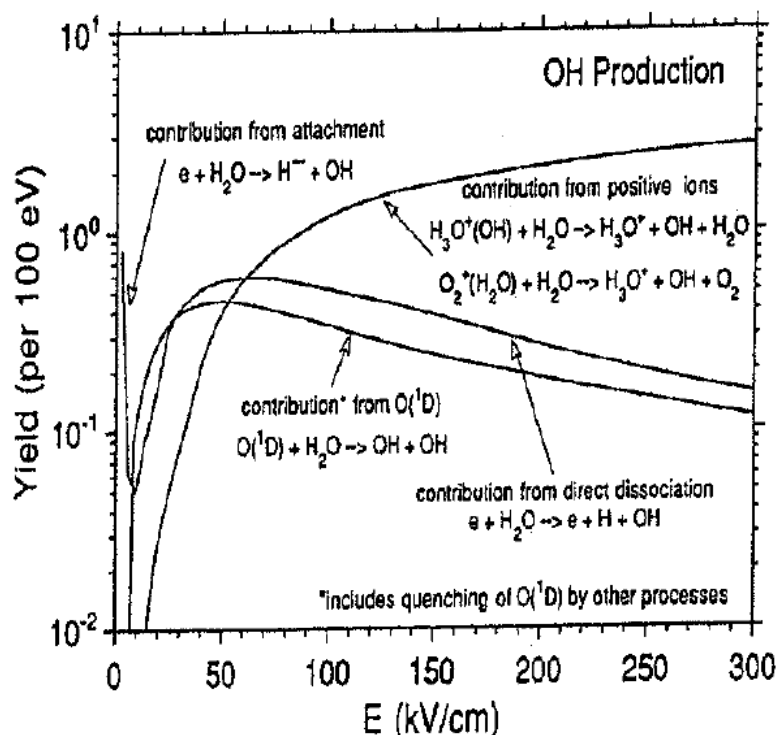
Figure 2.2 Calculated yield (per 100 eV) of primary and secondary OH generation processes in a NTP as function of electric field strength (kV cm^{-1}) (Hackam and Akiyama, 2000).

Consequently, non-thermal plasma can be defined as an ionized state of matter conformed by a quasi-neutral gas composed of short living charged and neutral particles (e.g. O, OH, HO$_2$, N, O$_2$*, N$_2$*, O$_3$, O$_3$*, O$^-$, OH$^-$, N$_2^+$, N$^+$, O$^+$, O$_2^+$, …) exhibiting a collective behaviour. NTP physics such as the calculation of the electron energy distribution or rate constants for excitation and dissociation reactions, has been modeled in great detail by solving Bolzmann equation (De Visscher et al., 2008). Research on NTP modelling using physical laws (Chen and Davidson, 2002; Kolobov and Arslanbekov, 2006) is essential to gain more knowledge about chemical and physical behaviour of NTPs. Next to simulations, also direct measurements of plasma species are recently being reported. Ono and Oda (2002) published data on direct measurement of OH radicals in NTPs, while Oda et al. (2006) were the first to measure atomic oxygen density in a atmospheric discharge using a two-photon excitation laser-induced fluorescence method.

There are many NTP types being investigated; dielectric barrier discharge (or silent discharge) (Wang et al., 1999; Sobacchi et al., 2003), pulsed corona discharge (Mok et al., 2002; Rudolph et al., 2003; Sobacchi et al., 2003; Vertriest et al., 2003), electron beam (Rudolph et al., 2003), radio-frequency plasma (Hu et al., 2002), capillary electrode reactor (Koutsospyros et al., 2005), DC glow discharge (Morent and Leys, 2005), DC corona discharge (this research), ferroelectric pellet packed-bed reactor ([b]Kim et al., 2005), surface discharge ([a]Kim et al., 2005), etc.

Each plasma has unique physical and electrical properties such as voltage/current characteristics, mean electron energy, ozone production, onset voltage, … Little work has been done towards comparing the behaviour of these different plasma configurations in terms of chemical efficiency. Indeed, comparing different plasma sources proves to be difficult since reported research results are obtained using different reactor type and geometry, type of power supply, temperatures, different target molecules, gas composition, etc. [a]Kim et al. (2005) published results of a comparative assessment of 5 NTP types (dielectric barrier discharge, surface discharge, pulsed corona, packed bed and plasma-driven reactor). This study revealed that for gas discharges, no differences in chemical efficiency (based on benzene decomposition data) could be indicated as long as the specific energy input is identical. On the other side, gas-solid heterogeneous NTPs (packed bed and plasma-driven catalysts) significant differences in performance were observed. These latter configurations typically lead to a higher mineralization rate and will be reviewed in more detail in the next sections of this chapter.

2.1.2 DC corona discharge

Corona gas discharges are low energy electric discharges with non-thermal ionization that takes place in the vicinity of an electrode of sufficiently low radius of curvature, at atmospheric conditions. Corona plasmas are self sustained and no external energy, other than that of the electric field, is needed to sustain the gas ionization processes (Rajch et al., 2006). Corona discharges can be operated both in positive as negative polarity. Both corona types have certain mechanisms in common. Both corona discharges are initiated by the acceleration of electrons, which are always present in air due to cosmic radiation, photoionization and other causes (Zhang and Adamiak, 2007). Due to electron collision processes, electron/positive-ion pairs are formed, which in their turn undergo similar separating processes creating an electron avalanche which sustains the corona discharge (Figure 2.3).
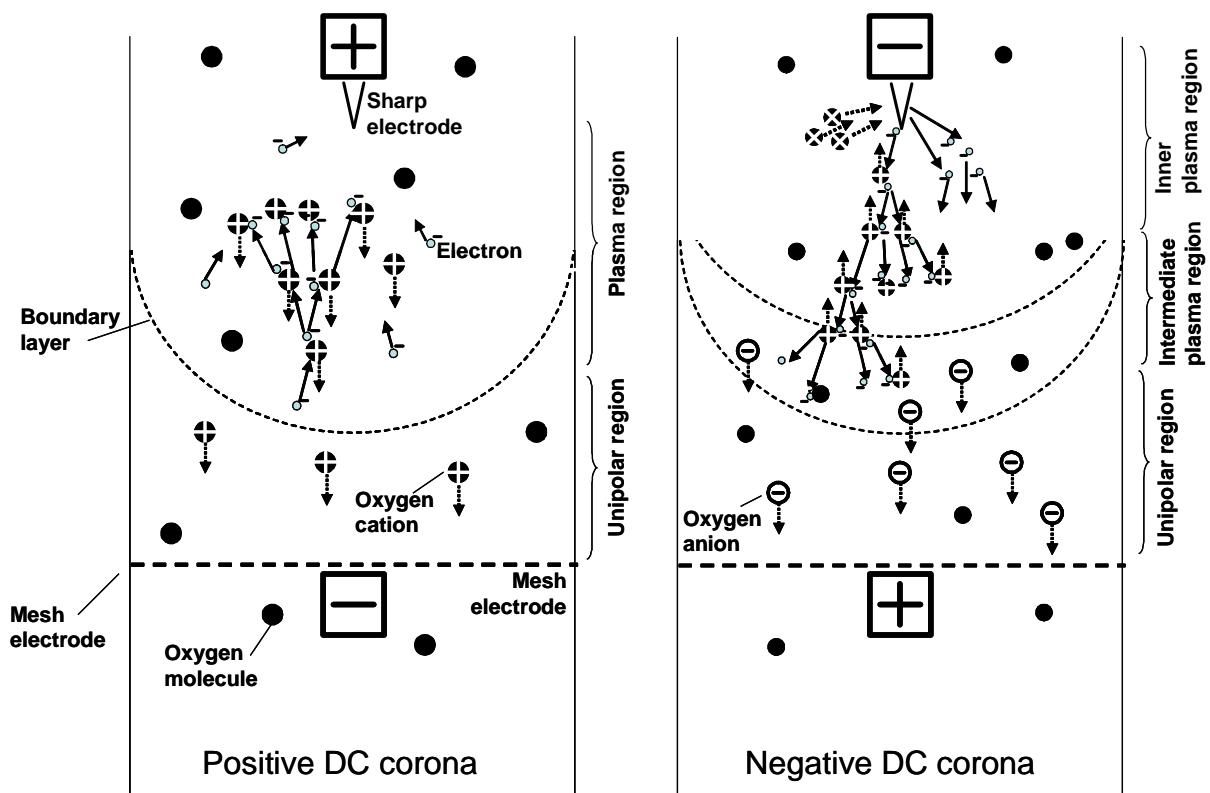
Figure 2.3 Schematic presentation of ionization processes in positive and negative DC corona discharge

2.1.2.1 Positive DC corona discharge

In Figure 2.3 a schematic presentation of a positive DC corona discharge indicates the occurrence of an ionization boundary. This boundary divides the interelectrode space in two regions; corona plasma region and unipolar region.

In the corona plasma region, field strengths typically exceed 3×10^6 V m^{-1} (Chen et al., 2002) accelerating electrons that produce electron-positive (O_2^+, N_2^+) ion pairs which in their turn release new electrons which are accelerated again. The resulting electron avalanche sustains the corona discharge. In Chapter 2.1.1 it was already discussed next to ionization processes, these energetic electrons also trigger excitation and dissociation processes, producing other reactive plasma species, such as radicals or excited molecules. The positive ions migrate towards the grounded electrode; outside the boundary layer the electric field strength is not sufficiently strong to produce secondary electrons. In this unipolar zone, positive ions complete the circuit and sustain the current flow. With increasing electric field strength, the corona plasma region becomes larger. When the number of electrons increases up to an amount where their spatial field is able to shield the electric field, streamers will be formed. Streamer discharges have a higher efficiency in the generation of chemical active species.

2.1.2.2 Negative DC corona discharge

Similar processes as discussed for positive DC corona discharges occur for negative DC corona discharges. A negative corona can be divided into three areas; inner plasma region, intermediate plasma region and unipolar region.

In the inner plasma region, electron impact ionization processes produce additional electrons and positive ions (N_2^+, O_2^+). The general movement of these electrons is outward from the curved electrode. By consequence the electron energy values decrease while electrons move

towards the boundary layer (Figure 2.3). The positive ions move back towards the electrode and hit its surface. Electrons are emitted from the corona electrode surface due to this ion impact. This is called the secondary electron emission (Zhang and Adamiak, 2002) (Figure 2.3). The work-function of the electrons (the energy required to liberate the electrons from the surface) is considerably lower than the ionization energy of air at standard temperatures and pressures. These new electrons move towards the grounded electrode, again producing electron/positive ions on their way.

In the intermediate region, electrons combine to form negative ions. In this region, energy levels are inadequate to cause further ionization processes. However, this intermediate region remains part of the plasma since different polarities of the species are present and species in this region are able to trigger characteristic plasma reactions.

In the outer region, only a flow of negative ions and, to a lesser extent, free electrons move towards the positive electrode.

When the electric field is increased to a level where the negative corona plasma region fills the complete interelectrode space, the discharge type is referred to as a DC negative glow discharge. Further increasing of electric field will eventually result in a spark discharge.

2.2 Hybrid plasma-catalyst configuration

A more effective use of plasma is possible by exploiting its inherent synergetic potential through combination with heterogeneous catalysts (Roland et al., 2005; Grossmannova et al., 2006; Guo et al., 2006). In the field of air purification, plasma driven catalytic technology has high potential as can be seen by increased mineralization efficiencies. Wallis et al. (2007) measured no CO_2 during the destruction of 500 ppm_v dichloromethane when using only plasma. However when γ-Al_2O_3 was introduced in the plasma discharge, CO_2 outlet concentrations were 32 ppm_v proving an increased mineralization rate. It can be concluded that by-product formation, such as aerosols, ozone and smaller organic compounds, is strongly reduced when using hybrid plasma catalyst technology ([c]Kim et al., 2005). In this study it is also observed that the energy efficiency for toluene degradation strongly increases using TiO_2 as in-plasma catalyst. Indeed, for dry air and an energy density of 17 $J.L^{-1}$, adding 15 g TiO_2 increased the toluene (C_{in} = 0.5 ppm_v) removal rate from 27 $\pm$ 4 % to 82 $\pm$ 2%. Similarly, introducing 15 g MnO_2-CuO/TiO_2 downstream the plasma discharge, resulted in 78% toluene removal efficiency for an energy density of 2.5 $J.L^{-1}$, while this was only 2% in the absence of a catalyst.

Based on recent papers (2004-2007) the different mechanisms occurring in plasma/catalyst hybrid configurations are reviewed. In a first part of this review it is shown that some authors report heterogeneous catalysts to affect plasma characteristics, while others claim that NTP initiate and influence catalyst mediated reactions. Secondly, the state-of-the art of plasma/catalyst combined systems in the field of waste gas treatment is presented.

2.2.1 Plasma catalytic mechanisms

Heterogeneous catalyst can be combined with NTP in two ways: by introducing the catalyst in the discharge zone (In Plasma Catalysis - IPC) or by placing the catalyst after the discharge zone (Post Plasma Catalysis - PPC) (Figure 2.3) (Holzer, 2005; [b]Subrahmanyam et al., 2006). For both IPC as PPC configuration, heterogeneous catalyst material can be introduced into the reactor in several ways (Figure 2.3): as coating on the reactor wall or electrodes, as a packed-bed (granulates, coated fibers, pellets) or as a layer of catalyst material (powder, pellet, granulates, coated fiber). In both designs many catalyst formulations have been proposed and tested. Reported in-plasma catalysts are $BaTiO_3$, Al_2O_3, SiO_2, TiO_2, MnO_2 and their derivates (Table 1) (Sano et al., 2006). Wallis et al. (2007) demonstrated that a variety of catalysts which were originally investigated in the field of thermal catalysis show similar synergy when combined with NTP. These kind of catalysts include platinum-based catalysts (Pinard et al., 2004), protonic zeolites, modified Y-zeolites, de-aluminated Y-zeolites, NaX and NaY zeolites, HZSM-5-supported manganese oxides and $LaCoO_3$. From recent publications it can be considered that the mentioned catalyst materials are also used in PPC configuration. However, Table 1 illustrates that in recent years most attention is given to IPC, particulary dielectric barrier discharge (DBD) packed-bed reactors are frequently used for experimental research.

a) In-plasma catalysis configuration

c) Overview of catalyst insertion methods
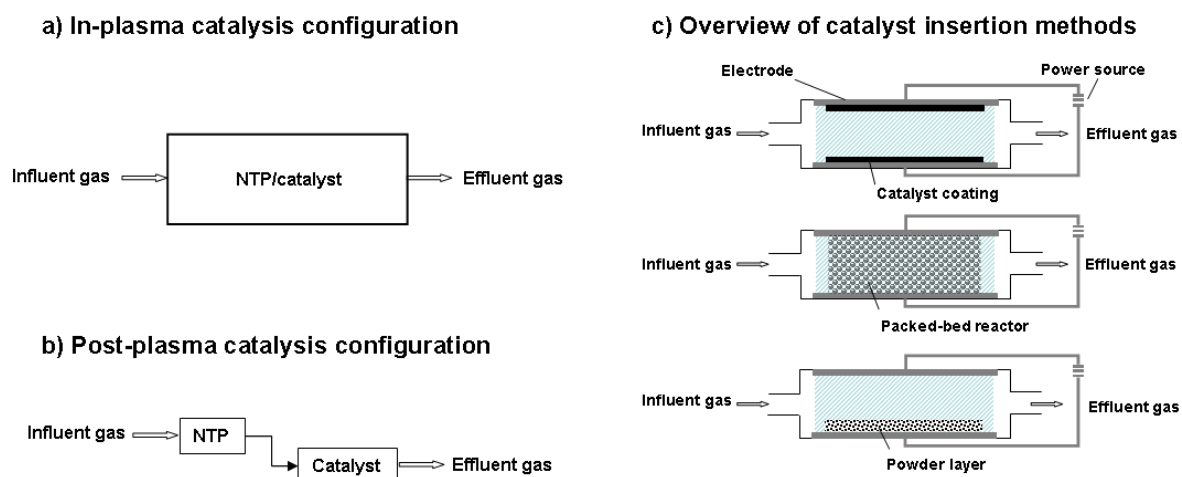
Figure 2.3 Schematic overview of two plasma-catalyst hybrid configurations; a) In-plasma configuration (IPC), b) post-plasma configuration (PPC). The most common catalyst insertion methods are summarized for IPC configuration (c)

Table 2.1 Overview of recently published papers on plasma catalysis

Plasma type	VOC	Flow rate (mL min^{-1})	Conc. range (ppm$_v$)	Catalyst	Position	Max. removal efficiency (%)	Energy cost (g kWh^{-1})	Reference
DBD	Toluene	315	240	MnO_2/Al_2O_3	IPC	55	11	Delagrange et al. (2006)
				MnO/AC	IPC			
				Fe_2O_3/MnO_2	IPC			
Corona	n-Heptane			TiO_2	IPC	50.4		Pekarek et al., 2006
DBD	Toluene	667×10^3	10 - 50	CuO/MnO_2	PPC	50		Chae et al. (2004)
	Ammonia							
DBD	Toluene	100 - 500	50	$MnO_2/Al/Ni$	IPC	> 95	1	Guo et al. (2006)
DBD	Benzene	250	300 - 380	TiO_2	IPC	16	3	Lu et al. (2006)
				MnO_2	IPC		4	
Corona (pulsed)	Toluene	100	300	AlO_2	IPC	> 95	156	Malik et al. (2005)
	Benzene			Silica gel	IPC	75		
	Hexane					25		
	Methane					5		
DBD	SF_6	600	300	$CuO/ZnO/MgO/Al_2O_3$	IPC	>99		Chang and Lee (2004)
	NF_3				IPC	>99		
	CF_4				IPC	66		
	C_2F_6				IPC	83		
DBD	Benzene	4000	75 - 110	Ag/TiO_2	IPC	96	11	[c]Kim et al. (2005)
	Toluene				IPC			
	o, m, p-xylene				IPC			
	formic acid				IPC			
DBD	Toluene	500	250	MnO_x/CoO_x	IPC	>99	2	[b]Subrahmanyam et al.
			100			>99	1	(2006)
Coil type (AC)	Benzene	4000 – 10,000	200	Ag/TiO_2	IPC	>99	10	Kim et al. (2006)
				Ni/TiO_2	IPC	>99		
				Ag/Al_2O_3	IPC	>99		
				Pt/Al_2O_3	IPC	>99		
				Pd/Al_2O_3	IPC	>99		
				Ferrierite	IPC	>99		
				Ag/H-Y	IPC	>99		
DBD	Formaldehyde	605	140	Ag/CeO_2	IPC	92	6	Ding et al. (2006)

Tabel 2.1 Overview of recently published papers on plasma catalysis (continued)

DC positive corona	TCE	1500	100	TiO_2	IPC	85	3	Morent et al. (2007)
Streamer	Toluene	133 x 10³	45	$CuOMnO_2/Al_2O_3$	PPC	96	33	Grossmannova et al. (2006)
DC positive corona	Toluene	10,000	0.5	$CuOMnO_2/Al_2O_3$ TiO_2	PPC IPC	>99 >99		This work
Coil type (AC)	Toluene	500	200	zeolites	IPC (discontinu)			Oh et al. (2005)
Dielectric pellet-bed reactor	CFC-12	1000	500	TiO_2	IPC	27	36	Wallis et al. (2007)
DBD	isopropanol	500	250	MnO_x/CoO_x	IPC	>100	9	Subrahmanyam et al. (2007)
DBD	Trichloroethylene	510	430	Au/SBA-15	PPC	>99		[a]Magureanu et al. (2007)
DBD	Trichloroethylene	500	250	MnO_2	PPC	97		Han and Oda (2007)
DBD	Dichloromethane	1000	500	γ-Al_2O_3 α-Al_2O_3 TiO_2 HZSM-5 NaZSM-5 NaA	IPC / PPC PPC PPC PPC PPC PPC	51 / 43 34 39 41 38 37		Intriago et al. (2006)

Table 2.1 summarizes several plasma driven catalytic processes which will be discussed in more detail during this review. It can be seen that introducing catalysts into the plasma discharge may affect the type of discharge or can induce a shift in the distribution of the accelerated electrons. These processes again influence the production of excited and short living reactive plasma species. New reactive species (e.g. atomic oxygen, superoxide species (O_2^-), hydroxyl radicals, …) can also be generated during the IPC process. Not only short-living unstable reactive species are produced in plasma discharges, a fraction recombines to form more stable species (e.g. ozone). Since these species have higher lifetimes, they are able to reach catalyst material positioned downstream the discharge zone (PPC). The presence of highly reactive plasma species and electrons trigger physical changes of the catalyst material and consequently affect VOC surface adsorption. Plasma driven catalytic systems show zeroth-order kinetics, indicating the important role of surface reactions during VOC decomposition. Accordingly, [a]Kim et al. (2005) reported that while VOCs with low ionization potentials usually have higher oxidation efficiencies in gas-phase NTP, this relationship is not observed in NTP-catalyst hybrid systems. Again, this proves that VOC decomposition is mainly influenced by adsorption processes, rather than by discharge characteristics. From Table 2.1 it is clear that gas temperature increase during plasma operation is able to thermally activate catalyst materials. Catalyst activation is also feasible by photon irradiation.
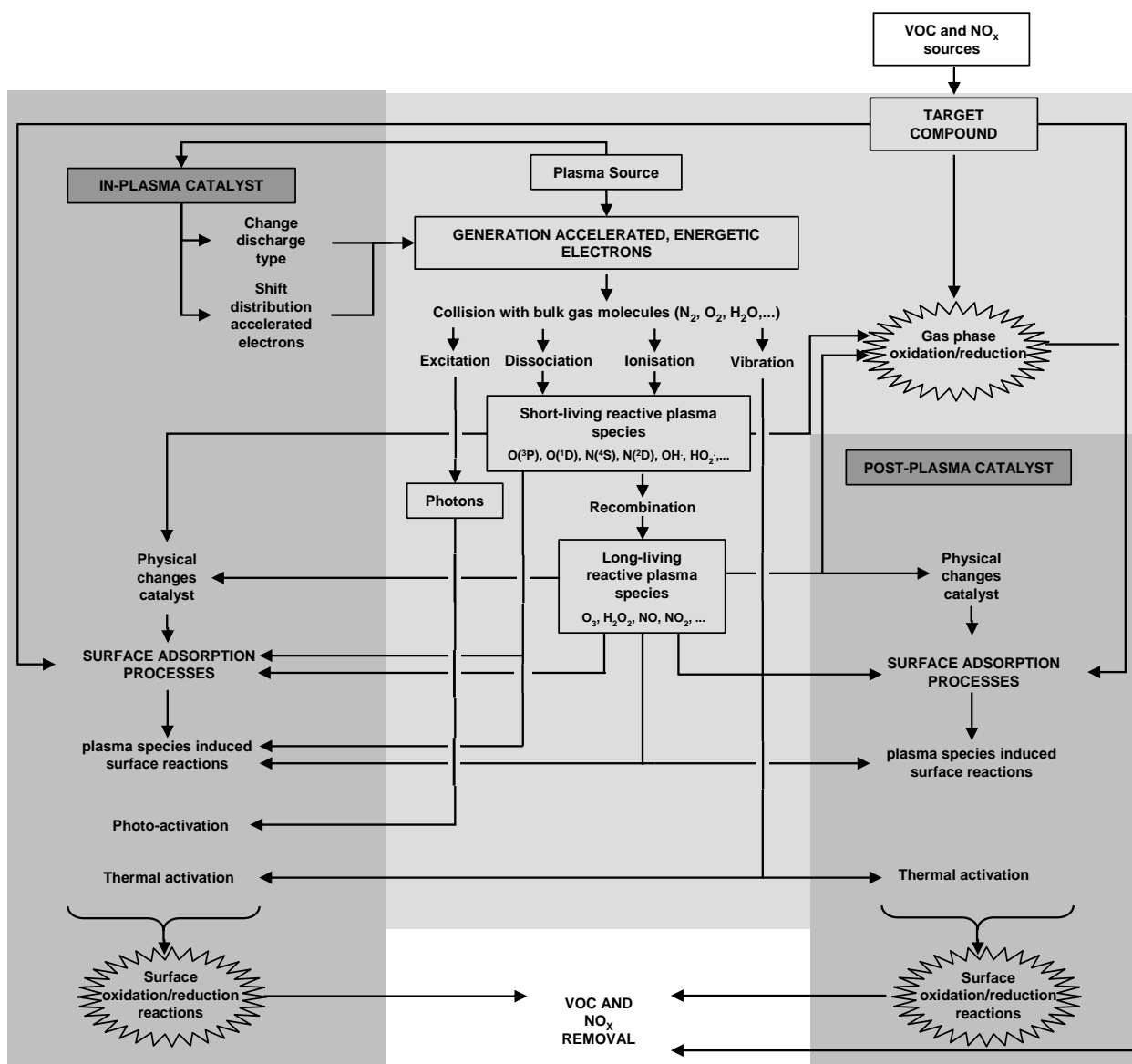
Figure 2.5 Schematic summary of plasma catalytic phenomena

To conclude, several processes are possible when catalysts are combined with non-thermal plasmas. Overall, it can be postulated that VOC removal becomes more efficient and higher mineralization rates, indeed own experiments proved that the energy efficiency of combining NTP with $CuOMnO_2/TiO_2$ in downstream position resulted in a toluene degradation energy efficiency of 1.06 g kWh^{-1} which was around 35 times higher than with plasma alone (0.03 g kWh^{-1}). In this study it was also illustrated what the effect of hybrid plasma catalysis was on by-product formation such as ozone.

Malik et al. (2005) wrote that in most of the research papers on plasma catalytic hybrid systems, the focus is put on catalytic reactions, whereas the adsorption processes at the catalyst surface has received less attention. Recent papers indicate that combining catalysts with NTP may result in physical chemical changes such as a shift of mean electron energy, change of discharge type, effect on catalyst properties or an impact on the VOC adsorption process (Figure 2.5) (Malik et al., 2005; Roland et al., 2005; Pribytkov et al., 2006).

2.2.1.1 Physical-chemical effects of catalysts on plasma properties

Change of discharge type and shift in distribution of accelerated electrons

The influence of changing the discharge type from streamers in air alone to streamers along insulator surfaces (surface flashover) has recently been described in literature (Malik et al., 2005). It is known that plasma streamers travel along insulators (Figure 2.6) (Akyuz, 2005; Malik et al., 2005), showing enhanced ionization compared to streamers in the gas space. As a consequence it is expected that VOC oxidation near insulators will be enhanced. In the presence of additional surface provided by heterogeneous catalysts, a similar effect has been noticed (Malik et al., 2005). Rodrigo et al. (2005) reported that corona interaction is the highest when surface is in direct contact with the electrode at which the corona originates. Indeed, it can be seen on Figure 2.6 that a glass surface, displaced 10 mm laterally from the electrode, enhances the propagation of the corona under negative polarity, but inhibits propagation with the positive polarity case (Rodrigo et al., 2005). Next, Hensel (2005) and Holzer (2005) reported that microdischarges might be generated inside the catalyst pores, resulting in more discharge per volume and increasing the mean energy density of the discharge. In addition, it has been reported that inserting ferroelectric materials in the plasma induces a shift in accelerated electron distribution. This phenomenon can be attributed to an

increased electric field with a factor of 10-250, leading to a more oxidative plasma discharge (Holzer, 2005). Similar conclusions were made for in-plasma zeolites (Liu et al., 2002) which easily interact with discharge plasmas due to a very strong natural electric field within their framework.
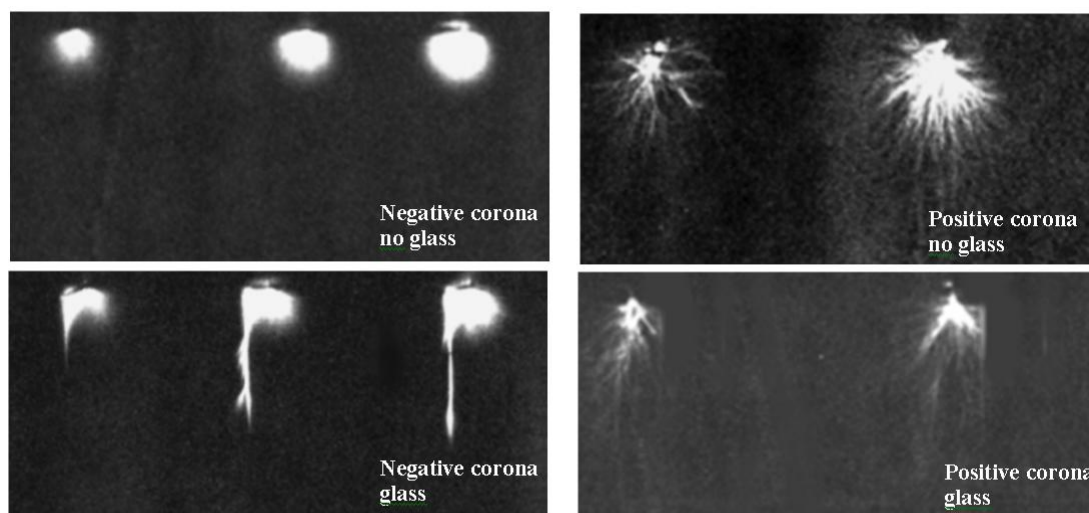
Figure 2.6 Photographs of the discharge under negative and positive polarities respectively, with glass displaced 10mm laterally from the high voltage electrode (Chae et al., 2004)

Generation of new reactive species

Introducing heterogeneous catalysts in the plasma discharge may increase the production of active species. This phenomenon was supported by Roland et al. (2005) who studied the oxidation mechanism of various organic substances immobilized on non-porous and porous carriers and concluded that these short-living oxidizing species are formed in the pore volume of porous materials when exposed to NTP. Also, Chavadej et al. (2007) found that insertion of TiO_2 in the discharge zone contributed to an acceleration of the superoxide radical anion (O_2^-) formation, consequently inhibiting recombination processes and increasing the total catalytic activity. Plasma generates intermediate species having a sufficiently long lifetime to trigger surface reactions on a catalyst placed downflow the plasma reactor (Hammer et al., 2004).

Short-living oxidizing species can not reach this post plasma catalyst ([b]Subrahmanyam et al., 2006). It is clear that mainly ozone is decomposed catalytically, forming molecular and highly-active atomic oxygen (Magureanu et al., 2005; Grossmannova et al., 2006; Wallis et al., 2007). This phenomenon is described for a number of catalysts such as silica gel, porous alumina and metal oxides (Roland et al., 2005). Lewis acid sites often appear to play a major role in the catalytic process. Sample pretreatment (e.g. calcinations temperature and residual water content) as well as the presence of additives and impurities influence the activity for ozone decomposition (Roland et al., 2005).

2.2.1.2 Physical-chemical effects of plasma on catalyst material

Effect on catalyst properties

Non-thermal plasma has been used in a series of surface treatment applications throughout the last few decades (Foest et al., 2005). This indicates that during plasma operation, catalyst surfaces might be affected in three different ways. First, discharges may enhance the dispersion of active catalytic components (Guo et al., 2006). NTP proved to influence the stability and catalytic activity of the exposed catalyst materials. Secondly, the oxidation state of the material can be influenced when exposed to plasma discharge (Guo et al., 2006; Jun et al., 2004; Pribytkov et al., 2006; Roland et al., 2005; Wallis et al., 2007). To support this, a Mn_2O_3 catalyst was exposed to a non-thermal plasma (energy density of 756 J L^{-1}) for 40 hours. After this experiment Mn_3O_4 was detected, this lower-valent manganese oxide is known to have a larger oxidation capability (Guo et al., 2006). Similarly, Wallis et al. (2007) reported that due to plasma catalyst interactions, less parent Ti-O bonds are found on TiO_2 surfaces. Pribytkov et al. (2006) and Jun et al. (2004) both agreed that in hybrid plasma catalyst configurations new types of active sites with unusual and valuable catalytic properties

may be formed. Similar conclusions were taken by Roland et al. (2005) who observed that during Al_2O_3 IPC, stable Al_O_O* paramagnetic species (lifetime > 14 days) are formed in the interior of the pores by direct plasma processes (electrons, UV, plasma species such as OH, OD ...). Finally, it was postulated that plasma exposure could even result in an specific surface area enhancement or in a change of catalytic structure (Guo et al., 2006). Indeed, Figure 2.7 compares SEM images of manganese oxide/alumina/nickel foam before and after DBD reaction. It was found that the granularity of the grain on the catalyst surface becomes smaller and the distribution is more uniform after discharge exposure. This results in the formation of ultrafine particles with higher specific surface and less-perfect crystal lattice having a large number of vacancies (Guo et al., 2006). These physical changes induce a higher catalytic activity, partially explaining the synergetic effect of plasma catalytic systems (Roland et al., 2005) (Guo et al., 2006). Contrary, Wallis et al. (2007) reported that BET surface areas can be reduced after plasma exposure: in the case of HZSM-5 (zeolite catalyst) a reduction of about 45% was measured while this was only about 6% for TiO_2 catalysts.
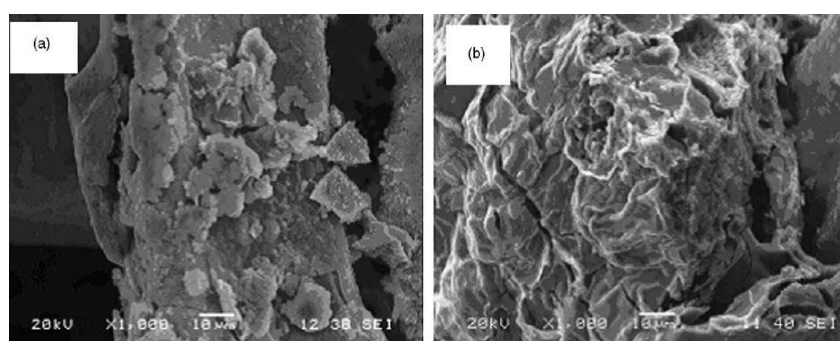
Figure 2.7 SEM images of manganese oxide/alumina/nickel foam before/after DBD reaction (1000x) (a) before and (b) after DBD exposure (Urashima and Chang, 2000)

Effect on adsorption process

Adsorption processes are strongly influencing the efficiency of plasma catalytic driven processes. A strong adsorption of the sorbate (VOC) combined with a large adsorption capacity of the sorbent is a prerequisite for a high performance of plasma-assisted catalysis used as air cleaning technology. Kwak et al. (2006) proved that differences in the amount and strength of NO_2 adsorption on Na-Y zeolites, mainly determine the NO_x removal efficiency. Lin et al. (2007) reported that the ionic wind may enhance plasma catalytic removal by increasing adsorption. Kinetic models commonly used in literature to study VOC surface oxidation corresponds to three types: Langmuir-Hinshelwood (LH), Eley-Rideal (ER) and Mars-van-Krevelen (MVK) (Miranda et al., 2007). LH models consider that the reaction takes place between both reactants adsorbed on the catalyst surface. ER mechanisms consider that the reaction takes place between one adsorbed reactant and the second reactant in the boundary layer. According to MVK models, the reaction takes place through alternative oxidations and reductions of the catalyst surface, the surface oxidation being produced by molecular oxygen (Miranda et al., 2007). Blin-Simiand et al. (2005) reported that the adsorption-desorption equilibrium of the molecule at surfaces is greatly influenced by the plasma discharge. In the case of interaction between adsorbed molecules and polar surfaces, electrostatic forces are more important than Van Der Waals forces. This effect can be quantified by the so-called parameter of specific interaction of polar solutes (Diaz et al., 2005). This parameter involves the surface properties in terms of potential and acid-base interactions, and includes different interactions (physical or electric) between molecules, such as Keesom and Debye interaction or hydrogen bonding (Miranda et al., 2007).

Thermal activation of catalyst

During non-thermal plasma operation, ambient gas temperatures increase due to inelastic electron-molecule collisions. Consequently, higher catalyst surface temperatures are often measured in hybrid plasma catalyst configurations (Lu et al., 2006). Ambient gas temperatures in non-thermal plasmas are determined by the gas mixture, gas residence time or type of discharge reactor. Hammer et al. (2004) measured that for a specific input energy density of 10 J L^{-1}, gas temperature in DBD discharges increase roughly 10 to 15°C. Other papers reported a temperature increase of approximately 70°C at 200 J L^{-1} (Kim et al., 2006). In a more detailed study by Staack et al. (2006), this effect was explained by an increase in rotational temperature with discharge current and electrode spacing. The vibrational temperature decreases with increasing rotational temperature and also decreases at low discharge currents and smaller electrode spacing. This results in an optimal regime for creating vibrationally excited species. This explains why gas temperature typically increases with discharge current and then levels off.

However, it has to be mentioned that the macroscopic gas temperature is often too moderate to explain thermal catalytic activation (Holzer, 2005). This indicates that hot spots can be formed on the catalyst surface. These hot spots are rather small zones which were equally distributed within the catalyst bed. These active volumes are presumably formed by strong micro-discharges appearing in particular between sharp edges and corners of adjacent pellets. Because ions and neutrals still have much lower temperatures compared to the accelerated electrons, the used discharges are still of the non-thermal plasma type. It has been proven that these increased catalyst temperatures promote catalytic VOC removal. This effect has been described by Kim et al. (2006) during benzene degradation experiments with Pt/Al_2O_3 catalyst. Holzer (2005) explained that complete ozone degradation in a $BaTiO_3$ packed bed plasma reactor for high energy densities was feasible due to thermally initiated decomposition

processes. Also Chae et al. (2004) reported that for temperatures above 100°C, ozone loss processes with $BaTiO_3$ catalyst were enhanced.

Plasma light emission triggering photo catalysis

Combining heterogenic photocatalysts with non-thermal plasma proves to enhance VOC and by-product degradation (Hammer et al., 2004). Among semiconductor photo-catalysts (i.e. ZnO, ZnS, CdS, Fe_2O_3, WO_3, etc.), titanium dioxide (TiO_2) is the most active, due to its photo-stability, strong oxidizing power, non-toxicitiy, chemical and biological inertness, stability, as well as its low cost (Wu et al., 2006).

Plasma triggered photocatalytic effects are not well understood. Some scientists state that UV wavelengths in the plasma discharge triggers oxidation reactions due to the formation of electron-hole pairs on the catalysts surface ([b]Demeestere et al., 2005; Kang et al., 2005). Indeed, UV light is produced by non-thermal plasma due to excited nitrogen molecules. Sano et al. (2006) reported that in the absence of TiO_2, UV light was emitted in a plasma discharge. The strongest emissions originate from the second positive system, which emits photons of 337.1 nm. The first negative system of N_2^+ emits 391.4 nm. In the presence of TiO_2 no UV light was detected, indicating that these wavelengths were absorbed by the catalyst (Figure 2.8).
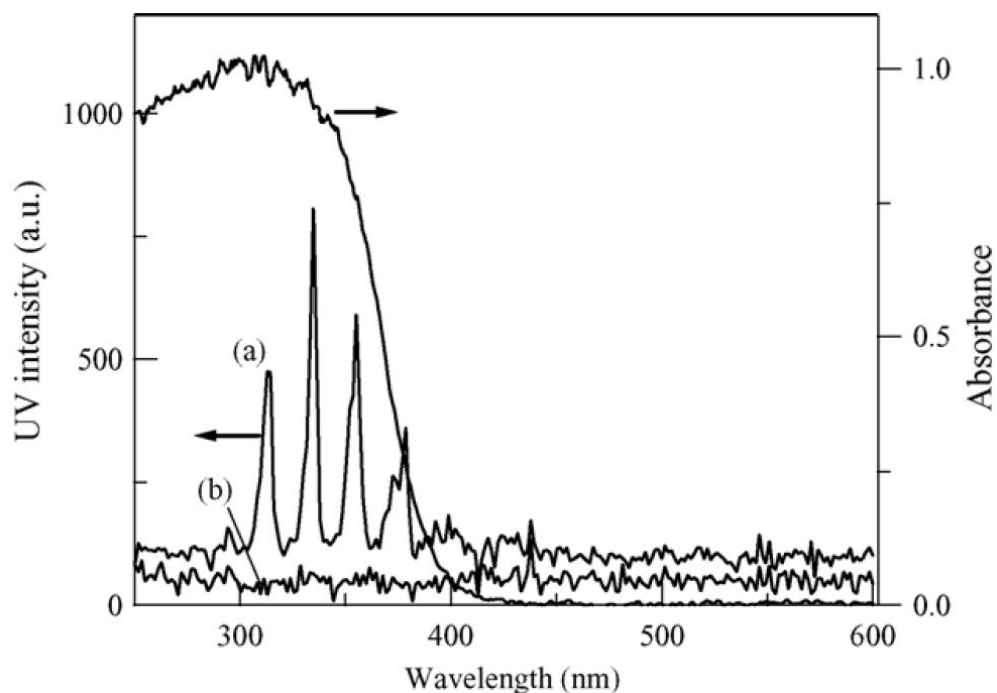
Figure 2.8 UV-vis emission spectra of surface discharge plasma observed from the outside of envelope without catalyst (a) and with TiO$_2$ (b), and the diffuse reflectance spectrum of TiO$_2$. Air was passed through a barrier tube with a flow rate of 100 mL.min^{-1}, the input power was 8W ([b]Magureanu et al., 2007).

Other scientists measured no increased UV emission in some plasma discharges (Ogata et al., 1999). The similar synergetic effects seemed to originate from the direct activation of the photocatalyst by the plasma discharge (Sano et al., 2006; Wallis et al., 2007). Chavadej et al. (2007) concluded that the catalytic property of TiO$_2$ is mainly due to the availability of reaction sites and its reducible property. Also [c]Kim et al. (2005) proved that UV emission is not always the controlling factor when photocatalyst are introduced. In Ar-O$_2$ gas streams only visible light is produced (400-850 nm). However, when combined with TiO$_2$, the synergetic effect was more important than in N$_2$/O$_2$ mixtures (Hammer et al., 2004; [c]Kim et al., 2005). It can be concluded that activation of the catalyst surface may also be explained by adsorption of high-energy species since metastable N$_2$[*] has an energy of 6.17 eV, while Ar

contains about 13 eV. Finally, as already described earlier, a generation of new reactive species on the catalyst surface might also be possible.

2.2.2 Environmental applications of plasma catalytic hybrid systems

2.2.2.1 Abatement of VOC

Table 2.1 gives an overview of recently published manuscripts about plasma catalytic VOC removal. From this table it can be concluded that dielectric barrier discharges (DBD) are most frequently used in recent plasma catalytic research. Most research has been done on inserting heterogeneous catalysts in the discharge. Nevertheless, post plasma catalysis is equally promising for environmental purposes. The main advantages of combining NTP with heterogeneous catalysts are an improvement of energy efficiency and a higher mineralization degree.

The type of VOC pollutant strongly determines the degree of VOC removal efficiency (Lu et al., 2006). These variations in removal efficiency are caused by the presence of different functional groups. To illustrate this, reaction rate constants ($cm^3.molecule^{-1}.s^{-1}$) for hydroxyl radicals and C_6 hydrocarbons having a varying number of unsaturated bounds, are 4.03×10^{-12}, 3.7×10^{-11} and 1.19×10^{-10} $cm^3.molecule^{-1}.s^{-1}$ for C_6H_{14}, C_6H_{12} and C_6H_{10} respectively. Generally, chlorinated VOCs can be removed with a higher energy efficiency due to the generation of chlorine radical chain reactions initiated by a chlorine atoms detachment. Generally, recent papers on hybrid plasma catalyst technology consider that the energy efficiency tends to increase with increasing initial pollutant concentration (Guo et al., 2006; Lu et al., 2006). Delangrange et al. (2006) concluded that the activity of the catalyst depends mainly on the support used. Kim et al. (2006) described the importance of metal-loading in

catalyst material during plasma catalytic processes. It was shown that conventional TiO_2 and Ag supported TiO_2 have different roles in the benzene decomposition (Kim et al., 2006). TiO_2 is responsible for the initial decomposition of benzene. However, Ag plays an important role in the decomposition of the surface intermediates. It was proven that the higher the Ag loading amount, the better the mineralization degree (Kim et al., 2006). Similar conclusions were taken by Kang et al. (2005). The insertion of 10.0 mol% Bi in TiO_2 catalysts resulted in smaller crystallic structure and an increased hydrophobicity. Wu et al. (2006) wrote that doping of TiO_2 with La resulted in increased porosity, uniformity and roughness, again resulting in better adsorption and decomposition of VOC. The conclusion that physical/chemical properties are dominating for the catalytic removal efficiency, is contradictory with processes as described by Kim et al. (2006) who reported that the degree of initial conversion was mostly determined by specific input energy, regardless of the type of catalyst. The catalyst surface area also proved to have little influence on the decomposition efficiency (Kim et al., 2006).

2.2.2.2 Reduction of nitrogen oxides

Non-thermal plasma applications for NO_x emission reduction has been widely studied in the last years (Higashi and Fuji, 1997; Lee et al., 2003; Penetrante, 1998; [a]Penetrante et al., 1999; [b]Penetrante et al., 1999). However, until today NTP and more recent hybrid plasma catalyst technology has not matured yet to meet 2007 regulations (Narula et al., 2005).

For these kinds of applications, plasma-facilitated catalysis is most a two-step process which consists of a plasma pretreatment of the exhaust before flow over a lean NO_x catalyst (Rappe et al., 2004; Tran et al., 2004). At lower reaction temperatures (<500 K), the efficiency of SCR (selective catalytic reduction) of NO_x strongly depends on initial NO_2 concentration in

the gas stream. About 30-50% of NO_2 in the gas stream greatly enhances the performance of SCR in $DeNO_x$ processes (Mok and Ham, 1998; Rappe et al., 2004; Tran et al., 2004). However, in real conditions the fraction of NO_2 present in the total NO_x seldom exceeds 5%. The plasma however, converts a part of NO into NO_2 (Okubo et al., 2005). Basically (plasma generated) ozone, hydroxyl radicals and atomic oxygen play an important role in the oxidation of NO to NO_2. When hydrocarbons are simultaneously treated by the plasma discharge, partially oxidized hydrocarbons and peroxy radicals (RO_2) are generated which react with NO and strongly influence NO_2 formation rates (Rappe et al., 2004; Tran et al., 2004). After the pretreatment step, NO_2 reacts over a catalyst while partially oxidized hydrocarbons are consumed during selective catalytic reduction producing CO_2, N_2 and H_2O (Lin et al., 2007).

Two main classes of catalysts, zeolites and metal oxides, have been reported to be highly effective for NO_x removal in combination with non-thermal plasma. It was proven that the addition of alkali and alkaline earth species (for zeolites) or transition metal ions (for γ-alumina) enhances catalytic activity (Rappe et al., 2004). In recent publications both designs, in-plasma catalysis (Hueso et al., 2007) and downstream catalysis (Kwak et al., 2006; Ogata et al., 1999; Okubo et al., 2005; Rappe et al., 2004; Tran et al., 2004), have been examined for NO_x reduction purposes. Niu et al. (2005) reported that NO_x conversion by a catalyst-filled dielectric barrier discharge with methane additive was much higher than with plasma alone. The NO_x conversion for pure plasma induced, pure catalyst induced and plasma-catalyst induced reactions was 24%, 25% and 65% respectively (Niu et al., 2005). Also Sun et al. (2005) described synergetic interactions in a one-stage plasma-over catalyst reactor between DBD plasma and Cu-ZSM-5 catalyst during C_2H_4 selective reduction of NO_x. Studies however proved that these in-plasma catalytic systems behave similarly to those with the catalyst positioned post plasma. This implicates that the catalytic mechanism does not involve

effects such as electric field enhancement or electron impact excitation of the catalyst surface. Instead, stable or metastable species created in the plasma may be central to the catalysis (Narula et al., 2005).

Okubo et al. (2005) reported that plasma pretreatment is not always effective. For higher temperatures (at high energy densities) less ozone is produced in the plasma. Secondly reaction rates of NO/$O^{.}$ and NO/$OH^{.}$ decrease, resulting in reduced NO_2 formation rates. Finally, during plasma pretreatment, OH radicals may convert the formed NO_2 into HNO_3 (Mok et al., 2002) and high $O^{.}$ levels may lead to a conversion back to NO (Okubo et al., 2005). For gas temperatures lower than 450K, ammonium nitrate formation should be considered in order to avoid deactivation of catalysts. It can be concluded that plasma characteristics and heating effects are important parameters in the design of plasma reactors used as a pretreatment technology.

Chapter 3

Chemical analytical techniques for monitoring of indoor air pollution: Accelerated solid-phase dynamic extraction of toluene from air

3.1 Introduction

The development of new analytical techniques to analyze trace levels of volatile organic compounds (VOCs) has received great attention, mainly due to the growing concern on indoor air quality. The main bottleneck and most time consuming step in the analysis of VOCs at ambient concentrations is often sample preparation and preconcentration. This has resulted in the development and optimization of a wide range of extraction, trapping and preconcentration techniques applicable to VOC analysis, as recently reviewed by Demeestere et al. (2007). Solvent-free microextraction based on the partitioning of analytes between a liquid or gaseous sample matrix and an immobilized sorbent as the preconcentration matrix, has received great attention in recent years (Baltussen et al., 2002; Demeestere et al., 2007). In the study of NTP, IPC and PPC, adequate VOC analytical techniques are indispensable. Therefore, solid-phase microextraction (SPME) has been used, but for some cases solid-phase-dynamic extraction (SPDE) can even be more useful. However SPDE has not matured yet to be used as a standard analytical sampling technique, this chapter focuses on its possibilities to be used for the detection of sub-ppm$_v$ VOC concentrations.

Solid-phase dynamic extraction has been reported for the first time by Lipinski (2001). SPDE is based on the same principles as solid-phase microextraction (SPME), but instead of using a coated fiber, SPDE uses a sorbent coating on the inner wall of a stainless steel needle. Due to this modified geometry, SPDE needle coatings possess around four to six times larger extraction phase volumes compared with a 100 µm SPME fiber (Jochmann, 2006). Other advantages include the reduced fragility of the needle. The most frequently used coatings for these applications are polydimethylsiloxane (PDMS), PDMS/divinylbenzene (PDMS/DVB), and Carboxen/PDMS (Martos and Pawliszyn, 1999). Analyte uptake on PDMS is via absorption, while it is adsorptive for PDMS/DVB and likely capillary condensation for

Carboxen/PDMS. Each of these polymers has a different selectivity for VOCs, eventually determining its sampling efficiency.

Due to the recent character of the technique, however, only few SPDE applications have been reported so far. Most applications for this technique to date have been for headspace sampling. Examples are the SPDE extraction of smoking-related compounds (Saito et al., 2007), amphetamines, cannabinoids and synthetic designer drugs (Lachenmeier et al., 2003; Musshoff et al., 2002; Musshoff et al., 2003) from the headspace of hair, next to applications in the field of food analysis. Bicchi et al. (2004) reported the SPDE of the volatile fraction from food matrices. However, the potential of this innovative technique has not being fully explored for the analysis of VOC in the field of environmental monitoring (Demeestere et al., 2007). Jochmann et al. (2007) reported the application of SPDE for the analysis of benzene and volatile halogenated hydrocarbons in groundwater samples; and Ridgway et al. (2006) investigated SPDE of non-polar volatile aromatic analytes from aqueous solutions in both headspace and liquid injection modes. As far as we know, SPDE as a tool for environmental air monitoring has not been reported. Next, despite the promising results recently obtained with SPDE, the fundamentals of this new technique have not been completely understood so far.

Therefore, the scope of this chapter is twofold. First, a home-made autosampling device has been constructed to systematically investigate the SPDE mechanism and the main parameters affecting SPDE of VOCs from air. Toluene has been chosen as a model compound. Particular attention has been given towards the extraction kinetics, and a new accelerated SPDE technique has been developed. Secondly, the applicability of SPDE to analyze VOCs at typical ambient/indoor air concentrations has been investigated. For toluene as a model indoor air pollutant, the limit of detection (=LOD) obtained with SPDE-GC-FID has been compared

with those achieved with more conventional sampling techniques such as SPME and gas syringe sampling.

3.2 Materials and Methods

3.2.1 Preparation of calibration standards

Toluene (>99.5%, CAS108-88-3) was purchased at Acros Organics (Geel, Belgium), and used as supplied without further purification.

Gaseous toluene calibration standards were prepared in two ways. For the mechanistic study, performed at ppm_v-level concentrations, a static method was used. Therefore, 10 mL of liquid toluene was introduced in a 118 mL glass bottle gastightly sealed with a Mininert Valve (Alltech Ass., Lokeren, Belgium). After equilibration of this two-phase system at 14.4 ± 0.1 °C for at least 8 hours, fixed volumes (100 – 1000 μL) of saturated headspace were injected into another series of gastight closed 118 mL glass bottles, thermostated at 25.0 ± 0.1 °C by using a Julabo ED heating device and/or a Huber TC45E cooler.

To determine LOD and LOQ of toluene, gaseous calibration standards were prepared at concentrations between 0.3 and 92 ppm_v using a dynamic VOC/air mixing system. Therefore, a clean and dry air stream ($[H_2O] < 3.0$ ppm_v; $[CO_2] < 1.0$ ppm_v; $C_xH_y < 0.5$ ppm_v) (Air Liquide, Luik, Belgium) with a flow rate set between 0 and 10 $L.min^{-1}$ was mixed with a second air stream (0 – 200 mL min^{-1}) enriched with toluene. Loading air with toluene was achieved by passing it through a thermostated capillary diffusion system ([b]Demeestere et al., 2005) or by bubbling it through an impinger filled with pure liquid toluene. More information on these VOC enrichment methods is given in Chapter 4.1, especially Section 4.1.2 in which the gas stream preparation procedure used in the experimental setup is discussed. All flow

rates were adjusted by mass flow controllers (5850E series, Brooks Instrument, Veenendaal, The Netherlands).

3.2.2 Analytical methods

3.2.2.1 Gas sampling techniques

The calibration mixtures prepared as described in section 3.2.1. have been sampled using three devices. First, a conventional 0.5 mL Hamilton 1700 gastight syringe (Alltech Ass.) has been used. Secondly, sampling was performed using a SPME device purchased at Supelco (Bornem, Belgium) consisting of a 1 cm fused silica fibre coated with polydimethylsiloxane (PDMS) (film thickness: 100 μm, volume: 0.66 μL) and mounted into syringe needle. Prior to extraction, the SPME fiber was heated at 220°C for 5 min in a gas chromatograph injector. A sampling time of 10 minutes was applied, being sufficiently long to achieve equilibrium partitioning of toluene between PDMS and the gas phase, as shown in preliminary experiments. Third, a SPDE needle (length 56 mm, outer diameter 800 μm, internal diameter 400 μm) coated at the inner side with 4 μL of PDMS (film thickness: 50 μm) (Chromtech, Idstein, Germany) was connected to a 0.5 mL Hamilton 1700 gastight syringe.

3.2.2.2 Home-made SPDE autosampling device

During SPDE, the syringe plunger is moved up and down several times at a controlled speed, hereby enriching the internal coating with the analytes of interest (Jochmann, 2006). Usually, the CTC-CombiPAL autosampler supplied by Chromtech (Idstein, Germany) is used for this purpose. These experimental data, however, were obtained using a home-made SPDE autosampling device that has been constructed with the ability to control important SPDE parameters (Figure 3.1 A).
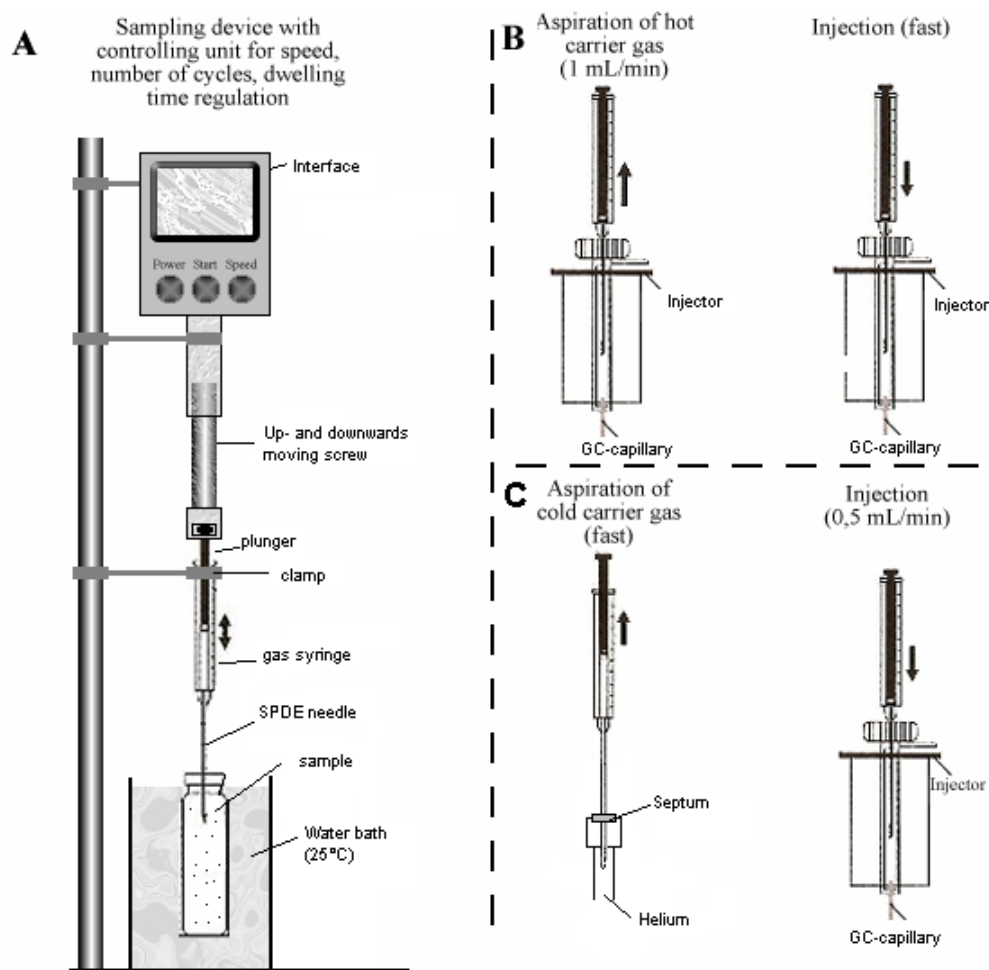
Figure 3.1 Schematic representation of home-made SPDE extraction device (A) and different SPDE desorption methods (B and C)

In essence, a computer unit (Siemens LOGO! 12/24 RC) and a 12 V DC power supply (Megane) controlled the movement of a converted drilling machine. The number of sampling cycles, with one sampling cycle being defined as one aspirating step followed by one dispensing step, could be regulated. Adjustable parameters included the aspirating and dispensing plunger speed (0 – 0.5 cm min^{-1}) corresponding with volumetric sampling rate between 0 and 6 mL min^{-1} when a 0.5 mL gas syringe is used. Next, the dwelling time can be regulated, i.e. the time span between an aspirating and dispensing step, which was set at zero seconds for all experiments.

3.2.2.3 Chromatographic analysis

A gas chromatograph (Chrompack 9200) equipped with a split/splitless injector (split ratio set at 1/10, 250°C), a 0.25 mL liner, a capillary column (CP-Sil 8CB, length 25 m, internal diameter 0.32 mm, film thickness 1.2 µm) and a flame ionization detector was used for toluene detection. Helium was used as a carrier gas with a column head pressure of 50 kPa. The GC oven temperature has been set in two different ways. A first series of experiments was conducted under isothermal conditions (T = 120°C), whereas subsequent analyses were performed using a temperature program starting at 40°C and ramped up to 120°C at a heating rate of 30°C min^{-1}.

3.2.3 Model description / development

In order to support the experimental conclusions, a model was built. In this model, the SPDE needle volume is discretised into $(n'' + n') \times m$ axisymmetric control volumes, where n'' is the radial cell number in the (mobile) gas phase (n = 10), n' is the radial cell number in the polymeric (stationary) phase (n' = 50) and m represents the number of cells in the longitudinal direction (m = 100). The volume discretisation is shown in Figure 3.2.

Figure 3.2 The model's discretisation scheme (n' and n": number of radial control volumes in gas (mobile) and solid (stationary) phase, m: number of longitudinal control volumes, L: length (m), r and x: radial and longitudinal coordinate (m), d₁: tubular inner diameter (m), d₂: inner diameter steel needle (m))

Within the range of gas velocities used and considering the geometry of the capillary needle, the gas flow was laminar, as exemplified by the Reynolds number Re (equation 3.1):

$$\text{Re} = \frac{\bar{v}_g d_1 \rho_g}{\mu_g} \ll 2300 \tag{3.1}$$

with $\bar{v}_g$ the mean gas velocity (m s⁻¹), d_1 the tubular inner diameter (m), ρ_g the gas density (kg m⁻³) and μ_g the gas viscosity (Pa.s). Because of the laminar flow regime, Equation (3.2) was used to describe the longitudinal gas velocity in each of the gas phase's control volumes $v_g(r)$. r being the radial coordinate of the control volume's centroid (m). Radial gas velocity was assumed to be equal to zero.

$$v_g(r) = 2\bar{v}_g \left(1 - \left(\frac{2r}{d_1}\right)^2\right) \tag{3.2}$$

In order to model toluene partitioning between gas and PDMS phase, a toluene mass balance was attributed to each control volume (i, j), with i ranging from 1 to $n'' + n'$ and j ranging from 1 to m, having the following generic form:

$$\frac{dC\ i,j}{dt} = \left(\begin{array}{c} convective \\ mass\ transport \end{array} \right) + \sum \left(\begin{array}{c} diffusive \\ mass\ transport \end{array} \right) - \left(\begin{array}{c} exchange\ at \\ gas/solid\ interface \end{array} \right) \tag{3.3}$$

In Equation (3.3), the convective mass transport term is only present in the gas phase control volume mass balance. The second term on the right hand side of Equation (3.3) describes mass transport by diffusion across all boundaries of the control volume. These transport terms were quantified using Fick's first law of diffusion, with Q and A the mass transfer rate (kg s^{-1}) and surface area (m²) respectively, and *Q/A* the diffusion flux (kg m^{-2} s^{-1}):

$$\frac{Q}{A} = -D\frac{dC}{dx} \ \ or \ \ -D\frac{dC}{dr} \tag{3.4}$$

In Equation (3.4), the coefficient D represents the diffusion coefficient (m² s^{-1}) of toluene, either in the gas phase (D_g = 0.086 cm² s^{-1} (Shih and Wu, 2002) or the PDMS phase (D_s = 0.0000012 cm² s^{-1} (Dhoot and Freeman, 2003)) depending on the type of control volume under consideration. The terms *dC/dx* and *dC/dr* are the longitudinal and radial gas concentration gradients, respectively.

The third term in Equation (3.3) represents the mass exchange occurring at the gas/PDMS interface. This component is based on the toluene concentration gradient across the gas phase boundary layer at the gas/PDMS interface. Assuming that the toluene concentration in the gas phase at the wall surface is in equilibrium with that in the PDMS phase (C$_{PDMS}$) to be equal to C$_{PDMS}$/K with *K* the gas/solid partitioning coefficient of toluene (K$_{25°C}$ = 1061 (Demeestere et al., 2007)). In that case, the gas/PDMS interface mass transport is equal to:

$$\frac{Q}{A} = k_m \left(C_g - \frac{C_s}{K_{g/s}} \right) \tag{3.5}$$

where k_m (m s^{-1}) is the convective mass transfer coefficient and C_g (kg m^{-3}) is the toluene concentration in the bulk of the gas phase.

In order to estimate the value of the convective mass transfer coefficient, the dimensionless Sherwood number (Sh), as calculated from the dimensionless Nusselt (*Nu*) and Lewis (*Sc/Pr*) numbers, was used:

$$Sh = \frac{k_m d_1}{D_g} = Nu \left(\frac{Sc}{Pr} \right)^{0.25} \tag{3.6}$$

where the dimensionless Schmidt (Sc) and Prandtl number (Pr) are calculated as:

$$Sc = \frac{\mu_g}{\rho_g D_g}, \; Pr = \frac{C_{p,g} \mu_g}{\lambda_g} \tag{3.7}$$

with λ_g the gas thermal conductivity (W m^{-1} K^{-1}). For fully developed laminar flow in a cylindrical tube, the Nusselt number is equal to 3.657.

Overall, the model constitutes of a set of *(n" + n') × m* ordinary differential equations (ODE's) which were solved using Euler's method and implemented on an Intel Pentium IV 3,6 GHz equipped PC using VB6.0 (Microsoft, US).

3.3 Results and discussion

3.3.1 Mechanistic study

3.3.1.1 Optimisation of SPDE desorption-based injection

Prior to gain insight in the fundamental SPDE mechanisms, it is essential to have knowledge on the appropriate way of desorption-based GC injection. Therefore, three different SPDE injection methods have been investigated which combine toluene desorption from the PDMS coating of the SPDE needle with simultaneous injection into the gas chromatographic column.
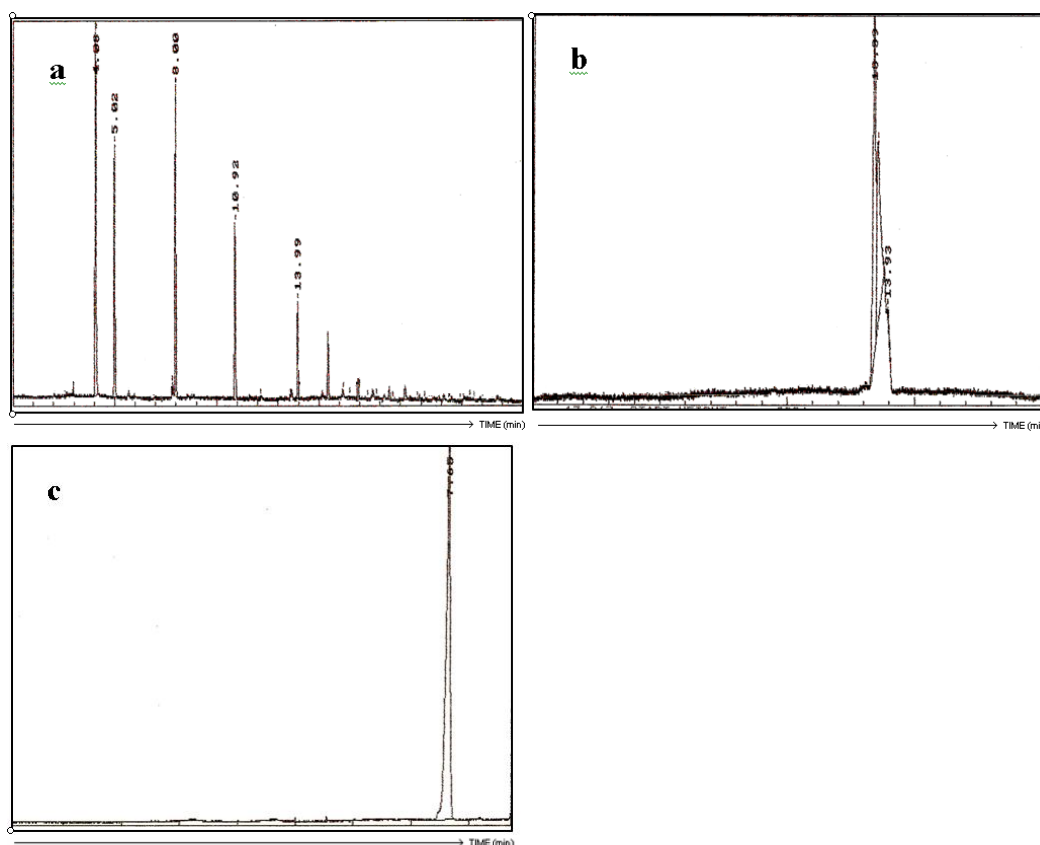
Figure 3.3 Comparison of three SPDE injection procedures (a, b, c) after toluene loading (volumetric sampling rate 0.8 mL min^{-1}, 5 sampling cycles, T = 298.15 K, conc$_{toluene,in}$ = 92 ppm$_v$)

Main criteria of evaluation hereby were the desorption/injection efficiency, expressed as the number of injections needed for complete toluene desorption; and the quality of the chromatographic peak, quantified by the peak width at half height and the asymmetry factor. In order to investigate the desorption techniques, SPDE needles were loaded with toluene by sampling 118 mL gas bottles, thermostated at 25.0 ± 0.1 °C and containing 92 ± 2 ppm$_v$ of toluene. For each desorption technique, five sampling cycles, an aspirating and dispensing volume of 0.5 mL and a volumetric sampling rate of 0.8 mL min^{-1} were used.

In a first desorption method, 0.5 mL of heated helium (T = 250 °C) was aspirated from the GC-FID injector through the toluene enriched SPDE needle at a flow rate of 1 mL min^{-1} (Figure 3.1b). During aspiration, desorbed toluene molecules are collected in the SPDE gastight syringe. Next, this toluene loaded gas volume was rapidly injected through the SPDE needle into the heated GC-FID injector. The GC oven temperature was set isothermally at 120 °C. Experiments proved that desorption was not complete after one desorption-injection cycle (Figure 3.3a). However, up to 10 cycles were necessary before toluene was totally removed from the SPDE coating, indicating a low desorption/injection efficiency.

The second desorption procedure was similar to the first one, but the GC oven temperature was programmed as described in Section 3.2.2.3. Again, multiple (n > 7) desorption-injection cycles were necessary to obtain > 99% toluene desorption from the SPDE needle. However, due to refocusing of the toluene molecules in the first part of the chromatographic column, kept at 40 °C during the multiple desorption-injection, one badly shaped peak was observed characterized by a peak width at half height of 3 min and an asymmetry factor of 4 (Figure 3.3b). Figure 3.3b indicates that several injection peaks are superposed and elute very close to each other giving the impression of being one single peak.

Finally, the third injection method (Figure 3.1c) involved the aspiration of 0.5 mL of cold helium (T = 25 °C) through the toluene loaded SPDE needle as shown in Figure 3.1c. Next,

the SPDE needle was inserted in the heated GC injector (T = 250 °C) and the 0.5 mL of helium was introduced slowly (flow rate of 0.5 mL min^{-1}). During injection, toluene gradually desorbs and is collected in the first part of the chromatographic column (trapping effect). Figure 3.3c proves that this injection method results in single peak characterized by a peak width at half height of 0.3 min and an asymmetry factor of 0.8. Experiments proved that sampling 92 ± 2 ppm$_v$ toluene with a PDMS-SPDE at these conditions corresponded with a peak area of 122,300 a.u. and a low standard deviation of 3.4% (n = 3), indicating the reproducibility of the desorption/injection method.

3.3.1.2   SPDE parameter study: number of sampling cycles and volumetric sampling rate

The number of sampling cycles and the volumetric sampling rate are both directly correlated with the sampling time. Jochmann (2006) reported that experimental peak integration data sigmoidally increases with larger number of sampling cycles. For several analytes, i.e. 1,4-dioxane, methyl tert-butyl ether, ethanol and 2-ethylhexanol, stable responses were obtained after 50 cycles sampled with a 50 μm thick WAX phase SPDE, corresponding to a sampling time of 33 minutes.

Vials containing 92 ± 2 ppm$_v$ of toluene were sampled with SPDE using the home-made device described in Section 3.2.2.2. (Figure 3.1a). The amount of toluene sorbed in the SPDE coating was determined as a function of the number of sampling cycles, ranging between 1 and 50, and at two different volumetric sampling rates, i.e. at 0.8 and 1.6 mL min^{-1} (Figure 3.4).
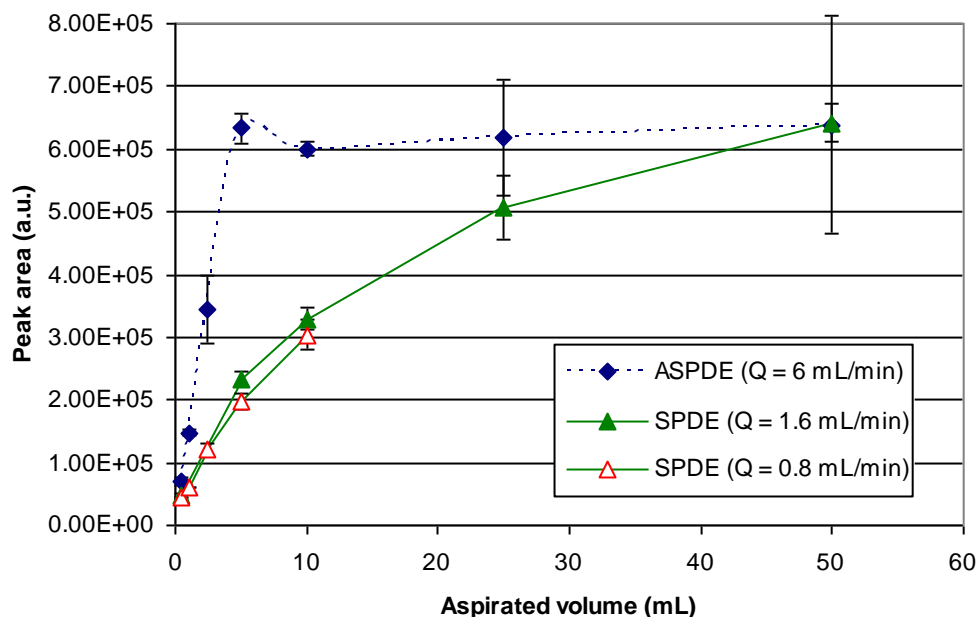
Figure 3.4 SPDE integration results as function of the aspirated volume during toluene sampling (T = 298.15 K, volumetric sampling rate = 6 mL min^{-1}, toluene gas phase concentration = 92 ± 2 ppm$_v$). Error bars express the standard deviation on the average measured value (n = 3).

Given that the syringe volume is 0.5 mL, 1 mL of gas passes through the SPDE needle during one sampling cycle, i.e. 0.5 mL is withdrawn from the sample during the aspiration step; after which 0.5 mL is introduced again in the sample during dispensing. It is clear from Figure 3.4 that the GC peak area - and thus the sorbed mass of toluene- gradually increases with increasing the aspirated volume, being in agreement with the results reported by Lipinski (2001) and Jochmann (2006). Within the experimental range, the highest peak area (641,900 ± 30,900 a.u.) is obtained at an aspirating volume of 50 mL, corresponding to a sampling volume of 100 mL, and with a volumetric sampling rate of 1.6 mL min^{-1}. At the same toluene gas phase concentration, sampling with a conventional 0.5 mL gastight analytical syringe resulted into a peak area of 16,300 ± 800 a.u., being a factor of 39 lower than the response obtained with SPDE. Despite this significant gain in sensitivity, the main drawback of SPDE proves to be the extraction time. Indeed, at the set sampling rate of 1.6 mL min^{-1}, the required

sampling volume of 100 mL corresponds to a total sampling time of 62.5 min, being clearly higher (at least a factor of 6) than needed using a more conventional preconcentration technique like SPME.

Figure 3.4 also reveals that the volumetric sampling rate does not have an important effect on the extraction yield, expressed as the amount of toluene sorbed per sampling cycle. This result is in agreement with Bicchi et al. (2004), and indicates that the partitioning process is not affected by the gas residence time in the needle.

3.3.2 Towards a better understanding of the SPDE mechanism and the development of an innovative accelerated SPDE procedure (ASPDE)

3.3.2.1 Experimental approach

In order to gain insight into the underlying SPDE mechanism leading to the rather long sampling times as observed in Section 3.3.1.2, an experimental set-up as depicted in Figure 3.5 has been constructed. One side of the SPDE needle was inserted through a septum into a cylindrical volume which was sealed with stainless steel unions and Teflon ferrules (Alltech Ass., Lokeren, Belgium). The other side (sampling side) of the SPDE needle was inserted into a glass vial containing toluene loaded air (92 ± 2 ppm$_v$). At the other side of the cylindrical volume, a 0.5 mL gastight analytical syringe equipped with a stainless steel needle was introduced (Figure 3.5a).
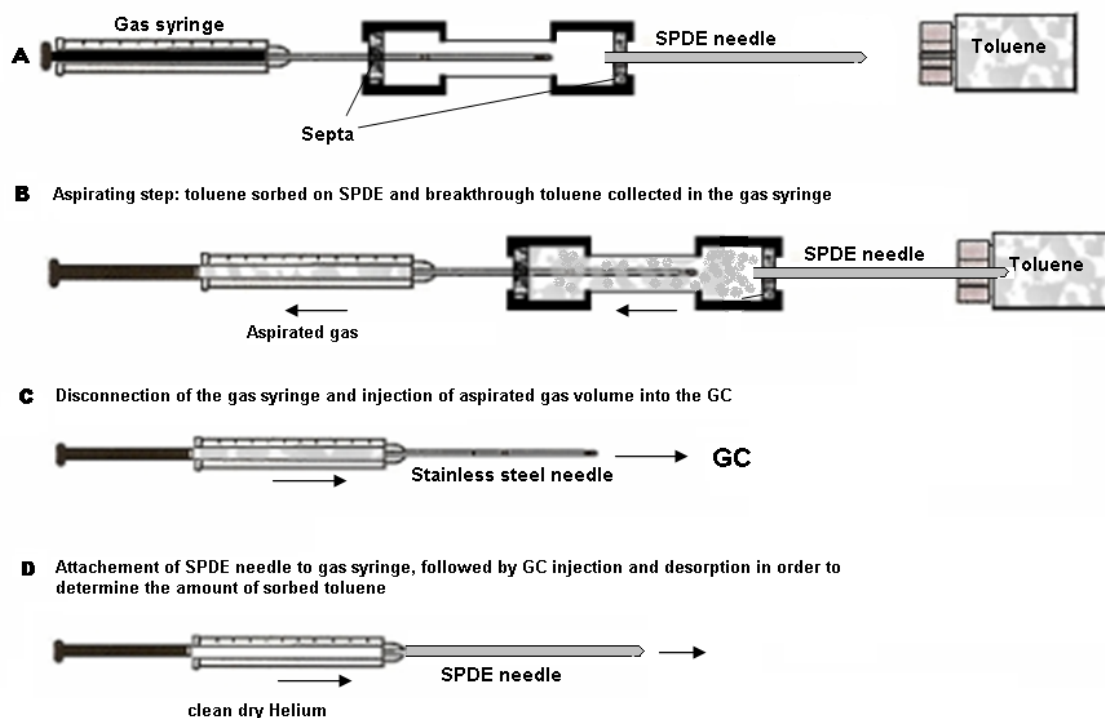
Figure 3.5 Experimental set-up used to study the SPDE mechanism

During aspiration, the plunger of the gas syringe was moved (flow rate = 6 mL.min^{-1}) in that direction that forced the toluene loaded air to be transferred through the SPDE needle (Figure 3.5b). After withdrawing of 0.5 mL of toluene loaded air, i.e. after 1 aspiration step, the gas syringe was disconnected from the cylindrical volume, and, without having a dispensing step through the needle, the gas collected in the syringe was introduced into the GC-FID system described in Section 3.2.2.3 (Figure 3.5c). Next, after flushing the gas syringe at least 3 times with air, it was reconnected to the sampling device and inserted again to the cylindrical volume after which the procedure described above was repeated multiple times.

Results revealed that no toluene could be detected in the gas collected in the syringe up to 2 aspiration cycles, i.e. after passing 1.0 mL of toluene loaded air through the needle. After 10 sorption steps, the peak area obtained by injecting the last 0.5 mL of aspirated gas collected in the syringe body amounted $5,400 \pm 1,000$ a.u. (n = 2), being 3 times lower than the peak area obtained by injecting 0.5 mL sampled directly from the toluene containing vial ($16,300 \pm 800$

a.u.) with the gastight analytical syringe (without SPDE). It can be concluded that no equilibrium is reached yet. Up to about 20 aspiration steps, corresponding to an aspirated volume of 10 mL, were necessary to obtain a GC peak area of 16,000 ± 200 a.u. (n = 3) and no further significant increase in peak area was observed at higher aspirating volumes. This indicates that breakthrough through the needle − and thus equilibrium portioning of toluene between gas and PDMS phase- is obtained at an aspiration of 10 mL.

In a similar experiment, the mass of toluene sorbed in the SPDE needle coating was measured after 1, 2, 5, 20, 50 and 100 aspiration steps, without performing any dispensing through the needle. Therefore, the procedure described above was repeated but after the appropriate number of aspiration steps, the SPDE needle was disconnected and mounted on a gastight syringe after which 0.5 mL of cold helium was sampled and injected into the GC, according to the third desorption/injection procedure discussed in Section 3.3.1.1 (Figure 3.5d). The GC peak areas obtained as a function of the aspirated volume are given in Figure 4 (circular points, connected by a dotted line). It can been seen that a peak area of 617,000 ± 24,700 a.u. is already obtained after an aspirated volume of 10 mL, i.e. after 20 aspirating steps. Moreover, this value does not increase significantly by enlarging the aspirated volume. This result is in agreement with the peak areas obtained by analyzing the gas collected in the syringe, and indicates complete breakthrough of the PDMS coating after passing of about 10 mL of toluene loaded air through the SPDE needle. For example, the peak area obtained after 100 aspiration steps amounted 638,664 ± 173,289 a.u, being not significantly different from that measured after 20 aspiration steps, nor from the maximum peak area obtained with the SPDE procedure described in Section 3.3.1.2. All data points plotted in Figure 3.4 could be measured with a standard deviation less than 10%, except the values obtained using set-up

shown in Figure 3.5 after 50 and 100 aspiration steps (no dispension steps) were higher due to the large number of experimental handlings.

A mechanistic explanation supporting the obtained results is proposed in Figure 3.6. During the first aspiration step, toluene molecules are completely sorbed in the PDMS coating, resulting into a zero toluene concentration measured in the gas phase collected in the syringe (Figure 3.6a). During subsequent dispensing of the needle, i.e. when passing the toluene free gas through the needle, the toluene concentration difference between the enriched PDMS phase and the toluene free gas phase forms a driving force initiating partial toluene desorption from the PDMS coating (Figure 3.6b). As a result, every dispensing step leads to a significant loss of retained analytes, leading to the rather low sampling yield in subsequent aspiration-dispensing sampling as observed in Section 3.3.1.2.
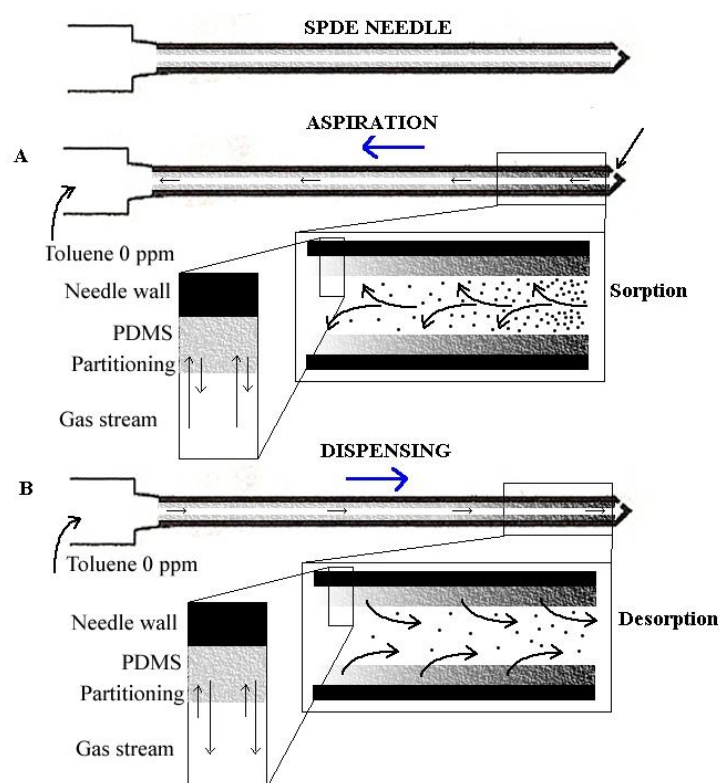
Figure 3.6 Proposed mechanistic explanation for the low SPDE yield based on sorption/desorption processes taking place in the SPDE needle during subsequent aspiration and dispensing.

3.3.2.2 Modeling approach

The model described in Section 3.2.3 has been run to support the proposed mechanistic processes. Both the SPDE procedure including aspiration and dispensing, and the SPDE method without dispensing (Figure 3.4) have been modelled to determine the mass of toluene loaded on the PDMS phase as a function of the aspirated volume.

Figure 3.7 clearly indicates for both processes a high correlation between the experimental and the modeled results, supporting the sorption-desorption processes discussed in section 3.3.2.
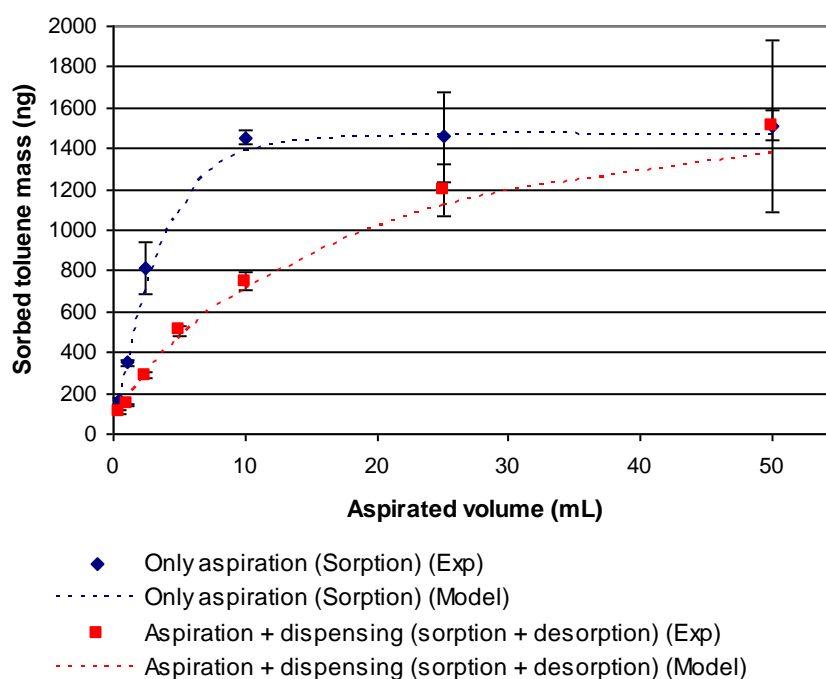
Figure 3.7   Comparison experimental and modeled toluene mass sorbed on PDMS coating for sorption and sorption-desorption measurements.

As an illustration of the loss of extraction yield during the dispensing step, Figure 3.8 represents as a function of the number of sampling cycles the predicted amount of toluene that is sorbed during aspiration next to the mass of toluene desorbed from the needle during subsequent dispensions. It is clear that the dispension step results into a high procentual loss

of extraction yield (up to 48 % during the first sampling cycles), indicating the rather low extraction efficiency of the SPDE technique. This explains the long sampling time needed to obtain complete partitioning equilibrium in the SPDE needle, as observed in Section 3.1.2.
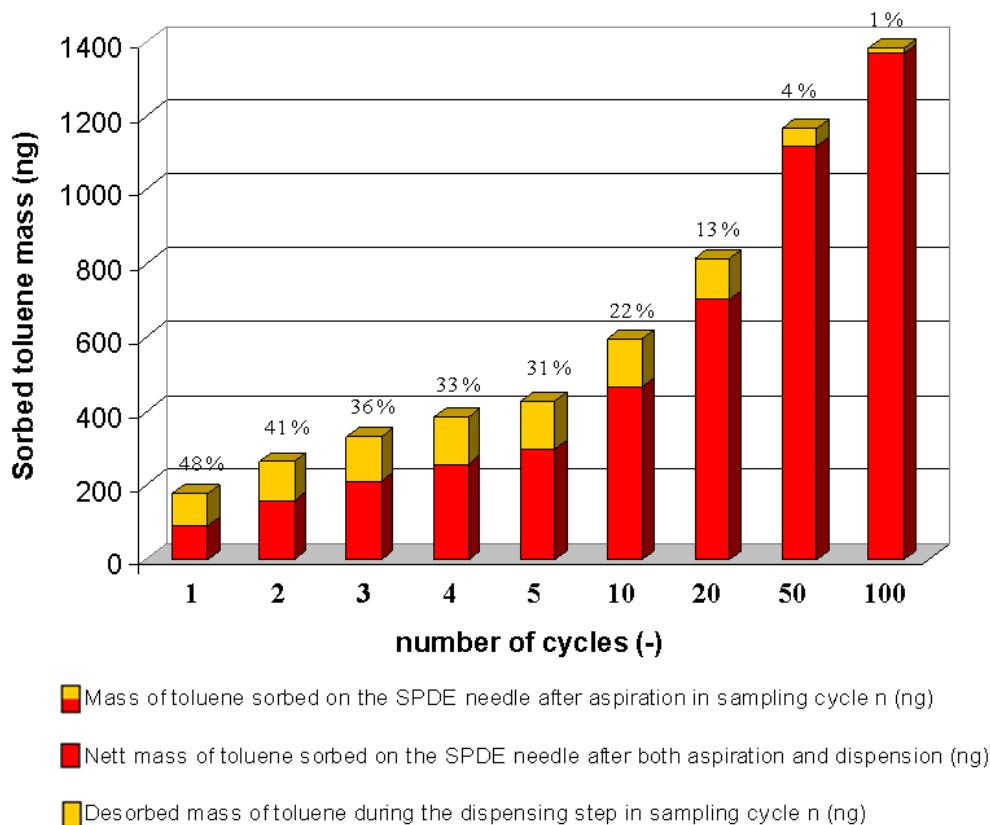
Figure 3.8 Predicted masses of toluene (ng) sorbed on the SPDE needle after aspirating and dispensing as a function of sampling cycle n. Procentual losses of sorbed mass of toluene due to desorption (dispensing) are inserted for each modeled cycle.

3.3.3 Innovative accelerated SPDE (ASPDE)

Regarding the results shown in Figure 3.4, and given the mechanistic explanation suggested in Section 3.3.2.1. and 3.3.2.2., it becomes obvious that the SPDE yield can be drastically improved by eliminating the dispensing steps and thus avoiding toluene desorption losses. Therefore, a new optimized ASPDE device is configured. A large volume syringe (50 mL) is connected to the SPDE needle and the required aspirated volume is withdrawn through the

needle in one single step at a volumetric flow rate of 6 mL min^{-1}. In this way, the PDMS coating in the needle is enriched with the analytes without any dispensing step. Next, the large volume syringe is replaced by a 0.5 mL analytical gastight syringe, and the SPDE needle is disconnected from the sample matrix. Finally, 0.5 mL of cold helium is aspirated through the needle and the optimized desorption and chromatographic methods described in Section 3.3.1.1 (Figure 3.1c) are applied to analyse the sorbed mass of analytes by GC-FID.

3.3.4 ASPDE potential for indoor air monitoring

The applicability of ASPDE in the field of ambient and indoor air quality monitoring has been explored for the first time. Therefore, gaseous standard solutions of toluene in a concentration range between 0.3 and 10.8 ppm$_v$ have been sampled and injected into the GC-FID by the 0.5 mL analytical gastight syringe and the SPME device described in Section 3.2.2.1, as well as by the optimized ASPDE procedure developed in Section 3.3.1. The aspirated volume and volumetric sampling rate applied during ASPDE of toluene amounted 10 mL and 6 mL min^{-1}, respectively. The calibration curves measured for toluene using the three sampling techniques, are given in Figure 3.9. In all cases, a linear regression curve could be fitted through the data points ($R^2 \geq 0.9994$, n $\geq$ 3), and statistical analysis (SPSS 14.0) revealed that the intercepts were not signifantly different from zero ($\alpha > 0.05$). Therefore, the slope of the curves forced through the origin can be considered to be a valuable parameter to compare the sensitivity of the three analytical techniques.

Considering Figure 3.9, it is clear that the ASPDE technique provides sensitivities for toluene sampling at least a factor of 37 higher than obtained with gas syringe sampling, and at least a factor of 6 higher than achieved with SPME.
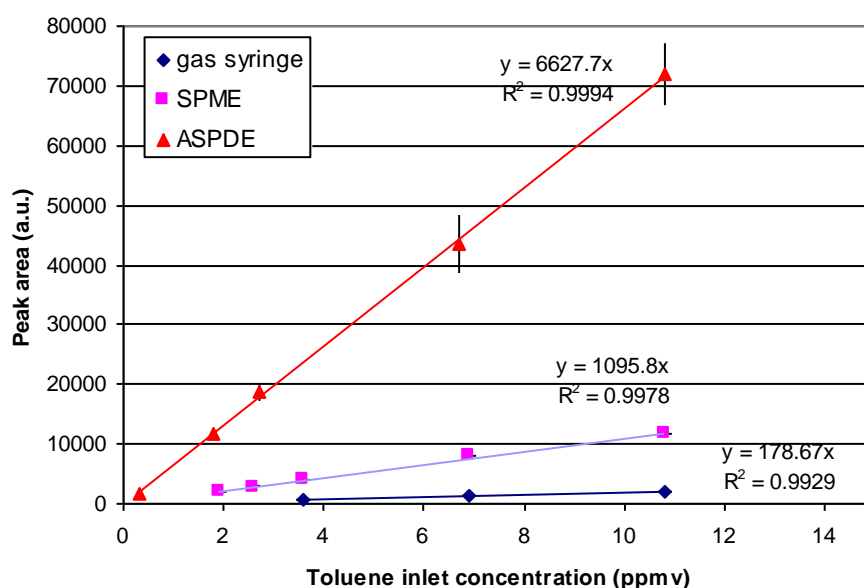
Figure 3.9 Toluene calibration curves obtained with three sampling techniques: ASPDE (aspiration volume 10 mL, volumetric sampling rate 6 mL min^{-1}), SPME and gas syringe sampling (0.5 mL injected volume, T = 298.15 K, p = 101.3 kPa).

Given that the enrichment phase in both preconcentration techniques is the same (PDMS), the partition coefficient applicable in both techniques is identical. Therefore, the higher preconcentration factor obtained with ASPDE can be explained by the larger volume of PDMS. Indeed, whereas the SPDE needle contains 4 µL of PDMS, the SPME fiber is coated with 0.66 µL of PDMS (Dewulf et al., 1999). The 6 times larger volume of sorbent phase is in good agreement with the observed difference in enrichment power. From the calibration curves LOD and LOQ values for toluene, determined as the signal-to-noise ratios of 3 and 10, respectively, have been calculated to be 345 ppb$_v$ and 1063 ppb$_v$ for SPME and 56 ppb$_v$ and 173 ppb$_v$ for ASPDE.

Moreover, due to the optimization of the SPDE procedure as described in Section 3.3.2, the equilibration time in the new ASPDE procedure amounts about 1.7 min being a factor of 5 shorter than that needed with SPME. This, in combination with the increased robustness of the SPDE needle, makes ASPDE to be a very promising tool for the detection of low levels of VOCs in air.

3.3.5 Conclusions

In this chapter, the applicability of SPDE to analyze VOCs at typical ambient/indoor air concentrations is investigated for the first time.

A home-made autosampling device is constructed to systematically investigate the SPDE mechanism and the parameters affecting the toluene extraction yield. After optimization of the SPDE desorption/injection mode, resulting into toluene detection as one sharp and symmetric peak, it is proven that the sorbed mass of toluene increases at larger number of subsequent aspiration-dispensing steps. Next, the volumetric sampling rate is shown not to have an important effect on the toluene extraction yield, i.e. the mass of toluene sorbed per sampling cycle.

One main conclusion of our study is that every dispensing step leads to a significant loss of retained analytes, leading to a rather low extraction yield and long sampling times (62.5 min). Experimental and modeled results revealed that up to 48 % of the analytes retained on the SPDE needle during aspiration are released again because of desorption during the dispensing step. Therefore, a new accelerated SPDE technique, characterized by a large volume aspiration through the needle, and the elimination of the dispensing step is developed, resulting into sampling times of about 1.7 min. This is 38 times shorter than with the SPDE procedure involving both aspiration and dispensing, and about 5 times shorted than the equilibrium time needed with SPME. Using ASPDE, sensitivities being at least a factor 37 and 6 times higher than those obtained with gas syringe sampling and SPME, respectively, are obtained. LOD and LOQ values for toluene are calculated to be 56 ppb_v and 173 ppb_v proving its promising potential for ambient/indoor VOCs monitoring.

Chapter 4

DC pin-to-mesh corona discharge: parameter study

4.1 Introduction - Experimental setup

4.1.1 DC corona reactor

As mentioned earlier, non-thermal plasma technology is an AOP having great potential for the treatment of gas flow rates exceeding 1000 m³ h^{-1} containing low pollutant concentrations (<10%). Non-thermal plasma processing is an AOP that has been considered as an effective and energy-saving method to remove VOCs due to its unique properties (Futamura et al., 2002; Morent et al., 2007). One of these advantages compared to other purification technologies is its non-selectivity. Plasma designs for removing VOCs include electron beam, surface discharge, dielectric barrier discharge, ferroelectric packed-bed, pulsed corona, DC discharge and microwave discharge processes (Li et al., 2002). The more or less effective removal of a wide variety of contaminants has already been described in literature: aliphatic, aromatic (Rudolph et al., 2002), chlorinated and fluorinated hydrocarbons as well as inorganic pollutants such as SO_2, H_2S and NO_x. Despite the importance of indoor air quality, only a few studies (Zhu et al., 2007) have reported on the feasibility of applying non-thermal plasma technology for the removal of indoor air pollutants.

In order to study NTPs for indoor cleaning purposes, a DC corona reactor was developed and mounted into a cylindrical tube with an inner diameter of 40 mm, as represented in Figure 4.1.
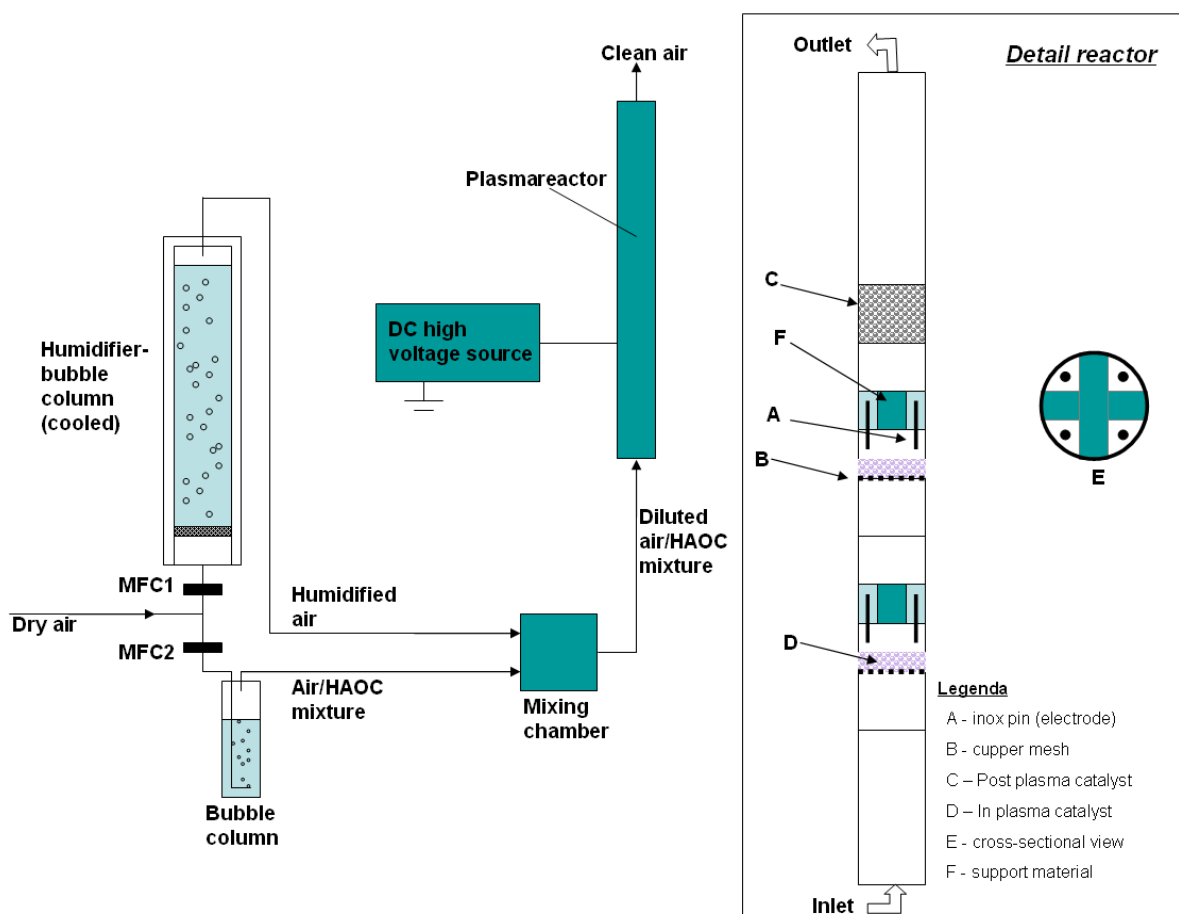
Figure 4.1 Experimental setup with detail of developed DC corona reactors

Each plasma unit consists out of a mesh cathode, and four crenellated inox pins as anodes. These home-made anodic electrodes are mounted onto a support and are constructed in such a way that the discharge connects to typically 8 anode spots for each pin. Each pin is ballasted with a 1.5 MΩ resistance. The fraction of the total electrical power that is dissipated in these resistors amounts to 10% at most (Morent et al., 2007). The pins and mesh are mounted in the tube in such a way that the inter-electron gap can be varied. Gas can freely flow along the pins (section 4.1.2). Since the plasma reactor is created in a modular way, several plasma source units can be placed in series along the gas flow. Different units can be electrically connected in parallel (two plasma reactor in series are represented in Figure 4.1). The gas flow pattern and velocity in each plasma unit is comparable. The discharge is powered by a 40 kV/5 mA

DC high voltage supply (HVS40005P). When a corona discharge is generated this is visualized by a purple plasma cone for each pin. Since each pin-resistor combination has an identical total resistance, no visual differences of corona discharge could be distinguished between the pins and it can be assumed that the current is distributed equally over the four pin electrodes.

4.1.2 Gas stream preparation

Figure 4.1 shows that two gas streams are controlled by mass flow controllers (MFC) (Brooks Instrument BV). Dry air (Alphagas 1, Air Liquide, < 3 ppm$_v$ H$_2$O) is humidified by bubbling through a temperature controlled water column. Simultaneously, VOC are dosed to a sidestream which is mixed downstream with the first clean (dry or humidified) air stream in a mixing chamber. The two gas stream preparation techniques to achieve this sub-ppm$_v$ VOC loaded gas streams are by means of bubbling or capillary diffusion.

Bubbling systems are based on gas and liquid partitioning. While gas bubbles move through the liquid pollutant phase, there is a VOC mass transfer to the gas phase. The VOC mass flux is mainly determined by vapour pressure (depending on temperature), but also the size of the bubbles or bubble residence time.

Capillary diffusion systems are based on dynamic VOC diffusion from a headspace reservoir to a gas stream. Therefore a T-section is installed in the side-stream and connected with a VOC reservoir by means of a capillary. Downstream the T-section a resistance is inserted to reduce the influence of fluctuations in atmospheric pressure on the diffusion process. The mass flux can be calculated as:

$$m_f = DM \frac{P_t}{RT} \frac{A}{l} \ln \frac{P_t}{P_t - P_s} \qquad (4.1)$$

With VOC mass flux m_f (g s^{-1}), VOC gas diffusion coefficient D (m² s^{-1}), molar VOC mass (g mol^{-1}), pressure at capillary P_t (kPa), universal gas constant R (8314 10^{-6} m³ kPa mol^{-1} K^{-1}), temperature T (K), cross-section A (m²), capillary length l (m), VOC vapour pressure P_s at temperature T (kPa).

4.1.3 Chemical analytical techniques

4.1.3.1   Volatile organic compounds

Since inlet VOC concentration are of sub-ppm$_v$ level, sampling preconcentration is necessary in order to obtain accurate and reproducible results. Next, the sampling technique has to be insensitive for ozone. Xiong et al. (2004) did not detect ozone when a 100 μm polydimethylsiloxane (PDMS) fiber was exposed to high concentrations of ozone (> 100 ppm$_v$), indicating that the coating is not efficient in extracting ozone. They also proved that the absorption capacity of the PDMS 100 μm SPME coating was not affected by repeated exposure to ozone and oxygen. Therefore, solid-phase microextraction is used for sampling in and outlet gas stream. As discussed in Chapter 3, ASPDE is developed as a more sensitive sampling technique. However, due to the very recent character of ASPDE (published results mid-2007) and the sufficient sensitivity of SPME for our measurements (inlet concentration typically a factor 10 higher than real-life indoor air concentrations), analytical measurements have mainly been done using SPME. Based on experiments reported in Chapter 3 it can be highly recommended to use ASPDE for sub-ppm$_v$ measurements in future research.

Temperature has an important effect on both SPME and ASPDE sampling procedure. Since indoor air temperature strongly fluctuates and the plasma reactor effluent temperature might increase due to thermal heating effect of NTPs,… a temperature correction is necessary.

Therefore, two relevant indoor air pollutants (toluene and limonene) were selected to study the influence of temperature on the SPME sampling technique.

Multiple two-phase batch systems having identical headspace concentrations were prepared and sampled. These systems were made at different temperatures being 10, 25, 30 and 40°C. The Henry's law states that at a constant temperature, the amount of a given gas dissolved in water is directly proportional to the partial pressure of that gas in equilibrium with that water volume. Based on Henry's data for the different temperatures, it can be calculated what amount of VOC has to be injected to obtain a similar VOC headspace concentration in every batch system. Henry's data for toluene and limonene were found in literature (Gorgenyi et al., 2006) or determined experimentally. Sampling of identical concentrations at different temperature indicated that the sorbed mass is indeed strongly influenced by temperature. For 1 ppm_v, toluene measurements average peak area (n=3) at 10°C was 41.7 ± 0.36 a.u. while this was 9.25 ± 0.50 a.u. at 40 °C. The same phenomena occurred for d-limonene. This phenomenon can be explained by a change in VOC distribution constant K as result of temperature change from T_0 to T;

$$ K = K_0 e^{\frac{-\Delta H}{R}\left(\frac{1}{T}-\frac{1}{T_0}\right)} $$

(4.2)

where K_0 is the distribution constant when both fiber and sample are at temperature T_0 (in K); ΔH is the molar change in enthalpy of analyte when it moves from sample to fiber polymer; and R is the gas constant.

Based on these experimental results, a correction equation could be calculated. Therefore, as well during SPME as for ASPDE measurements, temperature was consistently recorded in order to recalculate the obtained experimental results.

4.1.3.2   Ozone measurement

To measure ozone outlet concentrations, a constant gas flow ($Q = 200$ mL min^{-1}) was pumped from a sample point at the outlet towards the inlet of the Anseros ozone analyzer equipped with Picolog Data Acquisition software. A low pressure mercury vapor lamp provides a monochromatic source for 253.7 nm radiation. This UV wavelength is absorbed by ozone molecules. The principle of measurements is based on Lamber-Beer law. This law states there is a logarithmic dependence between light transmission through a UV measurement cuvet containing ozone and its corresponding concentration.

4.1.3.3   Nitrogen oxide measurement

NO_x concentrations were measured by a Chemiluminescence NO-NO_2-NO_x Analyzer (Model 42C, Environmental Instruments, Inc., Franklin). These measurements are based on the principle that nitric oxides (NO) and ozone (O_3) react to produce intermediates having a characteristic luminescence with an intensity linearly proportional to the NO concentration. NO_2 in the sample is converted to NO by a molybdene catalyst in order to conduct chemiluminescence measurements.

4.2 Plasma characterization

NTPs can be characterized by their voltage-current characteristics. Depending on reactor type, electrode configuration, temperature, humidity,… a typical electric field strength, thus applied voltages, is necessary to obtain a certain charge transfer (current) between two electrodes. Next to voltage-current relation, also ozone production is often used to characterize NTPs. This molecule results from recombination reactions of atomic oxygen generated in non-thermal plasmas. Oxygen radicals are produced by dissociation of molecular oxygen after impact with accelerated electrons.

$$e^- + O_2 \rightarrow e^- + O^. + O^. \tag{4.3}$$

Secondly, a substantial part of the atomic oxygen formed in air discharges results from processes with excited molecular states of nitrogen ($N_2(A^3\Sigma)$ and $N_2(B^3P)$) (De Souza and Touzeau, 1983)). Atomic oxygen is a strong oxidizer, but its stability is very limited, having a lifetime at atmospheric pressure of typically only a few microseconds (Oda et al., 2006). Ozone is formed by a three-body collision by the following reactions:

$$O^. + O_2 + M \rightarrow O_3 + M \tag{4.4}$$

In air, M can be either molecular oxygen or molecular nitrogen (Devins, 1956). It can be concluded that ozone is a good indicator of the plasma reactivity since its occurrence can be correlated with reactive species concentrations in the NTP.

4.2.1 Influence of the discharge polarity

Corona discharges can be generated in both positive or negative configuration (Chapter 2.1.2). In this section results are represented using 4-pins-to-mesh reactors operated with 10 L min^{-1} of dry and clean air, both corona polarities were researched. Figure 4.2 shows that the positive corona discharge is characterized by higher currents at the same applied voltage compared with negative coronas.
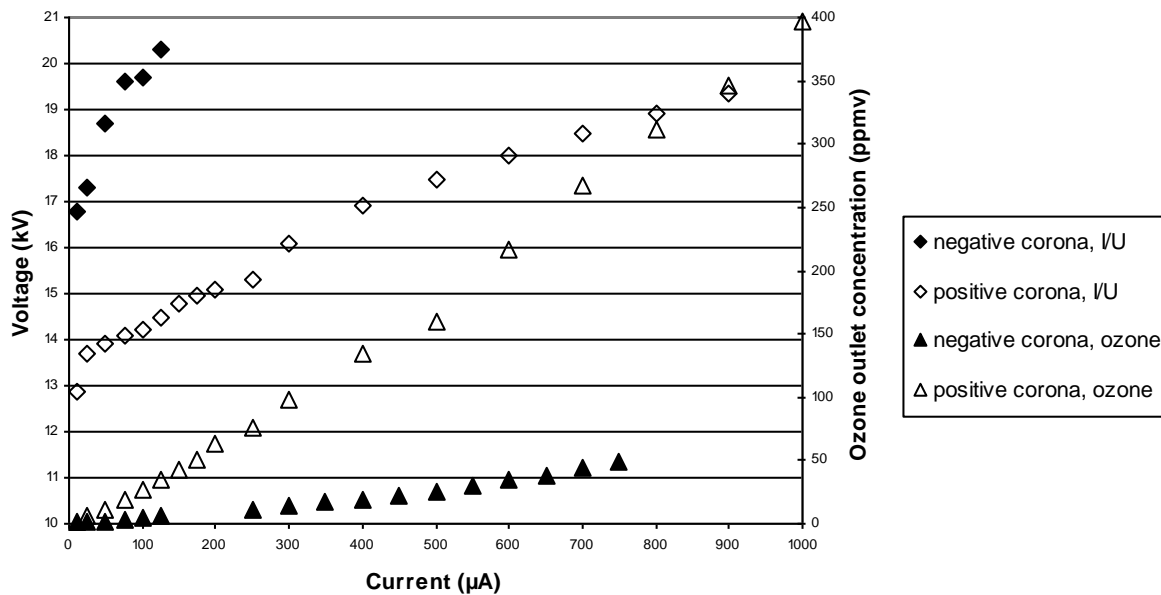
Figure 4.2 Voltage-current charactistics and ozone outlet concentration of both positive and negative corona 4-pins-to-mesh corona discharge (2 reactors in series) (Q= 10 L min^{-1}, P=101.32 kPa, T= 298.15 K, dry air)

Indeed, measured currents of the plasma reactors operated at both positive and negative polarity, are 600 µA and 50 µA respectively, when the applied voltage is 18 kV. It can be stated that positive corona discharges are 12 times more efficient in generating accelerated electrons and ions and by consequence result into the generation of an increased amount of reactive plasma species. This is reflected in the corresponding ozone production rates of both plasma configurations. For a current of 500 µA generated in a gas flow rate of 10 L min^{-1}, corresponding ozone outlet concentrations are 160 ppm$_v$ and 26 ppm$_v$ respectively, for positive and negative 4-pins-to-mesh corona discharge. A better way to compare the ozone production efficiency of both reactor polarities, is by using the parameter energy density which can be defined as the applied electric power (W) divided by the gas flow rate (m³ h^{-1}). Using this energy density parameter, it could be confirmed again that the positive polarity is most promising for the 4-pins-to-corona reactor. Indeed, for an energy density of 50 J L^{-1}, ozone concentrations for positive and negative corona were 224 and 21 ppm$_v$ respectively. Similar observations for corona discharges were obtained by Cooray and Rahman (2005),

again proving that polarity strongly influences O_3 formation. In the applied positive corona mode, electrons are concentrated as streamers in regions of high potential energy. In these streamers, electron concentrations are denser and they are accelerated to higher energies. Therefore, further experimental work has been done in DC positive mode.

To confirm that operation in DC positive mode using the 4-pins-to-mesh reactor setup, results in the occurrence of a positive streamer mode, discharge current waveforms are recorded with an oscilloscope. Repetitive current spikes are registrated which are indicative for a streamer discharge. These streamers are generated very fast (microsecond time-scale), therefore the visual aspect of the discharge is that of a luminous plasma column completely filling the inter-electrode space.
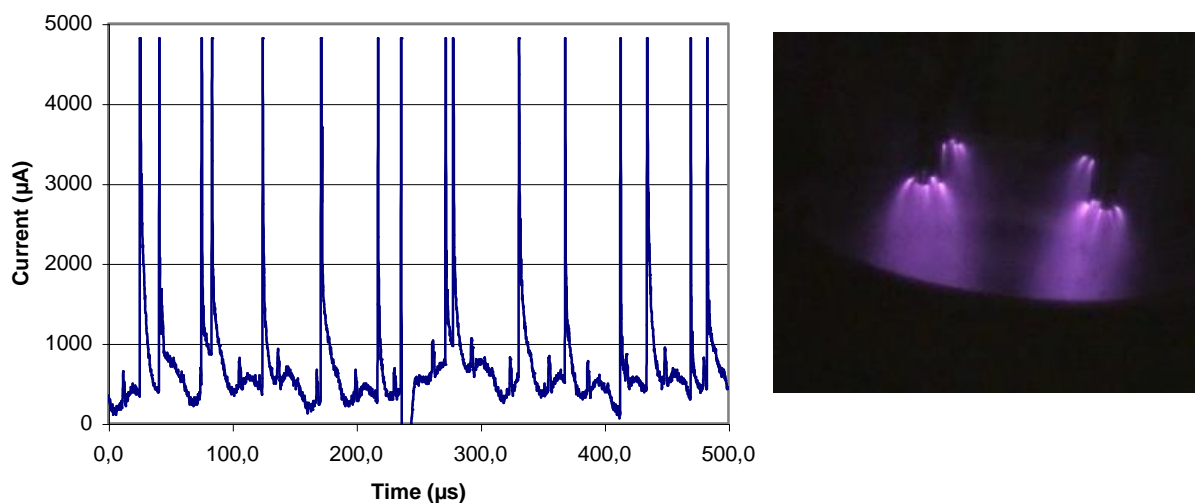
Figure 4.3. Left; Current (µA) waveform as function of DC positive corona operation time (µs) showing repetitive current spikes, Right; Picture of 4-pins-to-mesh DC positive corona discharge (Q= 10 L min^{-1}, P=101.32 kPa, T= 298.15 K, dry air)

4.2.2 Influence of electrode type and configuration

4.2.2.1   Electrode selection

Pin electrode

Four home-made crenallated pin electrodes are mounted onto a support, the resulting discharge connects to typically 8 anode spots for each pin. No further pin electrode adaptations have been done since this configuration was optimized by Morent et al. (2004).

Mesh electrode

The 4-pins-to-mesh reactor has been investigated using six ad random selected mesh electrode types (see Figure 4.4). Figure 4.4 represents the influence of mesh type on ozone outlet concentrations for the positive corona discharge.
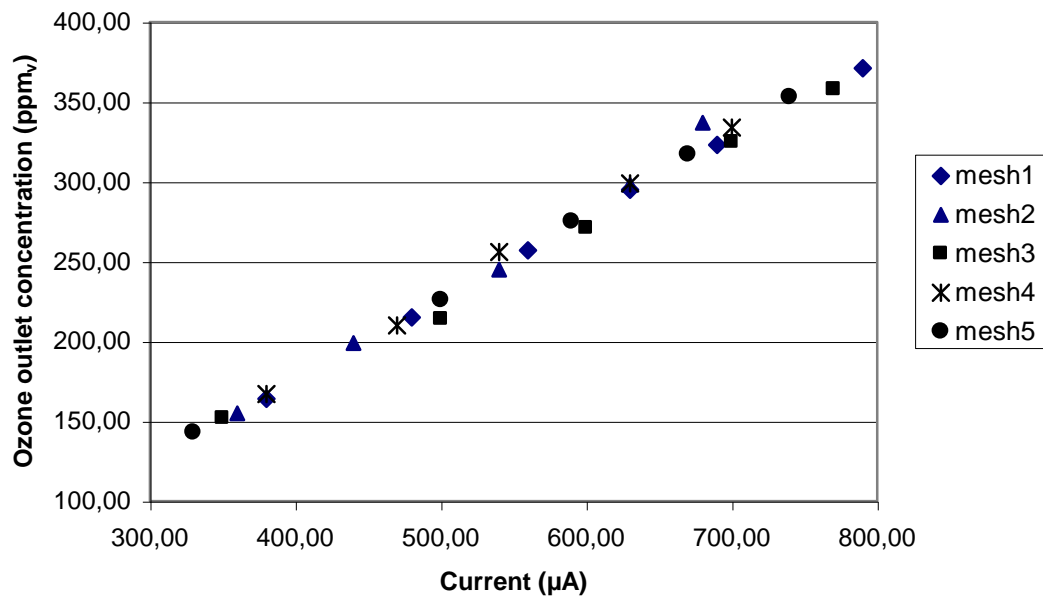
Name	Grid size (mm)	Thickness (mm)
Mesh1	1,49	0,63
Mesh2	0,80	0,32
Mesh3	0,104	0,065
Mesh4	0,025	0,025
Mesh5	0,51	0,28

Figure 4.4   Influence of mesh type (anode) on ozone outlet concentration as function of plasma energy density (J L^{-1}) (Q= 10 L min^{-1}, P=10.132 kPa, T=298 K)

From these measurements it can be concluded that no differences in ozone production can be detected in function of current (µA). This behaviour is expected since it is the mainly the sharp curvature of the electrode that determines the strength of the local electric field, and thus the total plasma oxidative strength (concentrations of accelerated electrons, ions, radicals, radiation, etc.). In further experimental work, mesh 5 was used as the anode electrode.

4.2.2.2 Effect of discharge gap

The discharge gap has to be selected in such a way that high energetic electrons (and by consequence highest concentrations of ion, charged species and radicals) are produced most optimally. Secondly, the plasma filling factor should be maximized; this factor is calculated by dividing the plasma zone volume by the total reactor volume. The plasma zone volume is a function of the reactor diameter, electrode distance, pin-to-pin distance, pin configuration, etc. When the plasma filling factor is high, the polluted gas effectively has to pass through the reactive plasma discharge and plasma residence times will be adequate for VOC abatement purposes. Finally, the gap distance has to be selected in such a way that the plasma has a high stability, while no transition of corona to spark discharge occurs.

The effect of discharge-gap was varied between 12 and 24 mm and the effect of this parameter was investigated by measuring voltage-current characteristics.
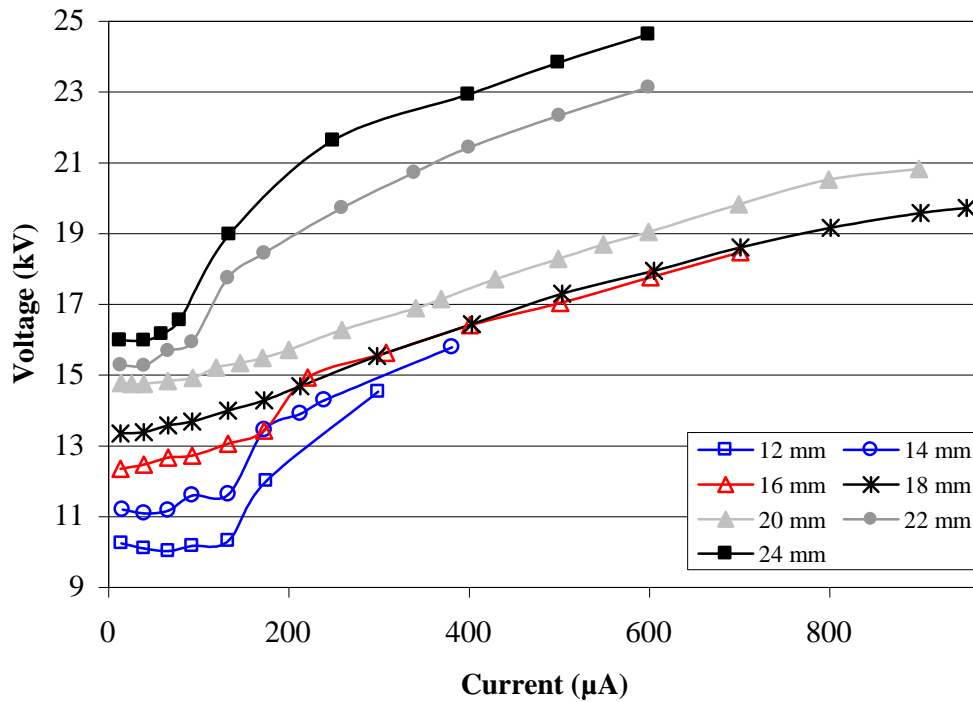
Figure 4.5 Effect of discharge gap on voltage (kV) – current (µA) characteristic of 4-pins-to-mesh DC positive corona discharge (dry air, Q= 10.8 L min^{-1}, C_{VOC} = 0 ppm$_v$, T = 295 K, P= 1.013 10^5 Pa)

The maximum current can be considered as a measure of the plasma discharge stability. Measurements revealed that for small discharge gaps the plasma is less stable and sparks often occurred. This is also reflected by a maximum current of only 300 µA. With increasing discharge gap, the maximum current raises above 900 µA for both interelectrode distances of 18 and 20 mm. However, further increase of the discharge gap resulted in a decreased stability.

Despite the effects of changing electrode distance on the voltage/current characteristics, little influence on the ozone production was observed as a function of current density.

It can be concluded that the reactivity of the NTP is not significantly influenced by interelectrode distance, which makes the filling factor and stability the main selection criteria for selecting the optimal interelectrode distance. Based on these findings, a 20 mm interelectrode distance has been selected to conduct further experiments.

4.2.3 Effect of gas flow rate

Experiments revealed that the gas flow rate has an effect on voltage-current characteristics. Figure 4.6 proves that for a constant applied voltage higher currents are measured with increasing gas flow rates.
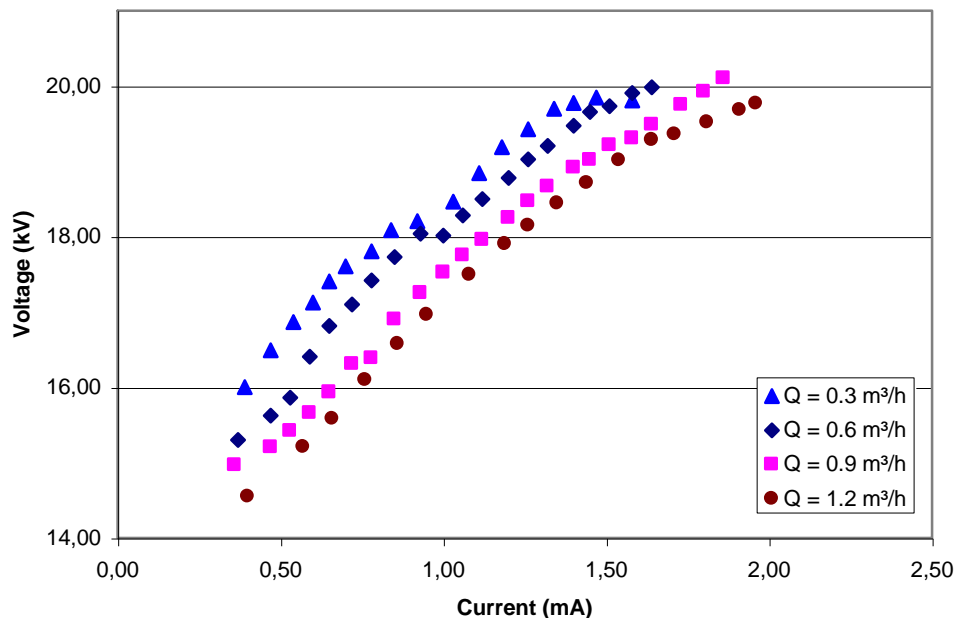
Figure 4.6 Effect of gas flow rate on voltage (kV) – current (mA) characteristics for DC positive DC corona discharge (two modules, dry air, Q= 10.8 L min^{-1}, C_{VOC} = 0 ppm$_v$, T = 295 K, P= 1.013 10^5 Pa)

Indeed, for a voltage of 18 kV (corresponding reduced electric field of 36 Td) a current of 780 μA, 930 μA, 1030 μA and 1200 μA is measured for gas flow rates of 5 L min^{-1}, 10 L min^{-1}, 15 L min^{-1} and 20 L min^{-1}, respectively. A possible explanation for this phenomenon is a change in gas composition at different plasma gas residence times. Indeed, experiments revealed that for a same voltage, higher ozone outlet concentrations are measured for decreasing gas flow rates. Experiments revealed that in the case of an applied voltage of 18 kV, ozone outlet concentrations were 553 ppm$_v$, 364 ppm$_v$, 300 ppm$_v$ and 265 ppm$_v$ for corresponding gas flow rates of 5 L min^{-1}, 10 L min^{-1}, 15 L min^{-1} and 20 L min^{-1}, respectively. Ozone outlet concentrations are lower for higher gas flow rates merely due to a dilution

effect, but for a same energy density indentical ozone outlet concentrations are measured. Figure 4.7 also indicates that the ozone outlet concentration as function of energy density is identical when the plasma modules are used separately or in series.
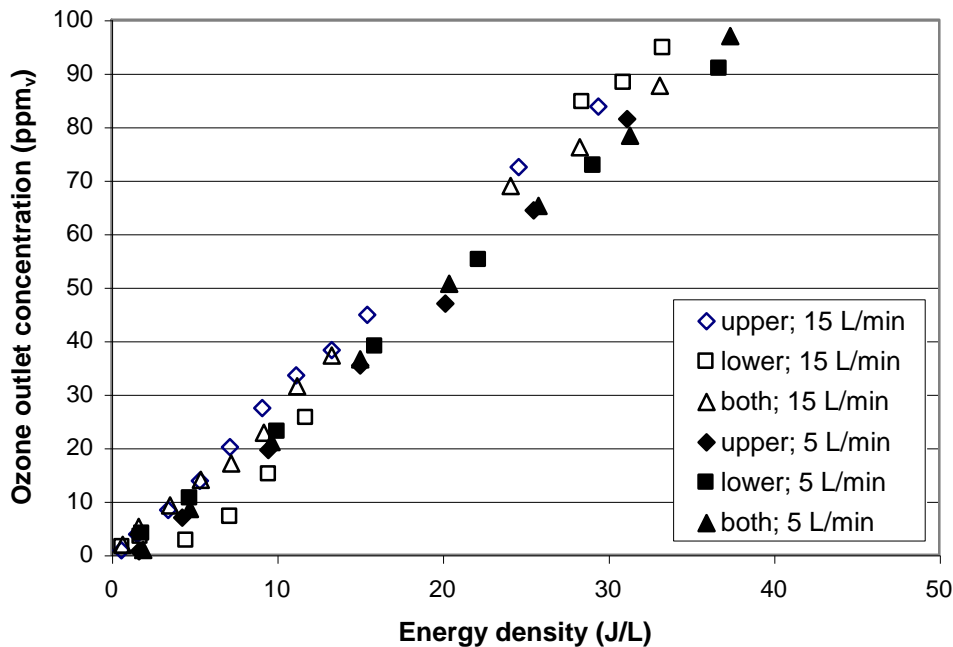
Figure 4.7 **Effect of gas flow rate (L min^{-1}) on the ozone outlet concentration (ppm$_v$) as function of the energy density (J L^{-1}) (dry air, Q= 10.8 L min^{-1}, C$_{VOC}$ = 0 ppm$_v$, T = 295 K, P= 1.013 10^5 Pa)**

4.2.4 Effect of air humidity

Indoor environments have variable humidity levels: Maki and Aoki (2006) reported that relative humidities typically range between 38% and 78% (T = 298 K) in concrete building rooms. To investigate the impact of the fluctuating air humidity, its effect on the discharge characteristics was examined. Figure 4.8 illustrates the influence of humidity on the plasma characteristics. With increasing humidity, lower currents are measured for a given voltage. For an applied voltage of 18.4 kV, a current of 0.6 mA is measured in dry air, while this is only 0.3 mA for 60% RH. Fouad and Elhazek (1995) concluded that for corona discharges, the electron attachment coefficient, η_h, is function of both the field strength and water vapor

content of the gas mixture. For higher RH, an increased attachment coefficient results in a shift of the ionization equilibrium leading to reduced electron densities.
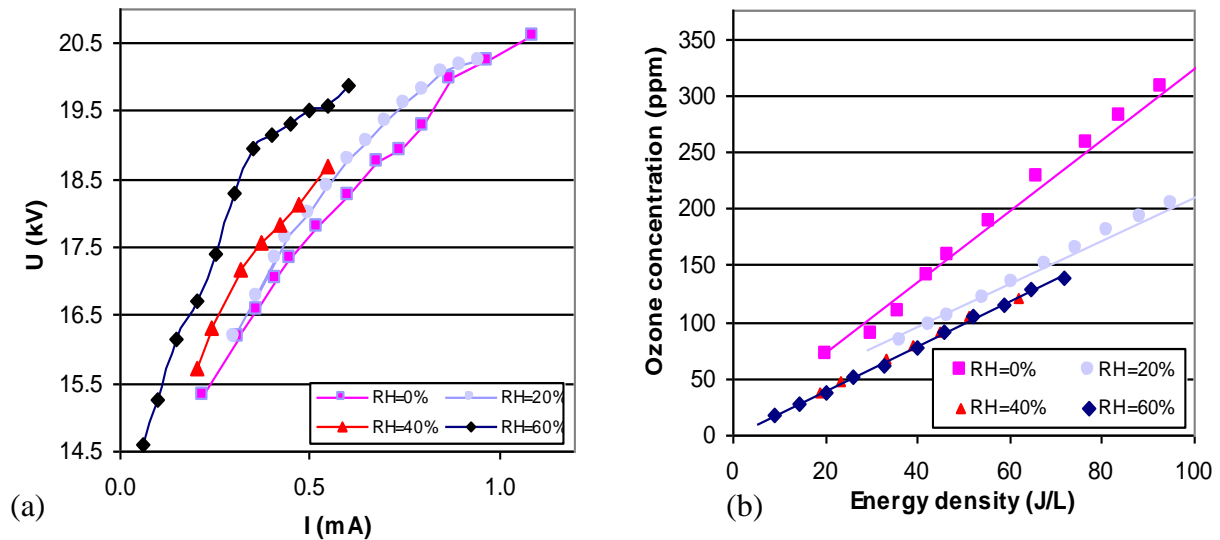
Figure 4.8 Effect of indoor air humidity on plasma characteristics: (a) voltage-current curves and (b) ozone outlet concentration (ppm$_v$) as function of energy density (J L^{-1}) (Q$_{air}$ = 10 L min^{-1}, p = 101.3 kPa, T = 298.15 K)

The effect of humidity is also reflected in changing ozone production rates. Measurements showed a decreasing ozone production at increased humidity levels (Figure 4.8). The ozone outlet concentration for an energy density of 40 J L^{-1} is 130 ppm$_v$ for dry air, while this decreased to 90 ppm$_v$ at 20% RH and 75 ppm$_v$ at 60% RH. A detailed study concerning ozone production by atmospheric glow discharge plasma, has also been conducted by Morent and Leys (2005). Chen and Wang (2005) modified existing ozone prediction models taking into account the water effect. The observed effects can be explained by a reaction between hydroxyl radicals and water molecules with oxygen radicals and ozone. Next, water affects the initial field strength, the mobility of charge carriers and the plasma composition.

4.3 Nitrogen oxide production by DC positive streamer discharge

NO_x concentrations formed by the corona discharge were measured using a nitrogen oxide measurement device as explained in section 4.1.3.3. The results are represented in Figure 4.9. In non-thermal plasma discharge, NO is mainly produced by reaction between air molecules (e.g. O_2, N_2) and atomic plasma species (e.g. O, N) or excited plasma species (e.g. N_2 ($\upsilon > 12$), $N_2^*(A_3\Sigma_u^+)$). The following mechanisms are proposed by Gordiets et al. (1995);

$$N_2 (\upsilon > 12) + O_2 \rightarrow NO + N \tag{4.5}$$

Because of a fast reverse process as;

$$NO + N \rightarrow N_2 (\upsilon = 3, 4) + O \tag{4.6}$$

the NO concentration is actually controlled by reactions;

$$N + O_2 \rightarrow NO + O \tag{4.7}$$

$$N + O_w \rightarrow NO \tag{4.8}$$

where reaction (4.8) is the wall recombination of N and O atoms.

Also the following mechanism can be proposed for NTP NO production;

$$N_2^*(A_3\Sigma_u^+) + O \rightarrow NO + N^*(^2D) \tag{4.9}$$

and

$$N^*(^2D) + O_2 \rightarrow NO + O \tag{4.10}$$

Ionikh et al. (2006) reported that the NO concentration is completely determined by oxygen radicals. Outlet concentrations of nitric oxide (NO) were below limit of detection (<10 ppb_v). This can be explained by an efficient oxidation of NO in the presence of excess O_3, $OH^\cdot$ and $O^\cdot$ (Table 4.1). The conversion of NO_2 into NO proves to have a slower chemical reaction kinetics. This trend is consistent with other experimental studies using non-thermal plasma discharges (Cooray and Rahman, 2005).

Table 4.1 Reactions and reaction rate constant for NO_x with reactive plasma species ($O^\cdot$, $OH^\cdot$, O_3) at standard conditions (T = 298.15K, P = 101.3 kPa)

a

reaction	k (cm³.molecule^{-1}.s^{-1})
$NO + O^\cdot \rightarrow NO_2$	$3.01\ 10^{-11}$
$NO_2 + O^\cdot \rightarrow NO + O_2$	$9.30\ 10^{-12}$
$NO + O_3 \rightarrow NO_2 + O_2$	$1.65\ 10^{-14}$
$NO_2 + O_3 \rightarrow NO + 2O_2$	$1.00\ 10^{-18}$
$NO + OH^\cdot \rightarrow HNO_2$	$3.30\ 10^{-11}$
$HNO_2 + OH^\cdot \rightarrow H_2O + NO_2$	$6.00\ 10^{-12}$
$NO_2 + OH^\cdot \rightarrow HO_2 + NO$	$7.70\ 10^{-16}$

b

reaction	k (cm³.molecule^{-1}.s^{-1})
$NO_2 + O^\cdot \rightarrow NO_3$	$2.16\ 10^{-11}$
$NO_3 + O^\cdot \rightarrow NO_2 + O_2$	$1.70\ 10^{-11}$
$NO_2 + O_3 \rightarrow NO_3 + O_2$	$7.80\ 10^{-17}$
$NO_3 + O_3 \rightarrow NO_3 + O_2$	$1.00\ 10^{-17}$

Figure 4.9 shows that the NO_2 production linearly increases with applied energy density in dry air. It can also be concluded that increased humidity results in decreased NO_2 outlet concentrations.
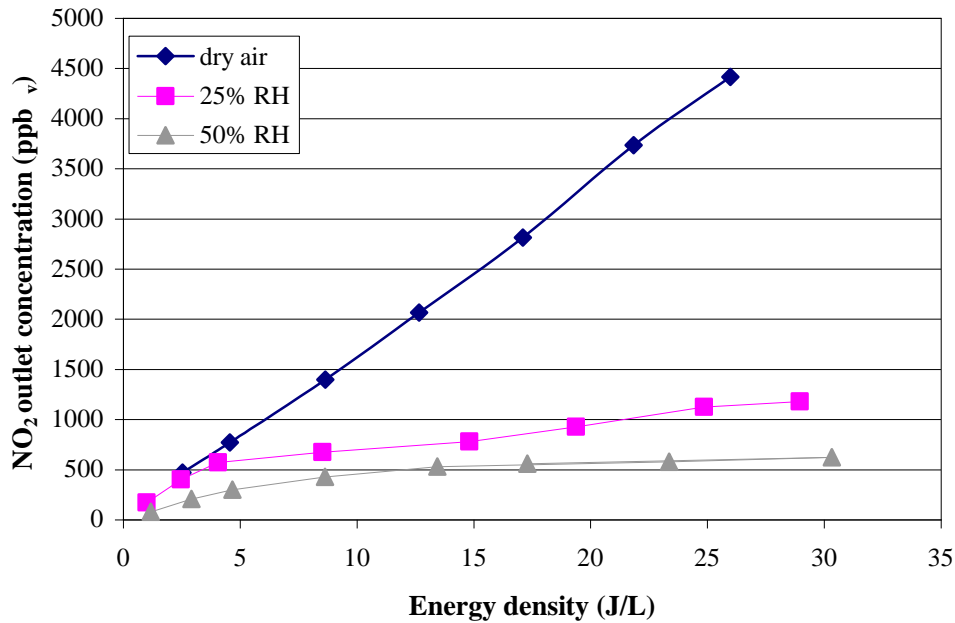
Figure 4.9 **NO$_2$ production as function of energy density (J L^{-1}) for three relative humidities; dry air, 25 and 50% RH (T=298K) (clean air , Q$_{air}$ = 10.8 L min^{-1}, P = 101.3 kPa, T = 298 K)**

Figure 4.9 confirms that for an energy density of 10 J L^{-1}, a NO$_2$ concentration of 1500 ppb$_v$ was measured in dry air. At a relative humidity of 25% and 50%, NO$_x$ outlet concentrations decreased to 800 ppb$_v$ and 500 ppb$_v$, respectively. This effect is even more pronounced at higher energy densities: for an energy density of 25 J L^{-1}, NO$_2$ outlet concentrations are 4210 ppb$_v$ and 1130 ppb$_v$ for 0 and 25 % RH (Figure 4.9).

The reduction of NO$_2$ outlet concentrations in humid gas streams can be explained in two ways. First, water affects the field strength, the mobility of charge carriers and the plasma composition. Due to enhanced electron attachment processes, the electron concentration and mean electron energy decreases for increased humidities, resulting in a reduced total production of oxygen radicals. Secondly, the production of hydroxyl radicals results in a more efficient reaction with NO$_2$ molecules (Table 4.1).

Experiments prove that the presence of toluene in the gas stream have an effect on the NO_2 outlet concentration. This effect is only observed at higher energy densities (>10 $J.L^{-1}$). In dry air the NO_2 outlet concentration was 4400 ppb_v at an energy density of 25 J L^{-1}, while this was 3600 ppb_v in the presence of 0.5 ppm_v toluene. This can be explained by a competition for atomic oxygen in the presence of toluene or by reaction between NO_x and toluene, both resulting in reduced NO_2 outlet concentrations.

4.4 Conclusions

This chapter discusses the experimental setup used during this PhD work. Since corona discharges have a proven potential for VOC abatement, a 4-pins-to-mesh plasma reactor was developed and characterized. The reactor configuration is constructed so that heterogeneous catalysts can be inserted. Corona discharges can be operated both in positive and negative mode. However, based on current-voltage characteristics and ozone production rates it was chosen to operate the discharge in the positive streamer regime.

In a second part, the influence of some physical and chemical parameters on the DC positive streamer discharge has been investigated. While the mesh type and size has no influence on the plasma properties, the discharge gap distance mainly influences the discharge stability. For an interelectrode distance of 12 mm, currents of 300 µA can be obtained prior to transition to spark regime. This maximum current is 900 µA when using a 20 mm gap distance. Similar experiments have been done to investigate the effect of gas flow rate and humidity. Particularly humidity significantly affects plasma discharge characteristics. For an applied voltage of 18.4 kV, a current of 0.6 mA is measured in dry air, while this is only 0.3 mA for 60% RH.

Finally, NO_x production by the plasma discharge was investigated. It is concluded that NO_2 concentrations are low and strongly influenced by humidity. For an energy density of 10 J L^{-1} NO_2 levels proved to be 1500 ppb_v and 500 ppb_v for relative humidities of 0% and 50%, respectively.

Chapter 5

Abatement and degradation pathways of toluene in indoor air by positive corona discharge

5.1 Introduction

In this chapter it is investigated whether the earlier discussed corona discharge is suitable for the abatement of low levels of toluene from indoor air. Toluene was selected as test compound since it is, together with benzene, ethylbenzene and o-xylene, grouped as BTEX compounds which are the major group found in indoor environments for different countries (Van Winkle and Scheff, 2001). Average indoor air concentrations of toluene vary between 5-50 ppb_v (Tillborgs et al., 2005), with maximum concentrations up to 9 ppm_v (AERIAS, 2006). To our knowledge, little is known about chemical reactions of toluene in a corona discharge or in non-thermal plasma discharges in general. Reactions are numerous due to the presence of several types of reactive species in the plasma zone. The focus is to identify reaction products, allowing a better understanding of the degradation pathway of toluene in a non-thermal plasma.

5.2 Materials and methods

5.2.1 Experimental setup – plasma reactor

The experimental setup is discussed in Section 4.1.1. A 4-pins-to-mesh electrode configuration was used to generate a positive DC streamer discharge. Two corona reactors were mounted in series during the experiments.

5.2.2 Chemicals

Abatement experiments were done using toluene as test compound. Toluene 99.5% was delivered from Aldrich (Steinheim, Germany). In Section 4.1.2. it is explained how the toluene loaded gas stream is prepared.

For the experimental determination of Kováts indices 3-methyl-4-nitrophenol, 4-methyl-2-nitrophenol, 5-methyl-2-nitrophenol were obtained from Aldrich (Steinheim, Germany), n-alkanes were delivered by Polyscience Corp (Niles, US).

5.2.3 Chemical analytical techniques

Inlet and outlet air samples were taken by solid-phase microextraction (SPME) (Chapter 3). The SPME device was supplied by Supelco equipped with a 57330-U SPME holder containing a plain hub fiber assembly.

Chemical analyses were carried out with an Agilent 6890 Series GC, equipped with a flame ionization detector (FID) and a HPCORE integration system. The FID detector (250 °C) was fed by 400 mL min^{-1} air and 40 mL min^{-1} hydrogen. The carrier gas was helium with a flow rate of 3 mL min^{-1}. A SPME inlet liner was installed and placed at a temperature of 200 °C. Separation was done on a 30 m x 0.53 mm cross linked methyl siloxane capillary column with a film thickness of 5.0 μm (HP-1) (HP, USA). Analyses were carried out isothermally (140°C). Sampling with a 100 μm PDMS SPME fiber (Supelco) combined with GC-FID, resulted in a limit of detection of 67 ppb$_v$.

Analysis of degradation products was done in two ways. First, for the identification of degradation products, a Trace DSQ GC-MS was used (Thermo Finnigan). The temperature program started at 35 °C and increased to 40 °C with a rate of 1.0 °C min^{-1}. Next, the temperature was increased to 60 °C at 2 °C min^{-1}, followed by an increase to 160 °C at 8 °C min^{-1}. Finally, the oven temperature reached 220 °C with a temperature increase rate of 12 °C min^{-1}. This final oven temperature was maintained during 10 min. A SPME liner was installed at the inlet. The injector had a constant temperature of 200 °C and was used in a splitless mode. The injector was connected to a capillary column VARIAN VF-1ms (FactorFour^{TM} GC columns), 30 m length, diameter 0.25 mm and coating thickness of 1 μm. Ionisation was

achieved by electron impact (70 eV), detection of fragments by an electron multiplier (Trace DSQ Thermo Finnigan). For the identification of the unknown compounds obtained mass spectra the NIST v.2.0. databank (NIST/EPA/NIH Mass Spectral Library) was used. Secondly, confirmation of identified compounds was done by determination of Kováts indices on a GC-FID (4890) equipped with a capillary HP-5 column (HP, USA), these indices were determined isothermally at 35, 90 or 170 °C. The Kováts retention index (KI) has received wide acceptance and is defined as (Girard, 1996);

$$KI = 100\,z + 100\,\frac{\ln t_{R(i)} - \ln t_{R(z)}}{\ln t_{R(z+1)} - \ln t_{R(z)}} \qquad (5.1)$$

Where $t_{R(z)} < t_{R(i)} < t_{R(z+1)}$, $t_{R(i)}$ is the retention time of a component I, and $t_{R(z)}$ and $t_{R(z+1)}$ are the retention times of n-alkanes with z and z+1 carbon atoms.

5.3 Results and discussion

5.3.1 Toluene oxidation experiments

A gas stream containing 0.5 ppm$_v$ toluene was treated by the non-thermal plasma reactor. Figure 5.1 shows the removal efficiency (%) of toluene for a constant flow rate of 10 L min^{-1}. Experiments were done at room temperature, atmospheric pressure and for different humidities (dry air, 26% and 50% RH). The detection limit of the 100 μm PDMS-SPME combined with GC-FID measurements was 67 ppb$_v$. Therefore, the maximum toluene removal efficiency that can be measured correctly is limited to 87%. Ozone exposure did not result in visual deterioration and change of sorption capability of the PDMS coating during our experiments.
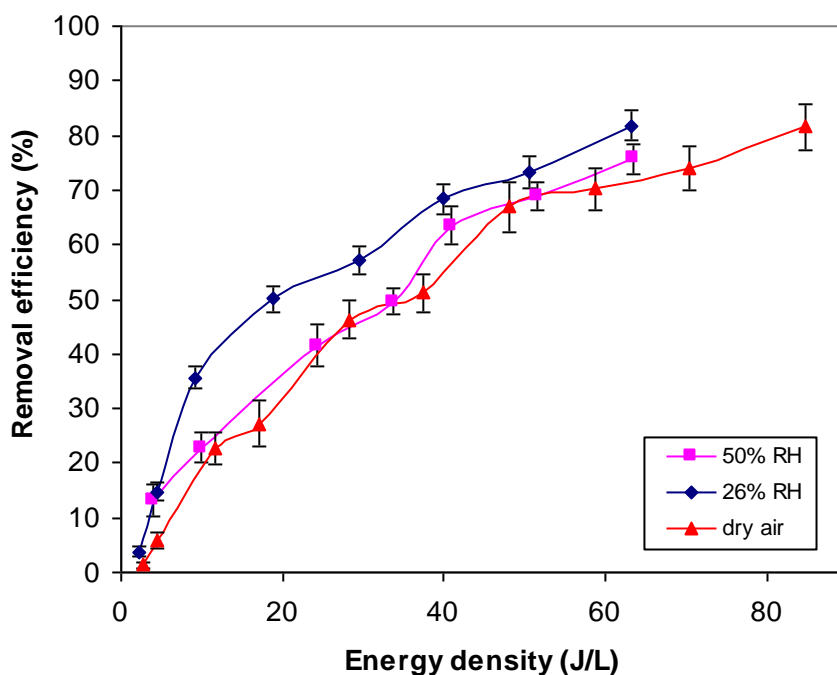
Figure 5.1 Removal efficiency (%) of 0.5 ppm$_v$ toluene by DC positive corona discharge and the effect of humidity (0, 26 and 50% RH) (Q$_{air}$=10 L min^{-1}, p = 101.3 kPa, T = 298 K) (n = 3)

Toluene degradation can be the result of direct electron impact dissociation. Since toluene concentrations are rather low, the probability for direct ionization, however, is very small. Collisions of accelerated electrons with other gas molecules such as N_2, O_2 or H_2O are more probable, resulting in active species such as atomic oxygen or hydroxyl radicals. The most powerful toluene oxidizing species are in fact the hydroxyl radicals (k = 5.7 x 10^{-12} molecule cm^{-3} s^{-1}) followed by atomic oxygen (k = 7.6 x 10^{-14} molecule cm^{-3} s^{-1}) (NIST, 2007). The reaction rate is smaller for ozone (k = 3.9 x 10^{-22} molecule cm^{-3} s^{-1}), resulting in a minor role in the oxidation kinetics of toluene (NIST, 2007). Next, excited nitrogen loses its excess of energy by emitting UV light which could also result in photolysis (Duten et al., 2002).

Humidity clearly has a significant effect on removal efficiency of toluene by plasma. In dry air 46% toluene is oxidized at 28.8 J L^{-1}, while this is 57% when the gas has a RH of 26%. Water molecules dissociate to form H$^{\cdot}$ and OH$^{\cdot}$ by collision with electrons or reaction with O$^{\cdot}$,

$O(^1D)$. From the reaction kinetics of toluene with available oxidizing species, it can be concluded that OH induced degradation is important (NIST, 2007). Ono and Oda (2002) explain that for low water concentrations (< 1% RH) the OH density is proportional to water concentration. This positive effect, however, is counteracted for higher humidities. For a constant applied voltage, the water concentration strongly influences the hydroxyl radical concentrations. Hydroxyl radical production saturates or diminishes as humidity increases. In the presence of higher water concentrations, increased plasma attachment processes result in a reduced hydroxyl radical production. It can be concluded that two opposite phenomena are seen: water partially dissociates in the plasma, producing reactive species, but humidity also negatively influences the plasma characteristics.

The concentration of all these reactive species (OH·, O·, O_3, charged species) can be linked with the energy density of the plasma. The relationship between energy density and removal efficiency can be expressed as (Vertriest et al., 2003);

$$\frac{N_{out}}{N_{in}} = e^{\left(-\frac{\varepsilon}{\varepsilon_o}\right)} \tag{5.2}$$

With N_{in} (N_{out}) the density of toluene molecules in inlet (outlet) gas stream (molecule cm^{-3}), the energy density ε (J L^{-1}) and the characteristic energy ε_o (J L^{-1}). This parameter ε_o is often used to express the energy efficiency of the used discharge reactor and is defined as the energy necessary to reduce the concentration of pollutants by a factor e. The characteristic energy for the oxidation of 0.5 ppm$_v$ toluene in dry air is 49.5 J L^{-1}. For 26% RH, the characteristic energy ε_o is 35 J L^{-1}, while it was 49 J L^{-1} for 60% RH.

Mok et al. (2002) found that alkenes and substituted alkenes have higher decomposition rates than aromatics and substituted alkanes in pulsed corona and dielectric barrier discharges. Vertriest et al. (2003) tested several VOCs, they proved that toluene was the most difficult to

remove with a negative DC glow discharge (e.g. $\varepsilon_{o,toluene}$ = 160 J L^{-1} > $\varepsilon_{o,octane}$ = 125 J L^{-1} > $\varepsilon_{o,1\text{-}octene}$ = 30 J L^{-1}). Since the presented data indicate that toluene can be efficiently removed, it may be expected that the positive streamer discharge reactor is able to oxidize several indoor VOCs in a rather efficient way.

5.3.2 Intermediates: toluene degradation products

In order to obtain measurable concentrations of degradation products, higher toluene inlet concentrations of 150 ppm$_v$ were used. The plasma reactor effluent of the oxidized toluene-air gas stream is analyzed in order to identify degradation products. It is known that non-thermal plasma has high potential in air cleaning technology, but a disadvantage could be that in some cases unwanted degradation products are formed which could be more harmful than the original VOC (Magureanu et al., 2005).

Identifying degradation products is done in order to understand reaction mechanism in a DC positive corona discharge.

Figure 5.2 shows that conversion of toluene into CO_2 is not complete at these inlet concentrations and partially oxidized intermediates can be formed. Analysis of the degradation products was done with SPME sampling combined with GC-MS analysis. Confirmation of identified products with a relative abundance of more then 10% was done on GC-FID by KI determination. Calculated and measured KI values of products identified by mass spectrometry are given in Table 5.1. For 3-methyl-4-nitrophenol, 4-methyl-2-nitrophenol and 5-methyl-2-nitrophenol, KI were not found in literature; they were determined experimentally.
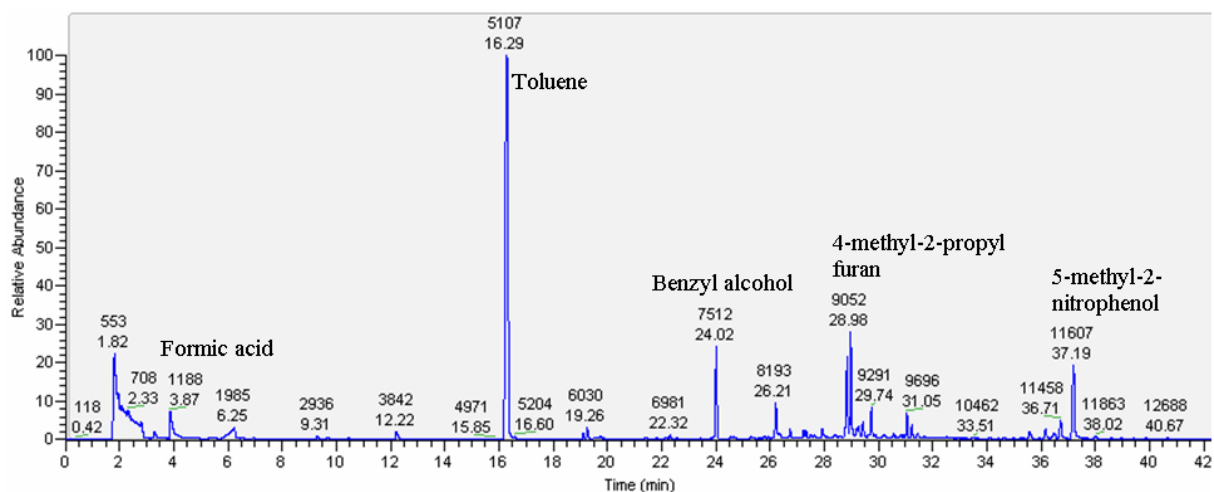
Figure 5.2   Chromatogram of GC/MS analysis for the identification of toluene degradation products (dry air (< 1% RH), Q = 10.8 L min^{-1}, C_{in} = 150 ± 1 ppm$_v$, ε= 54 J L^{-1}, P = 101.3 kPa)

Table 5.1   Most abundant oxidation products identified and confirmed by mass spectrometry and Kováts index determination (n = 3)

RT (min)	Compound	KI (-)$_{exp}$	KI (-)$_{lit}$	Reference
3.82	Formic acid	**582.0 ± 11.6**	**580.0**	(NIST, 2007)
24.00	Benzaldehyde	**960.8 ± 19.2**	**960.0**	Flavornet, 2006
26.21	Benzyl alcohol	**1023.6 ± 20.5**	**1039.0**	Flavornet, 2006
28.37	3-Methyl-4-nitrophenol	**1222.3 ± 24.4**	**1225.1**	This work
28.95	4-Methyl 2-propyl furan	**1236.5 ± 24.7**	**1241.0**	(NIST, 2007)
31.05	4-Methyl-2-nitrophenol	**1236.4 ± 24.7**	**1241.3**	This work
31.45	5-Methyl-2-nitrophenol	**1247.0 ± 24.9**	**1247.4**	This work
35.58	4-Nitrophenol	**1544.8 ± 30.9**	**1539.0**	(NIST, 2007)
38.20	2-Methyl-4,6-dinitrophenol	**1634.6 ± 32.7**	**1624.0**	(NIST, 2007)

Atkinson et al. (2000) showed that aromatic compounds react with OH radicals by two pathways: hydrogen atom abstraction and OH addition to the aromatic ring. This results in a complex oxidation mechanism of toluene via several pathways, producing either ring-retaining or ring-opening products Figure 5.3. (Pathways I through XII are illustrated in Figure 5.3).

Figure 5.3 Degradation pathway of toluene in non-thermal plasma discharge (Q_{air} = 10 L min^{-1}, P = 101.3 kPa, T = 298 K, 0% humidity). Compounds enclosed by full frame are identified and confirmed; compounds in dotted frame are tentatively identified.

5.3.2.1   Ring-retaining products after H atom abstraction

Benzaldehyde, benzoic acid and benzyl alcohol were identified in the outlet gas stream. An important pathway in toluene (I) oxidation, partially resulting in these degradation products, is a hydrogen abstraction from the methyl group leading to a benzyl radical (II) (d'Hennezel et al., 1998). In the non-thermal plasma, this H-abstraction could be the result of (a) direct electron impact, or (b) abstraction by hydroxyl radicals. The benzyl radical reacts with oxygen to form a benzylperoxy radical (III). The benzylperoxy radicals can couple to form a tetraoxide (IV). This intermediate can decompose according the Russell-mechanism to yield non-radical products: alcohols, ketones and singlet oxygen. The benzylperoxy radical can also react with a hydroperoxy radical to form a monoalkyltetroxide (V) that decomposes into benzaldehyde, molecular oxygen, and water. In the gas phase, Seuwen and Warneck (1996) proposed that the benzylperoxy radicals undergo self-reaction to form either benzaldehyde via a benzoxy radical or benzaldehyde and benzyl alcohol. Benzaldehyde oxidizes easily into benzoic acid.

Benzene-1-methyl-3-(phenylmethyl) (retention time (RT) = 36.49 min) was tentatively identified (not confirmed by KI) in the outlet gas stream (VI). The formation of this compound can be explained by benzyl radicals who can also react with an incoming toluene molecule, initiating a polymerization reaction. D'Hennezel et al. (1998) proved that during toluene oxidation, a methyl group attack with subsequent coupling could result in the production of o- and p-methyl-diphenyl-methane isomers and bibenzyl (VI).

5.3.2.2   Ring-opening products

During our measurements 4-methyl-propyl furan and formic acid were identified. These compounds indicate that the aromatic ring has been opened. The ring-opening pathways of the

toluene oxidation may proceed by a sequential addition of OH and O_2, resulting in hydroxycyclohexadienyl type peroxy radical (VII). Bartolotti and Edney (1995) wrote that in the atmosphere 85% of the time OH radical reactions with toluene lead to this intermediate. This unstable, reactive compound can form a peroxide bridged radical which is the precursor for both the carbonyl and the epoxide route. The dicarbonyl reaction route describes a ring opening via a series of peroxide-bicyclic intermediates (VIII) eventually forming α–dicarbonyls and conjugated α–dicarbonyls. Furanones (4-methyl-2-propyl furan) are proposed products of glyoxal and methyl glyoxal formed as primary products of the decomposition of the peroxide-bicyclic radical (Wagner et al., 2003).

Bartolotti and Edney (1995) described the epoxide route in which epoxides are the dominant reaction products during OH initiated oxidation of toluene. An epoxide (IX) (Figure 5.3) can be formed by addition of O_2 to the ring or by multi-step processes. This structure is unstable and undergoes further reactions. Based on analogies with less complex alkoxy radicals, the epoxide radical (IX) could undergo carbon-carbon scission and reaction with O_2. A first reaction pathway could be the scission of the 2,3-carbon bond in the presence of O_2, finally resulting in CHOCHO (X) and a reactive unsaturated epoxide dicarbonyl compound (XI). A second reaction pathway is the abstraction of H by O_2 producing an epoxide carbonyl ring compound (XII) which itself is subject to further oxidation reaction.

5.3.2.3 Ring retaining products after OH-addition

Another possible chemical pathway of toluene oxidation can be via an isomerisation and subsequent release of HO_2 to form cresol. This cresol route can explain partial conversion into nitro-aromatics by reaction with NO_2 and NO_3 (Hamilton et al., 2005). A detailed study on NO_x production in corona discharge has been discussed in Chapter 4.3. Reaction products of

NO_x and cresol were identified in the outlet gas stream; methyl-nitrophenols (3-methyl-4-nitrophenol, 4-methyl-2-nitrophenol, 5-methyl-2-nitrophenol), methyl-dinitrophenols (2-methyl-4,6-dinitrophenol) and others (4-nitrophenol) (Table 5.1).

5.4 Conclusions

Non-thermal plasma technology is proposed as a useful technology for indoor air purification. A DC positive corona is used to oxidize low toluene levels in gas streams. Humidity strongly influences the plasma characteristics, lower electron densities and ozone levels are measured when humidity increases. The removal of toluene is achievable with a characteristic energy density ε_o of 50 J L^{-1} ($C_{toluene}$ = 0.5 ppm_v, Q = 10 L min^{-1}). Removal efficiencies were higher for 26% relative humidity (ε_o = 35 J L^{-1}), compared with those at increased humidities (50% relative humidity, ε_o = 49 J L^{-1}). Degradation products are benzaldehyde, formic acid, nitrophenols, furans, and others. Hydroxyl radicals play a major role in the oxidation kinetics due to initiation by H-abstraction or OH-addition. Based on these by-products a toluene degradation mechanism can be proposed. Generally, it can be concluded that chemical pathways are similar to those in atmospheric chemistry, however, strongly accelerated.

Chapter 6

Efficient toluene abatement in indoor air by a plasma catalytic hybrid system

6.1 Introduction

Several conventional techniques are being used for off-gas treatment. However, for many applications, particularly for the removal of diluted indoor air concentrations, the non-thermal plasma (NTP) approach is likely to be more appropriate (Chapter 5). However, the efficiency of NTP can be improved in two ways: reducing power consumption and reducing the formation of undesired by-products ([a]Subrahmanyam et al., 2006). Reduction of size and energy cost are critical parameters in the design and development of indoor air purification technologies. Unwanted by-products of NTP processes are partially oxidized VOC, ozone and nitrogen oxides. Indeed, it was concluded in Section 4.3 that ozone and NO_2 can be detected in the outlet gas stream of the plasma reactor, and that ozone and NO_2 production increases linearly with the energy density, this relationship is also confirmed by Cooray and Rahman (2005).

These disadvantages may be resolved by combining plasma technology with heterogeneous catalysis. Heterogeneous plasma catalysis results in an increase in retention of the adsorbate molecules in the plasma zone which can lead to improved selectivity towards total oxidation (Roland et al., 2002). Sano et al. (2006) proved that atmospheric electric discharges emit radiation with wavelengths between 290 and 400 nm. This UV emission range lies within the absorption range of TiO_2 (Duten et al., 2002). IPC (In Plasma Catalysis) implies placing photocatalyst material into the plasma zone, e.g. semiconductors such as $SrTiO_3$, TiO_2, ZnO, ZnS and CdS can be used (Devahasdin, 2003). Next to UV triggered catalytic processes, the in-plasma catalyst can also be activated by adsorption of high-energy plasma species such as metastable N_2* (6.17 eV) ([c]Kim et al., 2005). Malik et al. (2005) wrote that plasma streamers might travel along the introduced additional surface, showing enhanced ionization compared to streamers in the gas space. Next, the synergetic effect may also be explained by the formation of short-living oxidizing species formed in the pores of the catalyst material

(Holzer, 2005). The introduction of catalysts may also shift the distribution of accelerated electrons towards higher energy levels, leading to a more oxidative plasma (Liu et al., 2002; Holzer, 2005).

Although a part of the energy dissipated in the plasma discharge is converted into heat, photons, etc., a significant part is used for the dissociation of oxygen molecules, resulting in ozone formation through recombination processes (Section 4.2). The oxidative capacity of these ozone molecules can be exploited by the introduction of an ozone degrading post-plasma catalyst (PPC). The decomposition of ozone into oxygen is a thermodynamically favored process. Nevertheless, ozone is thermally stable up to 523 K and a catalyst is necessary for decomposition at lower temperatures (Einaga et al., 2005). The synergetic effect of PPC is the result of two different phenomena: plasma physical chemistry and heterogeneous catalysis. At the plasma stage VOC are partially oxidized, while ozone is simultaneously generated and supplied to the post plasma zone. In the post plasma zone, both VOC adsorption and oxidation by newly formed active species occur on the catalyst. These active species result from the catalytic ozone decomposition with formation of molecular and highly-active atomic oxygen (Oh et al., 2005; Grossmannova et al., 2006). This does not only result in an increased energy efficiency, at the same time harmful ozone is removed from the outlet gas stream. Metal oxides are known to have these ozone decomposing properties. Noble metals like Pd or Pt, or oxides of transition metals such as Mn, Co, Ni and Ag could be used as ozone degrading catalyst. These compounds are often supported on materials such as γ-Al_2O_3, TiO_2, SiO_2, zeolites, activated carbon or on combinations of both (Heisig, 1997). Heisig (1997) found that combinations of metal oxides with various organic and inorganic additives are effective in enhancing the physical stability and activity of the catalysts. Sano et al. (2006) reported that ozone degrading catalysts often give better results than those obtained by heterogeneous photocatalysis during VOC oxidation experiments.

The purpose of this chapter is to optimize a positive corona reactor used for the abatement of low concentrations (C_{in} = 0.5 ppm$_v$) of toluene by introducing catalyst material. The effect will be evaluated on two aspects: increase of energy efficiency concerning toluene oxidation, decrease by-product formation such as ozone and NO_x. First, a photocatalyst, Aerolyst 7706 TiO_2, will be inserted between the reactor electrodes as explained in Section 4.1.1, doing this makes it possible to exploit emitted radiation. Next, the catalyst, $CuOMnO_2/TiO_2$, will be placed post-plasma in order to increase toluene removal and remove ozone and NO_x. The effect of humidity of the gas stream will be investigated. Finally, research on deactivation of plasma catalysts will be conducted.

6.2 Materals and Methods

6.2.1 Experimental setup-plasma catalytic reactor

The experimental setup is discussed in Section 4.1.1. This chapter discusses the observed effects when heterogeneous catalyst material is introduced for the first time. This catalyst material can be placed on the stainless steel mesh electrode (Figure 4.1). Aerolyst 7706 (commercially available, Degussa, Hanau-Wolfgang) was selected as in-plasma catalyst. This catalyst is an extrudate with cylindrical shape and average diameter and length of 2.7–3 mm and 4 mm respectively. Its chemical composition is > 85% TiO_2 (70% anatase, 30% rutile) and < 15% aluminum oxide and silicon dioxide, with a density of 3.8 g cm^{-3}. The BET surface of Aerolyst 7706 is 49 m² g^{-1} (physical-chemical data from Degussa, Hanau-Wolfgang). As ozone degrading catalyst, $CuO-MnO_2/TiO_2$ was selected for post-plasma catalysis (3% Cu, 6.8% MnO_2, commercially available, Heraeus, Hanau). This catalyst was also tested as in-plasma catalyst. However, results will not be discussed in this chapter since ozone breakdown efficiencies were much lower compared to results when used as post-plasma catalyst (Section

3.1). This extruded catalyst material is cylindrically shaped with an average diameter and length of 1.5 and 4 mm respectively, and a density of 0.925 g cm^{-3}. The catalyst has a BET surface area of 50 m^2 g^{-1}. When the in plasma catalysts were introduced, the in plasma residence time decreased to approximately 1.12 seconds. The residence time in the PPC unit was around 0.25 seconds.

An ozone generator (model LAB2B, Triogen) was used for the study of deactivation of catalyst materials. Ozone is produced by an electric discharge in dry air.

6.2.2 Chemical analytical techniques

Inlet and outlet air samples were taken by solid-phase microextraction (SPME) with a 100 μm polydimethylsiloxane fibre (Supelco) (Chapter 4.1.3.1). Chemical analyses were again carried out with an Agilent 6890 Series Gas Chromatograph, equipped with a flame ionization detector (FID) and a HPCORE integration system. The FID detector (250°C) was fed by 400 mL min^{-1} air and 40 mL min^{-1} hydrogen. The carrier gas was helium with a flow rate of 3 mL min^{-1}. A SPME inlet liner was installed and placed at a temperature of 200°C. Separation was done on a 30 m x 0.53 mm cross linked methyl siloxane capillary column with a film thickness of 5.0 μm (HP-1) (HP, Santa Clara). Analyses were carried out isothermally (140°C). Equilibrated water-gas systems with a known toluene headspace concentration were used for calibration (Dewulf et al., 1999). Sampling with a 100 μm polydimethylsiloxane (PDMS) SPME fiber combined with GC-FID, resulted in a limit of quantification of 67 ppb$_v$.

A chemiluminescence NO-NO$_2$-NO$_x$ analyzer (Model 42C, Thermo Environmental Instruments Inc.) was used for monitoring nitrogen oxides production.

A Dionex ion chromatograph ICS 90 was used for measuring nitrate and nitrite ions on the catalyst surface after rinsing with deionized water. 10g CuOMnO$_2$/TiO$_2$ and 15g Aerolyst TiO$_2$ pellets each were mixed with 50mL deionized water. Samples were stirred for 8 hours at

25°C. After filtering, 5mL of the samples was diluted with 60mL of deionized water before analysis with IC.

Temperature and humidity monitoring was conducted with a TESTO 110 device. For current and voltage measurements two multimeters (Velleman DVM 92) were used.

6.3 Results and discussion

6.3.1 Toluene removal efficiency by heterogeneous catalysis

Catalyst material can be introduced in IPC and PPC positions. Initially a systematic investigation is carried out in order to select the most optimal positioning. Two important criteria are considered; minimum ozone outlet concentration and maximum toluene removal efficiency.

Aerolyst 7706 TiO_2, both in IPC and PPC position, did not result in significant ozone reduction (Figure 6.1a). However, when this catalyst was positioned IPC, the highest toluene removal was measured (Figure 6.1b). It could be concluded that Aerolyst 7706 TiO_2 was most useful when inserted into the plasma discharge.

When used in PPC position, MnO_2-CuO/TiO_2 reduced ozone outlet concentrations up to 7 times when compared to the levels obtained without catalysis. When placed in the plasma discharge, limited ozone reductions were measured (Figure 6.1a). Both IPC as PPC positions increased toluene removal efficiency. Adding 10g $CuOMnO_2/TiO_2$ in the discharge zone resulted in 56 % toluene conversion for an energy density of 1.8 J L^{-1}. This removal efficiency increased to 77.8 % when used as post-plasma catalyst (Figure 6.1b). Taking into account both criteria, $CuOMnO_2/TiO_2$ is discussed in this manuscript as a post plasma catalyst.
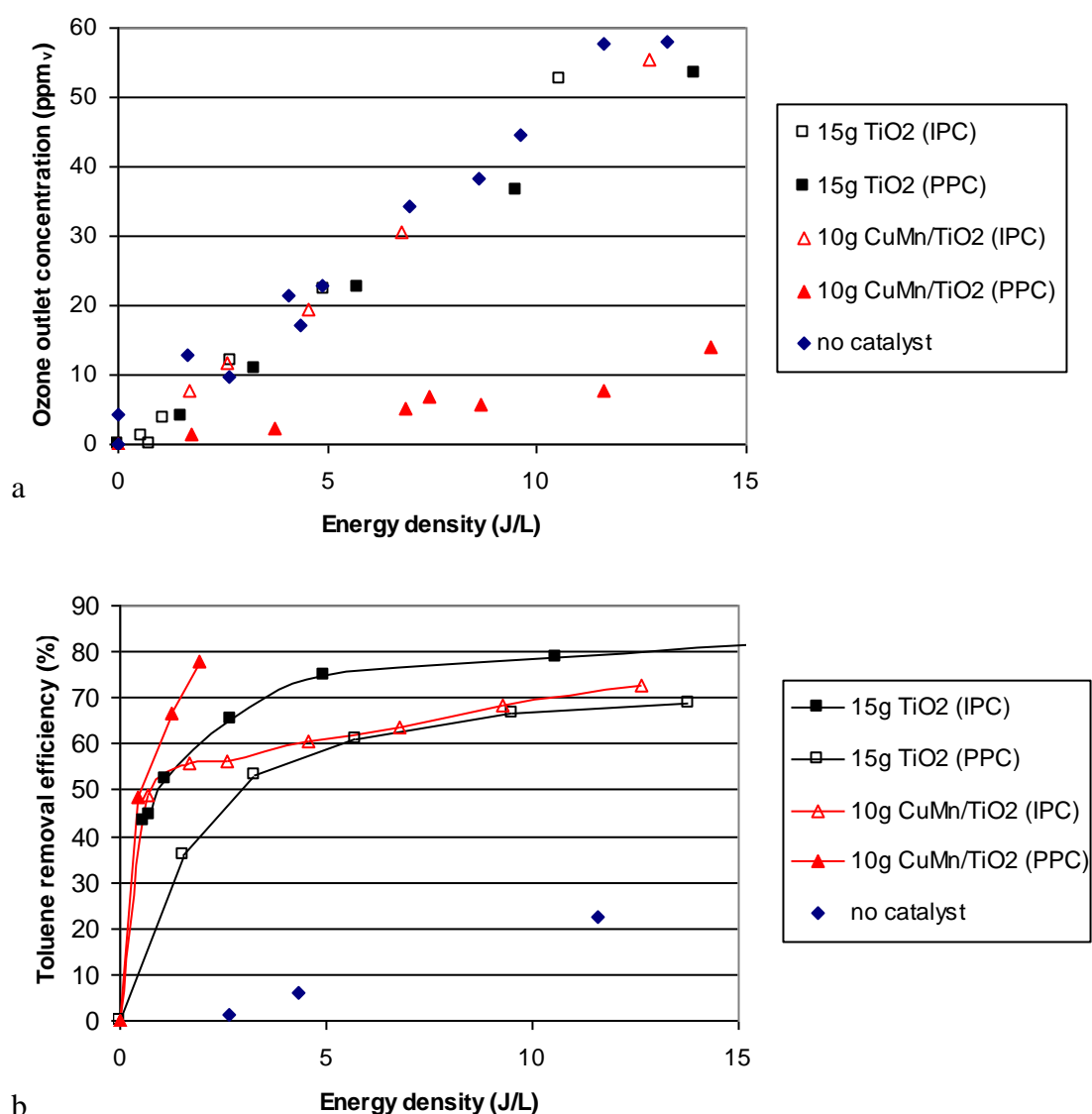
Figure 6.1 Effect of positioning on (a) ozone outlet concentration (ppm$_v$) and (b) toluene removal efficiency (%) as a function of energy density (J L^{-1}). Experiments were done with Aerolyst$^{®}$7706 TiO$_2$ and CuOMnO$_2$/TiO$_2$ catalyst in dry air ((Q$_{air}$ = 10.8 L min^{-1}, P = 101.3 kPa, T = 298 K)

6.3.1.1 Toluene abatement: in-plasma catalysis

When IPC is operated, the catalyst material is placed on the stainless steel mesh electrode. Atmospheric DC and pulsed glow discharges emit UV light due to excitation of nitrogen by accelerated electrons (Duten et al., 2002). UV light illumination of the photocatalyst is necessary to produce negative electron (e$^-$) and positive hole (h$^+$) pairs on the catalyst surface.

Next to plasma triggered photocatalysis, activation is possible due to adsorption of high-energy plasma species such as metastable N_2^* (6.17 eV) ([c]Kim et al., 2005). Other phenomena such as the storage and formation of oxidative species ([b]Kim et al., 2005) or a shift in average electron temperature (Liu et al., 2002; Holzer, 2005), may also contribute to the formation of a more oxidative environment than plasma alone.

Taking into account parameters such as stability of the corona discharge and degradation rates of toluene, an optimal amount of 7.5 g in plasma catalyst for each plasma module was found (height ~ 1 cm). The plasma became unstable when larger amounts (>20 g) of Aerolyst[®]7706 pellets were introduced. This might be explained by interactions with micro-discharges which arise between the charged catalyst pellets, negatively influencing the plasma characteristics.

Figure 6.2 summarizes the removal efficiency (%) of toluene as a function of energy density for corona, IPC (TiO_2) and PPC ($CuOMnO_2/TiO_2$) configuration. The toluene reaction rate constant with hydroxyl radicals is 5.7 x 10^{-12} molecules cm^{-3} s^{-1}, for atomic oxygen 2.32 x 10^{-13} molecules cm^{-3} s^{-1} (NIST, 2007). The reaction rates, combined with the high concentrations in the plasma discharge, make both radicals important towards toluene oxidation. Ozone, with a reaction rate constant of 1.2 x 10^{-20} molecules cm^{-3} s^{-1}, plays a minor role in the oxidation mechanism of toluene. In the absence of catalyst material, 27 ± 4 % of the toluene was removed in dry air for an energy density of 17 J L^{-1} (Section 5.3.1). Adding 15 g TiO_2 in plasma catalyst (Aerolyst 7706) in the plasma zone increased this removal rate to 82 ± 2 % due to in plasma catalytic processes.
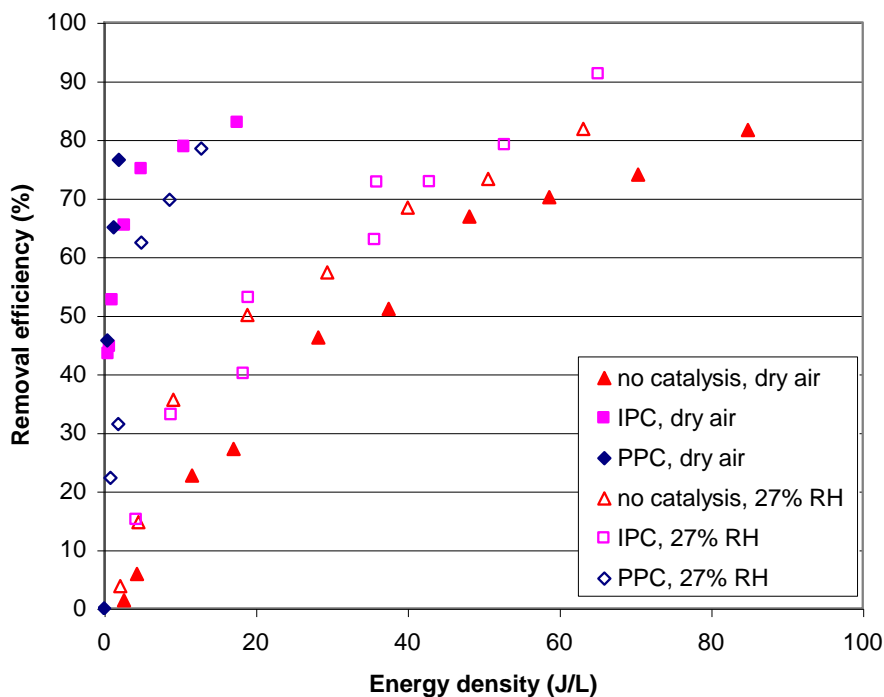
Figure 6.2 Removal efficiency (%) of toluene (C_{in} = 0.5 ppm$_v$) as a function of energy density. Data are shown for plasma without heterogeneous catalyst, TiO$_2$ in plasma and CuOMnO$_2$/TiO$_2$ post plasma. Experiments were conducted for dry air and 27 % RH (Q_{air} = 10.8 L min^{-1}, P = 101.3 kPa, T = 298 K)

Humidity proved to interfere within the oxidation mechanism of toluene in a non-thermal plasma (Section 5.3). In current work, the effect of humidity on IPC process was examined for two relative humidities. Experiments prove that water molecules negatively interfere within the plasma catalysis mechanism (Figure 6.2). For an inlet gas stream with 27% RH and a plasma with energy density of 17 J L^{-1}, a degradation efficiency of 40 ± 6 % was measured. This value is higher than the removal obtained by plasma without heterogeneous catalysis at dry conditions (27 ± 4 %). However, Figure 6.2 shows that this increased removal efficiency can not be attributed to the TiO$_2$ catalyst. Degradation results are equal to those obtained for humid air (27% RH) without catalyst. It can be concluded that for moderate relative humidities, higher removal efficiencies are obtained due to an enhanced production of hydroxyl radicals. Toluene reaction kinetics research showed that OH induced degradation is

one of the most important pathways in toluene oxidation (NIST, 2007) (Section 5.3.2). It may be concluded that water molecules adsorb on the TiO_2 surface to form mono- or multilayers (Demeestere et al., 2003). By this competitive adsorption, active sites are blocked which may result in a reduced catalytic activity with decreasing amounts of $OH^·$ formed on the catalyst surface. Another possible explanation is that toluene degradation rates in humid conditions are determined by slower diffusion rates through the water layers which cover the catalyst surface.

6.3.1.2   Toluene abatement: post-plasma catalysis

It is mentioned earlier that the degradation of ozone on the catalyst surface results in the production of reactive compounds (e.g. oxygen radical). By introducing 10g $CuOMnO_2/TiO_2$ post plasma, 78 % of toluene was removed at an energy density of 2.5 J L^{-1}. In the absence of this catalyst, removal efficiencies were only 2 %. It should be noticed that with this low amount of catalyst material, ozone is not removed completely. By introducing higher amounts of catalyst, ozone may be removed to a larger extent, resulting in an increased toluene removal efficiency.

Humidity proved to have an important impact on the performance of the post-plasma catalytic oxidation process. Rakitskaya et al. (1999) proved that catalysts with different amounts of absorbed water showed different activity in ozone decomposition. Indeed, for an energy density of 2.5 J L^{-1} and 27% RH, toluene removal efficiency was 30 %, which is 2.6 times lower than in dry gas streams. For a higher relative humidity of 50 %, toluene removal efficiency proves to be 5 times less effective than in dry air. This phenomenon can be explained by competitive adsorption of water molecules. Einaga et al. (2005) wrote that not only adsorption of VOC on the Mn sites is inhibited by the presence of water vapor, but that

also structural changes of the catalyst could influence the rate of decomposition. In own experiments a brownish color was seen after washing used catalyst material, indicating that Mn ions are extracted from the catalyst surface. An increased coordination of water to Mn sites during ozone decomposition in humid gas streams, might explain a bond cleavage of Mn-O-Al which is present in the tested Al_2O_3 supported MnO_2 catalyst.

Structural properties and chemical composition of the catalyst, strongly influence the interactions with water molecules. In the following chapter, it will be discussed to what degree plasma catalytic hybrid systems may benefit from introducing catalysts that are less susceptible to H_2O adsorption.

6.3.2 Reduction of ozone and nitrogen oxides by plasma catalytic processes

In Chapter 4 it was discussed that ozone and nitrogen oxides are formed as unwanted by-products. Figure 6.3 gives an overview of the effect of introducing in-plasma and post-plasma catalysts on the NO_2 production as a function of the relative humidity. Both catalysts proved to reduce outlet concentration of NO_x compounds. Table 6.1 summarizes the observed ozone levels with the plasma catalytic hybrid system.
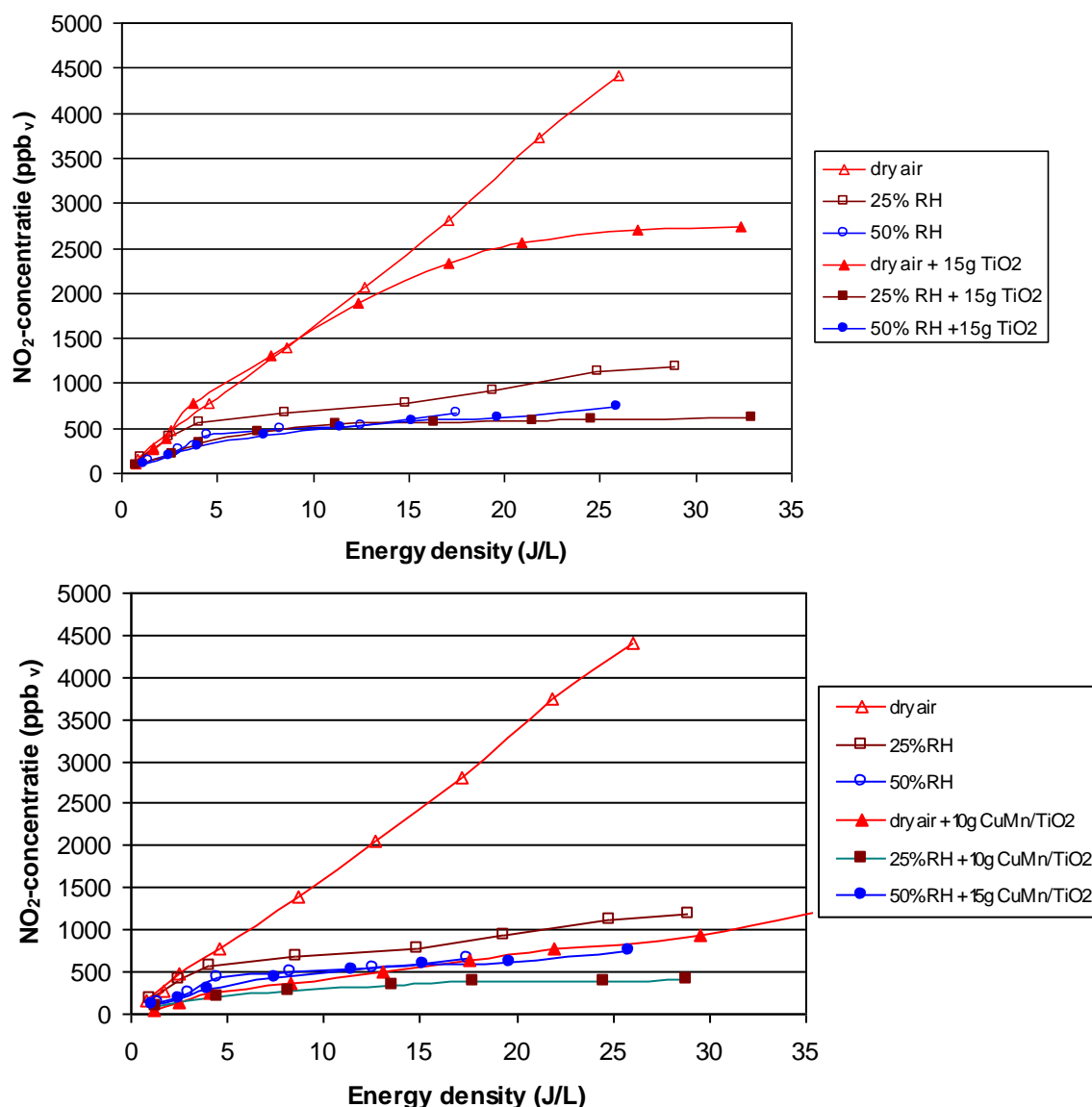
Figure 6.3 NO$_2$ production and effect of air humidity (dry air, 25% RH and 50% RH) as function of energy density (J L^{-1}); a) effect of introducing heterogeneous catalyst material (IPC (TiO$_2$)) and b) PPC (CuOMnO$_2$/TiO$_2$) (dry air or 28% RH) (pure air (no toluene), Q$_{air}$ = 10.8 L min^{-1}, P = 101.3 kPa, T = 298 K)

6.3.2.1 By-product reduction by in plasma catalysis

At energy densities lower than 10 J L^{-1}, no significant NO$_x$ removal was observed after introducing the photocatalyst (Figure 6.3). For higher energy densities, the increased current density results in more collisions of energetic electrons with N$_2$. This results in a larger amount of excited nitrogen molecules, subsequently leading to higher photon emission rates.

The UV intensity might be sufficient to activate the photocatalyst. As already mentioned earlier, the higher levels of metastable N_2^* may also result in an increased catalytic activation ([c]Kim et al., 2005). At higher energy densities, the storage and formation of oxidative species ([b]Holzer, 2005) or the shift in average electron temperature (Liu et al., 2002; Holzer, 2005) can become more significant. These phenomena might explain the suppression of NO_2 production when more energy is delivered to the plasma catalytic system. For an energy density of 15 J L^{-1} the NO_x removal rate in IPC system was 14 %, while this value increases up to 36 % for 25 J L^{-1}. For a identical energy density, but in humid conditions (RH = 25%), introducing 15 g in plasma catalyst resulted in a NO_2 outlet concentration which was 86 % lower ($C_{NO2,out}$ = 600 ppb_v) compared with levels produced by the corona discharge in dry air ($C_{NO2,out}$ = 4200 ppb_v).

Experiments showed that the photocatalyst under dry conditions was less effective in ozone reduction. Results indicate that no ozone degradation is measured by IPC in dry air (Table 6.1). However, Table 6.1 indicates that the presence of water molecules improve ozone removal performance of the in plasma catalytic reactor. For dry air and 27% RH no significant differences in ozone outlet concentrations can be observed. However, for higher relative humidities (45% RH) ozone outlet levels are typically 1.6 $\pm$ 0.3 (n = 3) lower compared with non-catalytic NTP.

Table 6.1 Ozone outlet concentrations (ppm$_v$) for plasma and plasma catalytic hybrid system and effect of IPC (Aerolyst 7706) and PPC (CuOMnO$_2$/TiO$_2$). Experiments were conducted at different humidities (0%, 27% and 45%) (pure air (no toluene), Q$_{air}$= 10.8 L min^{-1}, energy density 10 J L^{-1})

	Ozone outlet concentration (ppm$_v$)								
	Dry air			**27 % RH**			**45 % RH**		
Energy density (J L^{-1})	**5**	**10**	**20**	**5**	**10**	**20**	**5**	**10**	**20**
No catalysis	*27.7*	*49.9*	*91.8*	*16.2*	*31.2*	*N.A.*	*13.4*	*26.6*	*61.49*
IPC	*24.0*	*52.6*	*99.5*	*18.9*	*41.9*	*75.8*	*6.9*	*20.4*	*36.1*
PPC	*3.6*	*7.1*	*15.0*	*8.1*	*16.7*	*N.A.*	*3.9*	*9.9*	*18.3*

This trend might be explained by the presence of adsorbed water molecules which can enhance the generation of hydroxyl radicals (Pengyi et al., 2003). Previous experimental work proved that ozone diffusion through water layers on the catalyst surface is not rate limiting. Ozone can be consumed by three reactions: decomposed by UV light, acting as electron acceptor and as hydroxyl radical scavenger (Pengyi et al., 2003). The latter reaction might explain the reduced ozone outlet concentrations in humid conditions as seen in Table 6.1.

6.3.2.2 By-product reduction by post-plasma catalysis

It proved to be possible to reduce ozone outlet concentrations below limit of detection (14 ppb$_v$) when higher masses (20g) of catalyst were introduced in the system. Radhakrishnan et al. (2001) have reported that ozone decomposition on MnO$_x$/Al$_2$O$_3$ catalyst proceeds by electron transfer from Mn site to adsorbed ozone producing reactive atomic oxygen at the surface. Mn is reduced back during desorption of oxygen species.

Table 6.1 reveals that by adding only 10 g CuOMnO$_2$/TiO$_2$ PPC, ozone outlet concentrations in dry air are reduced with a factor of 6.9 ± 0.8 (n = 3) in the tested energy density range.

Also in humid conditions the ozone removal efficiencies proved to be higher than compared with IPC processes; ozone was reduced with a factor of 1.9 ± 0.1 (n = 3) and 3.1 ± 0.4 (n = 3) for relative humidities of 27% RH and 45% RH, respectively. First indications point that a high air humidity could negatively influence PPC ozone removal. More experiments are done and discussed in Section 7.3.1.2 to give more clarity on this topic.

Next, also NO_2 outlet concentrations could be reduced using a post-plasma catalytic system (Figure 6.3). When the energy density was 15 J L^{-1}, the outlet NO_2 concentration was 550 ppb_v, while this was 2520 ppb_v in the absence of the post-plasma catalyst at RH = 0%.

Best results were obtained after introducing 10 g $CuOMnO_2/TiO_2$ PPC in a gas stream with relative humidity of 25%: NO_2 outlet concentrations were only 360 ppb_v at 15 J L^{-1}, which is a reduction of 86 % compared to levels measured in the absence of heterogeneous catalysis.

6.3.3 Deactivation of catalyst materials

During normal reactor operation of total duration of 48 hours, no deactivation of both catalyst materials was noticed during ozone degradation experiments. Concentrations of toluene degradation products are low (Chapter 5), probably no significant amounts of active sites are blocked by these by-products. Secondly, adsorbed degradation products may also be oxidized efficiently due to the long residence time in a strong oxidizing environment. More volatile compounds, such as CO_2 and H_2O, could be formed followed by desorption of the catalyst material.

An experiment was conducted in dry air (Q = 1.5 L min^{-1}) at an energy density of 424 J L^{-1}, resulting in an inlet ozone concentration of 3050 ppm_v (6.1 g m^{-3}). During this experiment 10g $CuOMnO_2/TiO_2$ and 15g Aerolyst 7706 TiO_2 catalyst material was added to the plasma reactor. Initially, 98% of the ozone was removed by the catalysts; after 7 hours the ozone removal efficiency decreased to 47%. This indicated that there is a deactivation of the catalyst

under high loads. Einaga et al. (2005) reported that structural changes in alumina-supported manganese oxide catalyst were measured during ozone decomposition reactions. Sullivan et al. (2004) reported that regeneration for alumina-coated tubes that had been deactivated can be achieved by purging with dry CO_2 free air for periods of a few days. They however proved that there is only a partial recovery, ranging from a few percent to over 50% of the initial removal capacity. In this study we washed the deactivated $CuOMnO_2/TiO_2$ pellets with distilled water. Experiments with the washed catalyst material were repeated and results showed that the catalyst was reactivated completely: ozone and NO_2 could be decomposed to the same degree as initially achieved.

The washing water was analyzed with ion chromatography. No nitrite ions were detected in the washing water of both IPC and PPC catalyst. However, nitrate ions were detected, amounts of NO_3^- adsorbed on the photocatalyst were 0.184 mg m^{-2} and 0.143 mg m^{-2} NO_3^- on the $CuOMnO_2/TiO_2$ catalyst.

Sano et al. (2006) proved that plasma in atmospheric air produces HNO_3 and that these compounds are blocking the oxidation sites of the photocatalyst. Devahasdin (2003) wrote that HNO_3 is formed on a photocatalyst surface and can reach an equilibrium with its reverse reaction. Also during ozone degrading processes, similar reactions can occur on the catalyst surface producing HNO_3. Reaction rate constants in gas phase between NO_2 and atomic oxygen is $2.2.10^{-11}$ cm^3 molecule^{-1}s^{-1} (Atkinson et al., 2004) (Table 4.1). The fast removal kinetics with the formed atomic oxygen on the $CuOMnO_2/TiO_2$ surface, explains the measured levels of nitrate.

6.4 Conclusions

Non-thermal plasma technology is investigated for the abatement of low levels of toluene. A major drawback however is the production of by-products such as ozone, NO_x or secondary degradation products. A 4-pins-to-mesh corona reactor is used in combination with heterogeneous catalysts for the abatement of toluene in gas.

Energy efficiency for toluene degradation strongly increased using in-plasma catalysis (IPC). In dry air and for an energy density of 17 J L^{-1}, adding 15 g TiO_2 photocatalyst increased the toluene ($C_{in} = 0.5$ ppm_v) removal rate from 27 ± 4 % to 82 ± 2 %. Humidity had a limiting effect for toluene degradation, under the same conditions degradation efficiency decreased to 40 ± 6 %. Using MnO_2-CuO/TiO_2 as post-plasma catalyst, toluene removal efficiencies of 78% were obtained for an energy density of 2.5 J L^{-1}, while this was only 2% in the absence of the catalyst. Humidity proved to have a limiting effect on toluene degradation: removal efficiency decreased to 30% for 27% RH.

Outlet concentrations of NO_2 for dry air, 25% and 50% relative humidity are 770 ppb_v, 581 ppb_v and 431 ppb_v respectively at 4.5 J L^{-1}. Placing TiO_2 between the electrodes (IPC) resulted in NO_2 degradation for energy densities > 10 J L^{-1}. For an energy density of 25 J L^{-1}, NO_2 levels were reduced to 2685 ppb_v in the IPC configuration, while this was 4208 ppb_v for the corona discharge. Best results were obtained for humid gas streams: the NO_2 degradation efficiency increased from 36% to 86% when relative humidity was increased up to 25%. No degradation of ozone by TiO_2 was measured.

Placing 10g MnO_2-CuO/TiO_2 post-plasma resulted in ozone outlet concentrations below limit of detection. Also NO_2 was removed in the PPC configuration. For an energy density of 15 J L^{-1} in dry air, the outlet NO_2 concentration was 553 ppb_v, while this was 2524 ppb_v in the absence of this catalyst. Humidity had a positive influence, NO_2 outlet concentrations were reduced to 360 ppb_v at relative humidity of 26%.

Deactivation of catalyst materials used in combination with non-thermal plasma, may be explained by formation of HNO_3. It was experimentally determined that nitrate ion concentrations were 0.184 mg m^{-2} and 0.143 mg m^{-2} for TiO_2 and MnO_2-CuO/TiO_2 catalysts respectively. After washing with water and drying, the catalysts were fully reactivated again.

Chapter 7

Post plasma catalytic technology for the

removal of toluene from indoor air

7.1 Introduction

Volatile organic compounds (VOC) in indoor environments have been suspected to cause sick-building symptoms like headache, eye and mucous membrane irritation, fatigue, and asthmatic symptoms (Jarnstrom et al., 2006). Next to that, other parameters such as inorganic pollutants, particulate matter, biological pollutants, temperature and humidity are important for indoor air quality. Humidity levels are optimally controlled between 30 and 60%. Air that is too dry is harmful for building structural integrity and human health. Excess humidity is a breeding ground for mold, pests, and rot in homes and is more likely to cause heart stroke, heat exhaustion, headaches, and dehydration.

In Chapter 6 it is discussed that the combination of heterogeneous catalysts with non-thermal plasma offers great potential as indoor air purification technology, particularly toward VOC degradation. Catalysts can be introduced in (In Plasma Catalysis - IPC) or downstream from the discharge zone (Post Plasma Catalysis - PPC). One of the most important by-products formed in a non-thermal plasma discharge is ozone. Although the decomposition of ozone into oxygen is a thermodynamically favored process, ozone is thermally stable up to 250°C, and a post-plasma catalyst is necessary for decomposition at lower temperatures. This process produces active species on the catalyst surface able to induce secondary oxidation reactions.

However, for both the IPC and PPC configurations, the RH of the treated gas stream showed to be a critical parameter, having a limiting effect on the plasma catalytic toluene oxidation. Also Zhang et al. (2007) reported a negative impact on (photo)catalytic processes when treating humid air.

In this chapter, the effect of humidity on both ozone and toluene removal in a hybrid PPC device is investigated in a systematic manner. Therefore, six different catalysts were tested downstream a DC corona discharge at a RH ranging between 0 and 83% at 25°C; and the effect of water molecules on the synergetic power observed during PPC is investigated in

more detail. In order to better understand the observed results, equilibrium sorption constants of three model VOC including toluene on two selected catalysts were determined as a function of RH using the Equilibrium Partitioning In Closed System (EPICS) methodology (Demeestere et al., 2003).

This quantitative approach provides new insights on the effect of humidity on PPC systems, and for the first time, a relationship has been established between sorption data and plasma catalytic VOC degradation results.

7.2 Materials and Methods

7.2.1 Experimental setup - Post-plasma catalytic reactor

The experimental setup is discussed in Section 4.1.1. In Chapter 6 it was discussed how heterogeneous catalyst materials can be inserted in both in-plasma as post-plasma position.

7.2.2 Heterogeneous catalysts

Six different catalysts, divided in two subgroups, were selected in our experiments. In a first set of four catalysts (supplied by Hereaus (Hanau, Germany), the active compound is deposited on a support material. Two catalysts contain Pd (0.5 wt%) as the active compound with Al_2O_3 as a support material (Pd/Al_2O_3(a) and Pd/Al_2O_3(b)). The active material in two other catalysts involves a mixture of CuO (3 wt%) and MnO_2 (6.8 wt%) deposited on a TiO_2 support (Cu-Mn/TiO_2(a) and Cu-Mn/TiO_2(b)). According to the supplier, the Brunauer-Emmett-Teller (BET) specific surface area and the pellet size of Pd/Al_2O_3(a), Pd/Al_2O_3(b), Cu-Mn/TiO_2(a) and Cu-Mn/TiO_2(b) catalysts amount 230, 280, 32 and 50 m² g^{-1}, and 2-4, 2-5, 1.5 and 1.5 mm, respectively.

In the second set of catalysts, the active compound is dispensed in the bulk of the material. Two such catalysts, N150 and N140, were supplied by Süd-Chemie (München, Germany). The first contains >40 wt% Fe_2O_3 and >25wt% MnO_2 as active compounds, with an average pellet size of 6 mm and a specific BET surface area of 100 m² g^{-1}. The latter contains >15wt% CuO and >25wt% MnO_2, with an average pellet size of 5 mm and a specific BET surface area of 100 m² g^{-1}.

7.2.3 Chemical analytical techniques

Gas sampling at the reactor in- and outlet was done using solid-phase microextraction (SPME) with a 100 µm polydimethylsiloxane fibre (Supelco) (Chapter 4.1.3.1). A SPME liner was installed in a Agilent 6890 Series gas chromatograph having a split-splitless injector set at 220°C. After separation on a cross linked methyl siloxane capillary column (length: 30 m, column diameter: 0.53 mm, film thickness: 5.0 µm (HP-1) (HP, Santa Clara), the analytes were detected using a flame ionization detector (FID) and peak areas were integrated with HPCORE integration software. The FID detector (250°C) was fed by 400 mL min^{-1} air and 40 mL min^{-1} hydrogen. The carrier gas was helium with a flow rate of 3 mL min^{-1}. Analyses were carried out isothermally (140°C). Equilibrated water-gas systems with a known toluene headspace concentration were used for calibration (Dewulf et al., 1999). The limit of quantification, corresponding to a signal-to-noise ratio of 10, was determined to be 67 ppb$_v$.

Again ozone was monitored using an Anseros ozone analyzer (UV at 253 nm) equipped with Picolog Acquisition software. Therefore, a constant gas flow of 200 mL min^{-1} was pumped from a sample point to the detector. Temperature and humidity monitoring was conducted with a TESTO 110 device. For current and voltage measurements, two multimeters (Velleman DVM 92) were used.

7.2.4 EPICS methodology.

Equilibrium adsorption constants K (mL g^{-1}) were determined using an optimized EPICS methodology (Equilibrium Partitioning In Closed Systems) (Dewulf et al., 1999; Demeestere et al., 2003). Three clean and dry vials were filled with an appropriate amount of catalyst ($m_{catalyst}$ = 0.40 ± 0.01 g) and gastightly closed using Mininert valves (Alltech Ass., Lokeren, Belgium). Next, each vial was flushed for at least 8 hours with clean air (Air Liquide, Luik, Belgium) having a controlled relative humidity. Air humidity was set by bubbling dry air (<1% RH) through a cooled water column. In a next step, a known amount of gaseous toluene, trichloroethylene and acetone, was introduced in all two-phase systems. In a similar way, three one-phase vials without catalyst material were loaded with an identical mass of VOC (concentration$_{VOC}$ = 125 ppm$_v$). To avoid photolytic effects, both one- and two-phase systems were wrapped into aluminium foil during incubation at 25.0 ± 0.1 °C for at least 8 hours. Headspace sampling was done using a 0.5 mL gas syringe (Alltech Ass.) followed by GC injection.

The equilibrium adsorption coefficient K (mL g^{-1}) is calculated according to equations (7.1 and 7.2) (Demeestere et al., 2003);

$$K = \frac{rV_{g,1} - V_{g,2}}{m_{catalyst}} \left(mL\middle/ g \right) \tag{7.1}$$

$$r = \frac{C_{g,1}/m_1}{C_{g,2}/m_2} \tag{7.2}$$

m_1 and m_2 (g) represent the mass of VOC introduced in the one and two-phase system; $m_{catalyst}$ the mass of catalyst material (g); and $V_{g,1}$ (mL), $V_{g,2}$ (mL) and $C_{g,1}$ (g mL^{-1}) and $C_{g,2}$ (g mL^{-1}) the gas volumes and equilibrated VOC concentration in the one- and two-phase systems, respectively.

7.3 Results and Discussion

7.3.1 Post-plasma catalysis: ozone decomposition.

7.3.1.1   Effect of catalyst characteristics on ozone decomposition.

Figure 7.1 represents the concentration of ozone which is produced by the DC corona discharge ('no catalyst'-curve) next to ozone outlet concentrations after passing the heterogeneous catalysts.
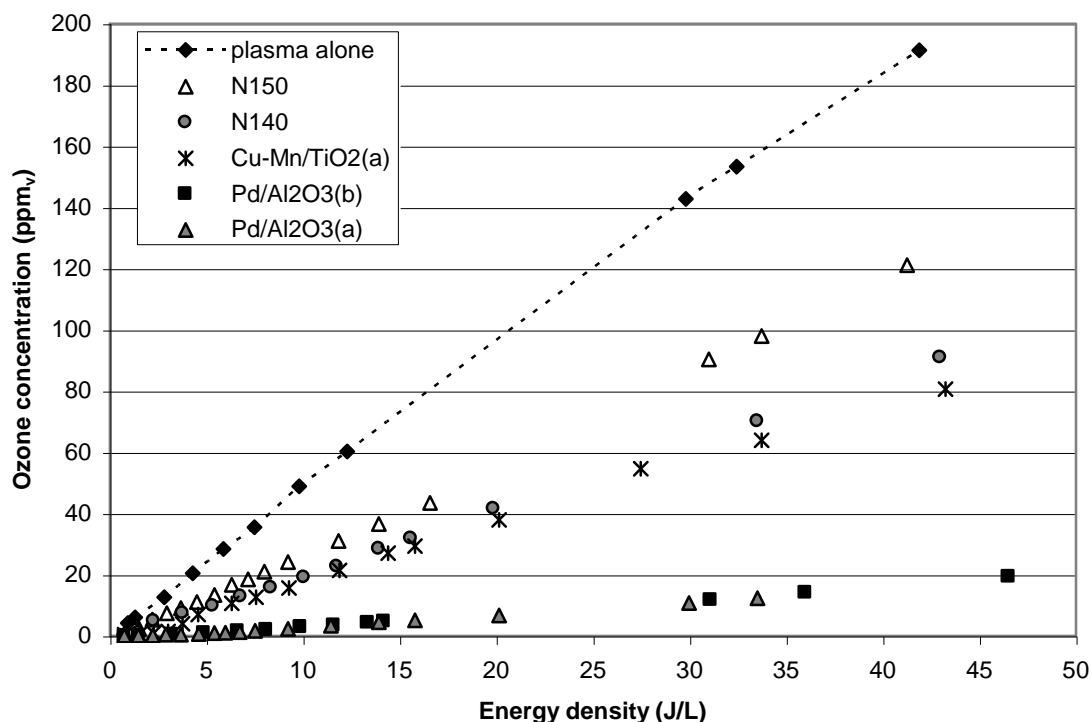
Figure 7.1   Ozone production (plasma alone) and ozone outlet concentrations (ppm$_v$) after passing the catalyst bed as a function of (i) energy density (J L^{-1}) applied to the positive DC corona discharge, and (ii) the type of heterogeneous catalyst (m$_{catalyst}$= 15.0 g, Q= 10.0 L min^{-1}, P=101.3 kPa, T= 298.15 K, dry air).

Results indicate that both physical and chemical properties of the catalyst materials strongly affect ozone decomposition efficiencies obtained in PPC configuration. Indeed, when 15 g of Pd/Al$_2$O$_3$(a) is introduced in the reactor, ozone outlet concentrations are reduced by 94%, while this is only 48% using an equal mass of N150 catalyst. Among the catalysts

investigated, Pd/Al_2O_3 catalysts are the most efficient towards ozone decomposition. A similar ozone removal is obtained for both Pd/Al_2O_3 catalysts despite a difference in specific surface area (SSA) (230 vs 280 m² g^{-1}). This indicates that SSA is not the main parameter affecting catalytic ozone decomposition. This is supported by comparing experimental data obtained for $Cu-Mn/TiO_2$(a) with those of N140 showing similar ozone degradation data, but having SSA of respectively 32 and 100 m² g^{-1} (Figure 7.1). N150, containing Fe_2O_3 and MnO_2 as the active compounds and having a SSA of 100 m² g^{-1}, is less efficient in ozone decomposition than $Cu-Mn/TiO_2$(a), having a SSA up to a factor 3 lower.

Our measurements reveal that mainly the active compound, rather than the presence of a support material and the SSA of the catalyst, determines the rate of ozone decomposition. Differences in ozone decomposition when using other active compounds might be explained by the existence of different decomposition mechanisms. Radhakrishnan et al. (2001) suggested that ozone decomposition on a MnO_x/Al_2O_3 catalyst occurs through an electron transfer from Mn^{n+} to an ozone molecule. In this way, ozone is decomposed into an oxygen molecule and an atomic oxygen. Next, unstable $O_2^{2-}Mn^{(n+2)+}$ complexes decompose by reducing the oxidized manganese back to Mn^{2+} and through desorption of an oxygen molecule. Similar mechanisms can be expected for other metal oxides (e.g. CuO) or noble metals (e.g. Pd) (Tidahy et al., 2007). On the other hand, Rakitskaya et al. (1999) reported other processes for ozone degradation using Co(II)-catalysts, based on $HO_2^·$ formed through the reaction of an ozone molecule and a hydroxyl radical. The latter can be produced from catalytic reaction between water and atomic oxygen. This variety of reported ozone reduction mechanisms may offer a possible explanation for the differences in catalytic performance illustrated in Figure 7.1.

7.3.1.2 Effect of humidity on ozone decomposition using catalysts in PPC position.

Humidity strongly affects ozone production rates in plasma. Indeed, for an energy density of 10 J L^{-1} in dry air, the ozone concentration in the plasma outlet gas stream is 48.9 ppm$_v$. The ozone production in the plasma decreases at higher humidities which is illustrated by an outlet ozone concentration of 28.4 ppm$_v$ at 35% RH, and 18.9 ppm$_v$ at 74% RH for an energy density of 10 J L^{-1}. First measurements using $CuOMnO_2/TiO_2$ PPC (Section 6.3.2) indicated that humidity negatively influenced the catalytic ozone removal. Indeed, it was measured that the ozone outlet concentrations were reduced with a factor of 7 in dry air condition, while this was a factor of 3 at 45% relative humidity. To examine this effect in more detail, dry and humidified air (0% < RH < 74%) is passed through the reactor containing 15 g of Pd/Al_2O_3(b) catalyst material. For this PPC configuration at an energy density of 10 J L^{-1}, ozone outlet concentrations decreased to 2.9 ppm$_v$ in dry air; and to 3.8, 3.7 and 2.0 ppm$_v$ at RH = 26, 35 and 74%, respectively. Similar results were obtained for other energy densities ($0 - 46.5 \text{ J L}^{-1}$). In conclusion, for all tested humidities and energy densities, the relative catalytic ozone decomposition efficiency by Pd/Al_2O_3(b) amounted 89 ± 3 % (n=4). Based on these data, a linear relationship could be observed between ozone production levels (ppm$_v$) and the amount of ozone removed (ppm$_v$) in the PPC unit containing 15 g Pd/Al_2O_3(b) (Figure 7.2). It can be concluded that humidity (0% < RH $\leq$ 74%) has no direct effect on the catalytic activity towards ozone decomposition. Again this proves that depending on the type of catalytic ozone removal mechanism, the effect of humidity can be more or less significant; exemplified by no significant impact for Pd/Al_2O_3(b) catalyst, while an efficiency loss of up to two was measured for $CuOMnO_2/TiO_2$(a) (Section 6.3.1.2). Finally, it can be stated that the Pd/Al_2O_3(a) remains the most efficient ozone degrading catalyst, both in dry and humid conditions. Consequently, further PPC research has been done using this PPC catalyst type.
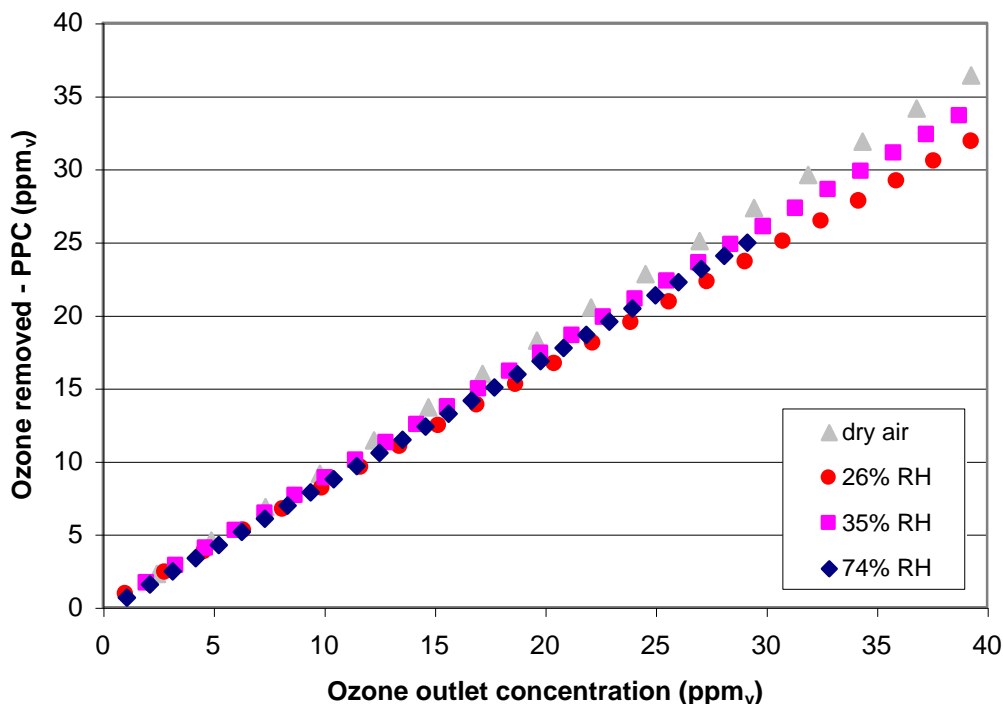
Figure 7.2 **Relation between inlet ozone concentration (ppm$_v$) and amount of ozone removed (ppm$_v$) in a PPC unit using Pd/Al$_2$O$_3$(b). Experiments were done in dry air and at RH = 26%, 35% and 74% (m$_{catalyst}$= 15.0 g, Q= 10.0 L min-1, P=101.3 kPa, T= 25°C)**

Also Sekiguchi et al. (2003) and Sullivan et al. (2004) reported a RH independent catalytic ozone degradation on MnO$_2$ and alumina, respectively, in a similar RH range. This might be surprising given the large amounts of water that are known to adsorb. Consequently, hydroxyl radicals can be formed on the catalyst surface by reaction between ozone and water. These hydroxyl radicals can interfere with the ozone decomposition mechanism (Chapter 4). Next, water might also compete with ozone for catalyst sorption sites (Chapter 6). Raoof et al. (1998) reported that typically a few layers of water (<10) are adsorbed on silica surfaces in humid air (<90% RH). One reason for the minimal RH effect may be attributed to a reactive ozone chemistry being considerably more exothermic than the physisorption interactions between water molecules and catalyst surface (Sullivan et al., 2004), resulting in the repelling of sorbed water molecules. A second explanation might be that the ozone diffusion time through the multilayers of water covering the catalyst surface are short enough to prevent

mass transfer limitation. Finally, it is also possible that water simply adsorbs at sites which are physically separated from the sites reactive for ozone (Sullivan et al., 2004).

7.3.2 Post-plasma catalysis: toluene degradation.

7.3.2.1 Effect of catalyst characteristics on toluene degradation at dry air conditions.

Since the ozone decomposition is related to the formation of oxidative species at the catalyst surface (e.g. atomic oxygen), similar trends for PPC toluene oxidation are expected as in ozone decomposition (Figure 7.1). Toluene degradation experiments were performed in dry air using different catalysts in downflow position (PPC). The selected catalysts, i.e. Pd/Al_2O_3(b), Cu-Mn/TiO_2(a), Cu-Mn/TiO_2(b), N140, N150, were in equilibrium with initial toluene concentrations. For all cases, resulting toluene outlet concentrations in dry air using a plasma energy density of only 2.5 J L^{-1} decreased below the limit of detection (67 ppb_v) representing a PPC toluene removal efficiency of at least 90%. It can be concluded that despite the difference in ozone removal capacity as observed in Figure 7.1, all catalysts proved to be able to remove toluene in an efficient way.

7.3.2.2 Effect of humidity on PPC toluene degradation.

The post-plasma catalytic toluene removal in humid air is investigated in two series of experiments. First, toluene removal is determined in a PPC unit, containing 15 g Pd/Al_2O_3(b) and treating a 10 L min^{-1} gas stream enriched with 0.5 ppm_v of toluene at $8\% \leq RH \leq 72\%$. At an energy density of 10 J L^{-1}, toluene removal efficiencies amounted 61%, 50% and 39% at RH = 30, 51 and 72%, respectively. This indicates the adverse effect of humidity on Pd/Al_2O_3(b) mediated PPC toluene removal, being in agreement with recent results obtained with a Cu-Mn/TiO_2 catalyst (Section 6.3.1.2). PPC toluene decomposition in dry air is shown to be up to 5 times more efficient than obtained in gas streams of 50% RH. However, even for

the highest RH level (72%), toluene degradation is still 2 times higher than in the absence of a catalyst. This proves the importance of PPC even in humid conditions.

Moreover, results reveal that for a given RH, toluene removal correlates well with ozone decomposition at the catalyst surface (Figure 7.3). This can be explained by the increased production of new oxygen active species from O_3 on the catalyst surface.
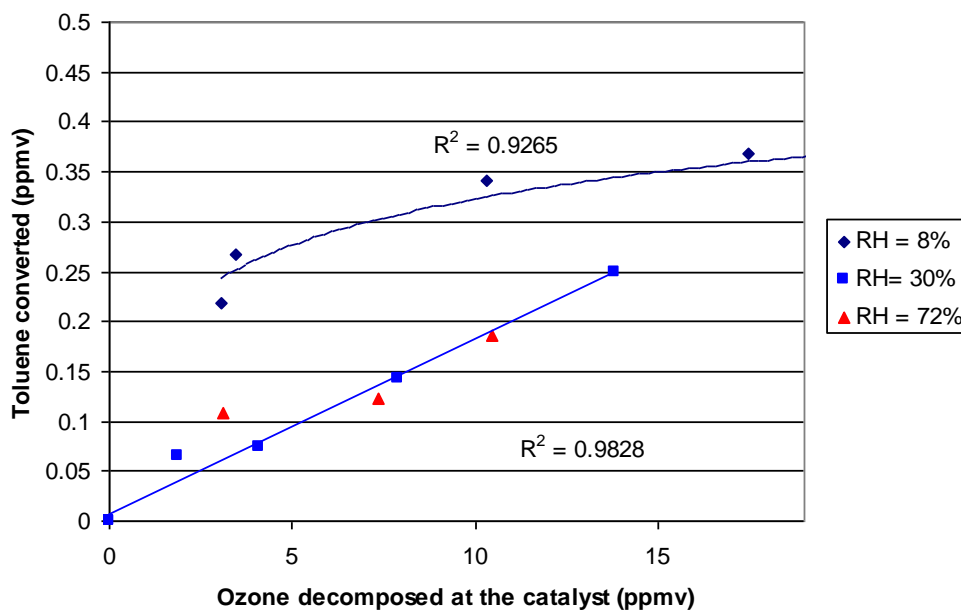
Figure 7.3 Converted toluene (ppm$_v$) as a function of removed ozone (ppm$_v$) for a Pd/Al$_2$O$_3$(b) PPC configuration at RH = 8%, 30%, and 72% (m$_{catalyst}$ = 15.0 g, Q=10.0 L min^{-1}, inlet concentration toluene = 0.5 ppm$_v$, T= 25°C, P= 101.3 kPa)

Figure 7.3 also shows that for an equal amount of converted ozone, toluene is removed more efficiently at lower relative humidities. Indeed, when 10.2 ppm$_v$ of ozone is decomposed catalytically, 0.34 ppm$_v$ of toluene (C$_{in}$ = 0.5 ppm$_v$) is removed at 8% RH, while this is only 0.18 ppm$_v$ at RH between 30% and 72%.

Secondly, the catalytic activity of five different catalysts towards toluene degradation has been compared with each other at a RH of 50% and at energy densities between 2 and 20 J L^{-1} (Figure 7.4).
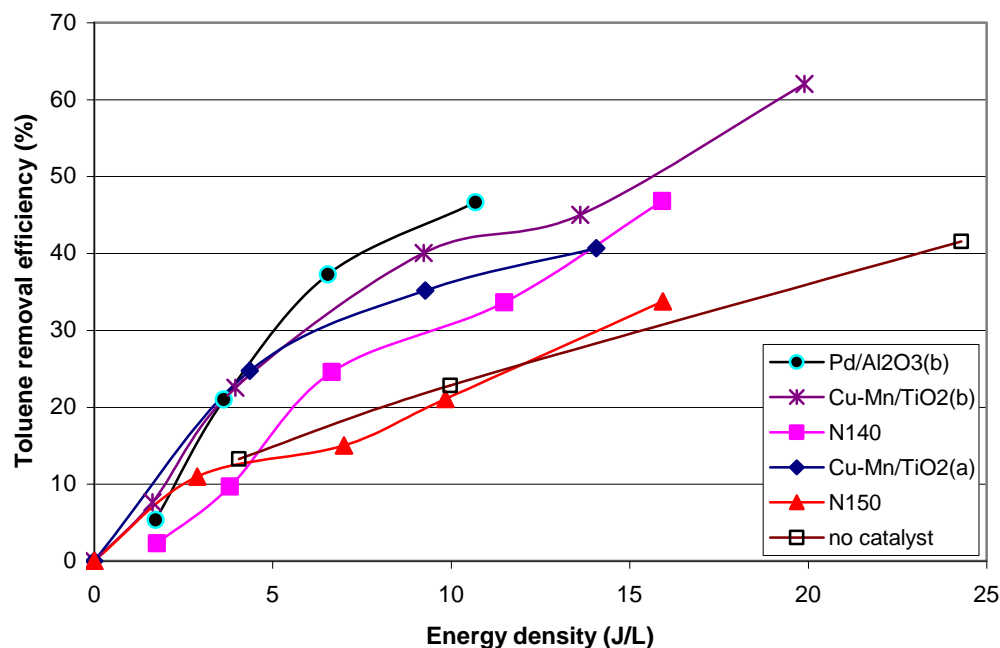
Figure 7.4 **Toluene degradation efficiencies in humid air (50% RH) for different catalysts (Pd/Al$_2$O$_3$(b), Cu-Mn/TiO$_2$(b), N140, Cu-Mn/TiO$_2$(a), N150) positioned in PPC (m$_{catalyst}$ = 15.0 g, Q=10.0 L min^{-1}, inlet concentration toluene = 0.5 ppm$_v$, T= 25°C, P= 101.3 kPa).**

It proves that significant differences in PPC toluene removal efficiency exist between the selected catalysts at an identical relative humidity (RH = 50% at T = 25°C). For example, the toluene removal efficiency obtained at an energy density of 4 J L^{-1} using Cu-Mn/TiO$_2$(a) and N140 as PPC catalysts amounts 25% and 10%, respectively. However, Figure 7.1 shows that both catalysts decompose a similar amount of ozone in dry air. As it was previously discussed, humidity has no influence on the ozone decomposition efficiency, suggesting a similar production of new oxygen active species from O$_3$, even under humid conditions.

It can be concluded that although toluene decomposition is related to ozone decomposition efficiencies for a given catalyst, differences between catalysts should also be explained by other processes playing an important role towards toluene decomposition.

A possible explanation can be found in the adsorption behavior of toluene on the catalyst. Indeed, the prerequisite for catalytic VOC decomposition is that molecules reach the catalyst interface, or at least contact a radical species formed within the boundary layer near the solid/gas interface (Zhang et al., 2007). On hydrophilic surfaces (such as most mineral oxides), the adsorption of water is hardly influenced by competing VOC. Water concentrations in indoor air are a factor of 10^6 greater than those of VOC. Next, due to strong hydrogen bonds the affinity of water to hydrophilic surfaces is larger than that of organic molecules (Goss, 2004). Therefore, the adsorption of organic molecules on hydrophilic surfaces is strongly determined by the presence of sorbed water. However, as far as we know, no specific data are available for VOC adsorption on the selected catalysts. Therefore, a detailed study on this partitioning process providing quantitative data is required to better understand the effect of RH on the toluene PPC removal.

7.3.3 Equilibrium sorption: effect of relative humidity.

Equilibrium adsorption constants (K) of three relevant indoor air pollutants (toluene, acetone, trichloroethylene) have been determined on two catalysts, i.e. Pd/Al_2O_3(b) and N150, under different humidity levels and using the EPICS methodology. These two catalyst were selected based on results shown in Figure 7.4, indicating respectively highest and lowest toluene degradation efficiencies in humid air (50% RH). Sorption results of both catalysts are represented in Table 7.1.

Table 7.1 Effect of relative humidity on the sorption coefficient K (mL g^{-1}) of toluene, trichloroethylene (TCE) and acetone on Pd/Al$_2$O$_3$(b) and N150 (n=3). VdW and electron donor/acceptor energies (mJ m^{-2})$^{0.5}$ of both PPC catalysts are included (P=101.3 kPa, T=25°C).

Catalyst	RH(%)	K$_{toluene}$ (mL g^{-1})	K$_{TCE}$ (mL g^{-1})	K$_{acetone}$ (mL g^{-1})	VdW$^{0.5}$ (mJ m^{-2})$^{0.5}$	HD$^{0.5}$ (mJ m^{-2})$^{0.5}$	HA$^{0.5}$ (mJ m^{-2})$^{0.5}$
Pd/Al$_2$O$_3$(b)	<1	62500 ± 600	12100 ± 900	103300±22700	10.2	4.0	4.2
	8	5020 ± 520	430 ± 20	19500 ± 1100	7.4	4.8	3.0
	17	1490 ± 180	350 ± 40	13200 ± 910	6.2	4.7	2.9
	31	790 ± 50	200 ± 20	5190 ± 420	5.6	4.3	2.6
	37	650 ± 50	180 ± 20	4300 ± 530	5.4	4.2	2.9
	55	180 ± 10	50 ± 10	2420 ± 180	4.0	4.7	2.1
N150	13	1960 ± 190	500 ± 50	22450 ± 2000	7.3	5.4	6.7
	31	900 ± 80	160 ± 15	13370 ± 1700	6.4	5.7	2.8
	55	250 ± 25	100 ± 10	1025 ± 85	5.7	3.6	5.4
	83	130 ± 20	30 ± 10	1130 ± 75	4.8	4.5	0.8

At humidity levels that do not result into a monolayer coverage of water molecules on the catalyst surface, a strong decrease of K with increasing RH is noticed. For example, the equilibrium sorption coefficient of toluene on Pd/Al$_2$O$_3$(b) in dry air (62500 ± 6000 mL g^{-1}) is reduced with a factor of 12 by increasing the RH to 8%. This may be explained by a competitive adsorption between water and target VOC molecules on unoccupied catalyst sites (Demeestere et al., 2003). Secondly, sorption equilibrium data obtained at relative humidities covering the catalyst surface with at least one water monolayer reveal another sorption behavior, characterized by a less pronounced decrease of K at increasing RH. Indeed, Goodman (2001) reported that a complete monolayer of water is adsorbed on an α-Al$_2$O$_3$ catalyst surface at RH = 17% and 296 K. Our results show that at this humidity level, the toluene sorption coeffient on PdAl$_2$O$_3$(b) amounts 1490 ± 200 mL g^{-1}. Increasing the RH to 31% decreases the K-value only by a factor of 1.9 (K = 790 ± 50 mL g^{-1}), whereas decreasing the RH to 8% leads to a 3.4 times higher K. At humidity levels covering the catalyst surface

with more than one monolayer of water, VOC can sorb on the water surface and/or dissolve in the bulk of this water film. According to Goss and Schwarzenbach (2002), adsorption onto the surface of the adsorbed water film is dominating even at the highest RH.

For all VOC-catalyst combinations, a logarithmic relationship is observed between the partitioning constant and the relative humidity (8% < RH < 83%) as exemplified by R² values of at least 0.927 (n=4) (Table 7.1). However, K-values determined at dry air conditions (RH ≤ 8%) do not fit to this logarithmic correlation, supporting the occurrence of two different sorption mechanisms depending on the humidity level and the water coverage of the surface.

Figure 7.5 shows that equilibrium sorption constants (K) and corresponding removal efficiencies (η) for toluene are logarithmically correlated for a constant energy density (R² ≥ 0.93, n = 4). This means that the highest VOC removal efficiency in hybrid plasma catalyst configurations are expected for catalysts and/or RH conditions that favour VOC adsorption. This is an important conclusion for the synthesis, selection and production of catalysts suitable for PPC. Given the results shown in Table 7.1, this also indicates that the PPC removal of acetone might be less affected by RH than those of more apolar compounds like toluene and TCE. Indeed, whereas the K-values of toluene and TCE on Pd/Al_2O_3(b) decrease by a factor up to 350 when increasing RH from <1% to 55%, the decrease of the acetone sorption coefficient in the same RH range is only a factor of 40.
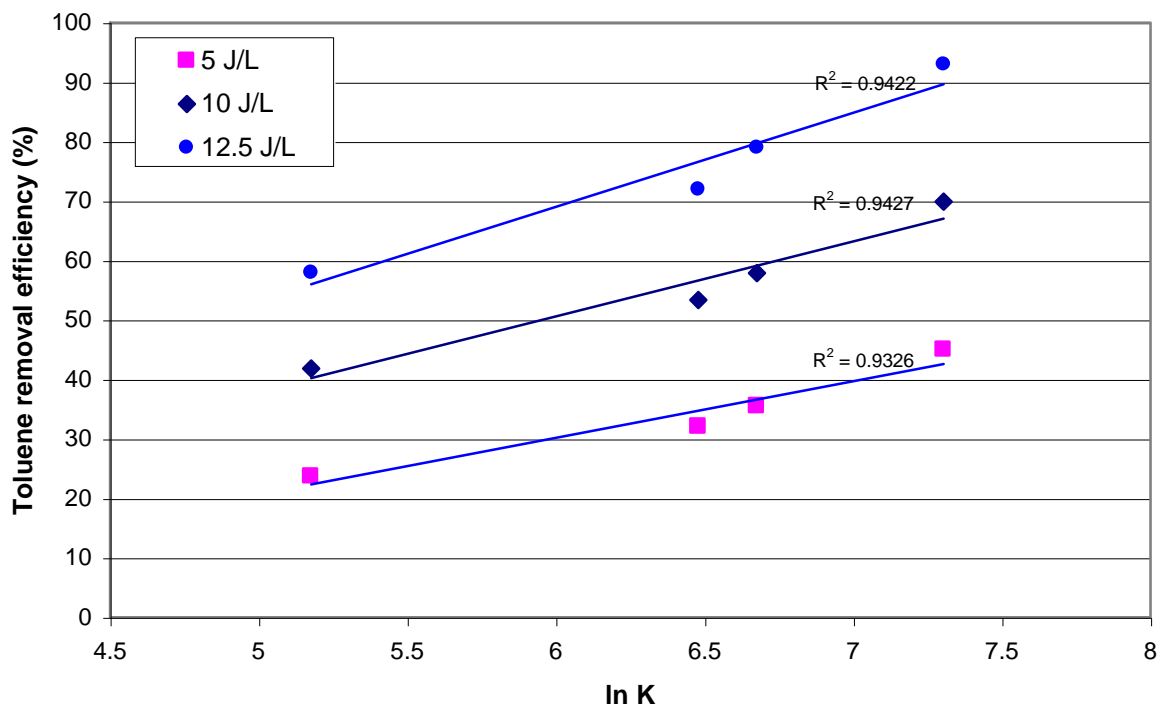
Figure 7.5   Toluene removal efficiency (%) with Pd/Al$_2$O$_3$(b) catalyst at different energy densities (5.0; 10.0; 12.5 J L^{-1}) (P= 101.3 kPa, T= 25°C) as a function of the equilibrium sorption coefficient (8% < RH ≤ 55%).

In order to better understand the sorption behavior of VOC on the (humid) catalyst surface, two kinds of interactions must be considered: (a) Van der Waals interactions (VdW) and (b) specific proton donor-acceptor (HD + HA) interactions (Goss and Schwarzenbach, 2002). The ability of a surface to interact with an adsorbate is dominated by the properties of its outermost molecular layer due to the exponential decrease of intermolecular interactions with distance and is quantified by the Van der Waals forces. Proton donor/acceptor properties are connected to a change in the orientation of the adsorbed water molecules (Goss and Schwarzenbach, 2002). The VOC equilibrium partitioning coefficient K between an air matrix and a mineral oxide surface is related to the total free energy of adsorption ΔG_{ads} (J mol^{-1}) (Demeestere et al., 2003), as given by

$$\Delta G_{ads}(J/mol) = -RT \ln \left[1.99 \, x10^8 (m^{-1}) K' \right] \tag{7.3}$$

with K´ (m³ m^{-2}) calculated from K (mL g^{-1}) and the specific BET surface area (m² g^{-1}) of the catalyst material. Based on thermodynamic parameters (Goss, 1997; Demeestere et al., 2003), a model was developed expressing ΔG_{ads} (J mol^{-1}) as;

$$\Delta G_{ads}(J/mol) = (-5092 + 324.1 \ln p_L^o)\sqrt{VdW_{surf}} - 5071\beta\sqrt{HD_{surf}} - 3344\alpha\sqrt{HA_{surf}}$$ (7.4)

where VdW$_{surf}$, HD$_{surf}$, HA$_{surf}$ (mJ.m^{-2}) characterize the ability of the surface to engage in Van der Waals, H-donor and H-acceptor interactions, respectively. Next, p$°_L$, α and β represent the saturated liquid vapour pressure (Pa), and the solvatochromic H-donor and H-acceptor parameters (dimensionless) of the adsorbing compounds, respectively (Abraham et al., 1994; Howard and Meylan, 1997). Values for the target VOC selected for our experiments are given in Table 7.2.

Table 7.2 Saturated liquid vapor pressures p$°_L$ (Pa) and dimensionless solvatochromic H-acceptor (α) and H-donor (β) values for acetone, TCE and toluene

VOC	p$°_L$ (Pa)	α (-)	β (-)	References
Acetone	30600	0.04	0.51	Goss (1994)
TCE	9200	0.08	0.03	Demeestere et al. (2003)
Toluene	3800	0	0.14	Demeestere et al. (2003)

From the equilibrium partitioning coefficients given in Table 7.1 and p$°_L$, α and β values given in Table 7.2, the surface parameters VdW$_{surf}$, HD$_{surf}$ and HA$_{surf}$ could be calculated according to equations 7.3 and 7.4. Based on these surface parameters, the relative importance of each type of interaction in the overall sorption process can be estimated. For the more apolar compounds such as toluene and TCE, the total free energy of adsorption ΔG_{ads} (J mol^{-1}) on both Pd/Al$_2$O$_3$(b) and N150 catalysts is mostly determined by Van der Waals interactions. This is exemplified by procentual contributions to the total free energy of adsorption ranging

between 74 and 93%, depending on RH. For acetone, Van der Waals interactions contributed to 36-62% of the total free adsorption energy, indicating more important H-donor interactions for polar compounds. In all cases, H-acceptor interactions proved to be negligible (contributions less than 10%).

Overall, it can be concluded that the humidity effect on sorption and thus on PPC (see Figure 7.5) is largely determined by VdW interactions. Indeed, Table 7.1 reveals that for both catalysts, VDW_{surf} systematically decrease at increasing RH, whereas the trend for HD_{surf} and HA_{surf} is less clear. In dry air (RH<1%), a $(VdW_{surf})^{0.5}$ value of 10.2 $(mJ\ m^{-2})^{0.5}$ was calculated for the $Pd/Al_2O_3(b)$ catalyst, being in good agreement with measurements of Goss and Schwarzenbach (2002) who reported that the $(VdW_{surf})^{0.5}$ values of a dry mineral oxide surface are in the range of 8-10 $(mJ\ m^{-2})^{0.5}$. Table 7.1 also shows $(VdW_{surf})^{0.5}$ values for $Pd/Al_2O_3(b)$ decreasing by a factor of 2.5 for a RH of 55%, approximating the $(VdW_{surf})^{0.5}$ value of bulk water 4.67 $(mJ\ m^{-2})^{0.5}$. This indicates again that the $Pd/Al_2O_3(b)$ catalyst is covered with multilayers of water at RH $\geq$ 55%, consequently minimalizing direct catalyst/VOC intermolecular interactions. Similar trends in $(VdW_{surf})^{0.5}$ are noticed for the N150 catalyst (e.g. $(VdW_{surf})^{0.5} = 4.8$ $(mJ\ m^{-2})^{0.5}$ for RH = 88%). Thus, the large contribution of VdW interactions to the total free energy of adsorption, next to the similar trends in $(VdW_{surf})^{0.5}$ and the toluene PPC removal, strongly indicates the importance of the $(VdW_{surf})^{0.5}$ parameter in further catalyst preparation and optimization for PPC applications.

7.4 Conclusions

In this chapter ozone and toluene removal is investigated using six different catalysts in post-plasma configuration. It is proven that the ozone removal efficiency is strongly correlated by the active compound of the tested catalysts. For the tested catalyst, the effect of humidity on ozone abatement ranged from negligible (e.g. $Pd/Al_2O_3(a)$) to a performance reduction (e.g. $CuOMnO_2/TiO_2(a)$).

In a second part it is discussed that for an equal amount of converted ozone, differences in corresponding toluene removal efficiency occur. This is for example the case for $CuOMnO_2/TiO_2(a)$ and N140, having a toluene removal efficiency at an energy density of 4 J L^{-1} of 25% and 4%, respectively. This reveals that not the amount of converted ozone, but VOC sorption is one of the most critical parameters determining the efficiency of catalytic VOC oxidation.

Equilibrium adsorption constants K of different catalyst were determined using EPICS methodology. Significant differences were measured between the several catalysts, next it was proven that the K values strongly decreased at increased humidities. For $Pd/Al_2O_3(b)$ the equilibrium adsorption constant was 12 times lower at 8% RH in comparison with that in dry air (62500 ± 6000 mL g^{-1}). A logarithmic correlation is found between equilibrium sorption constants and corresponding toluene removal efficiencies, explaining the observed differences at dry or humid condition between the tested catalysts.

Finally, it is concluded that the humidity effect on sorption and thus PPC is largely determined by VdW interactions.

Chapter 8

General discussion, conclusions and perspectives

In this dissertation the use of non-thermal plasma technology for indoor air cleaning is investigated. NTP performances were quantified based on VOC oxidation experiments and ozone production rates. One of the main accomplishments of this work is a strong improvement of energy efficiency, and thus mineralization achievements, due to the combination of NTP technology with heterogeneous catalysts. New insights have been achieved both on direct-plasma and on catalyst surface oxidation mechanisms.

In the first part of this work, the impact of indoor air pollution and related problems on both human health and economics were discussed. **Chapter 1** also summarizes technologies used nowadays to purify indoor air. Real-life testing of four economical indoor air cleaning devices revealed that they all were not able to reduce the indoor VOC concentration (VITO, 2008). In **Chapter 2** it was suggested that NTP technology offers major opportunities for treating polluted indoor air, especially in combination with heterogeneous catalyst materials. Surprising synergetic effects have been reported. Chapter 2 reviews the state-of-the-art of this hybrid plasma catalyst technology. This review focuses on changes of plasma properties caused by the insertion of catalyst material. These changing plasma characteristics eventually enhance the production of new active species, and thus increase the oxidation power of the plasma discharge. Similar, it is also discussed how plasma discharges on their turn affect catalyst properties. Finally, an overview of recent (2004-2007) published hybrid plasma catalyst configurations for VOC and nitrogen oxide abatement is given in this chapter.

In **Chapter 3** solid-phase dynamic extraction (SPDE) is explored as a sensitive preconcentrating sampling technique to detect low VOC levels in gas matrices. A continuous development of new analytical sampling techniques is essential to realize further indoor air related research. Therefore, a mechanistic study of this SPDE technique has been conducted, finally resulting in the development of "accelerated" SPDE, characterized by a limit of detection of 56 ppb_v and 38 times reduced sampling duration compared with that of

conventional SPDE sampling. By further optimization of post-sampling procedures such as injection procedure and detection method, ASPDE sampling will be applicable to measure VOC concentrations at sub-ppb$_v$ levels.

In **Chapter 4** the limits of application for a four pins-to-mesh reactor design were explored. Especially relative humidity, one of the most fluctuating parameters in indoor air, has shown to affect the characteristics and stability of the DC positive corona discharge design. Compared with measurements in dry air, discharge current at 60% RH decreased by a factor 2 (0.3 mA) at 18.4 kV. Generally, it can be concluded that operation of our plasma type at high humidities (> 80% RH at T = 298.15 K) is less stable and might even become problematic when condensation occurs on the electrodes.

In **Chapter 5** it was proven that the 4-pins-to-mesh reactor is able to oxidize low levels of toluene. Degradation experiments at 26% RH (T= 298.15 K) showed to be the most optimal; toluene conversion rates were reduced at higher humidity levels. This can be explained by two counteracting phenomena: reduced electron densities due to an enhanced number of electron attachment processes by water molecules, versus an increased hydroxyl radical production. The first process becomes dominant for high humidities. Plasma chemistry proves to be extremely complex and difficult to model or measure. The collection of accelerated electrons, nitrogen oxides, ozone, radicals and ions influence each other depending on internal and external conditions (temperature, pressure, humidity, electric field strength, pollutant types and concentrations, etc.). Despite this complexity, an effort has been done to avoid further black box thinking by investigating the toluene plasma oxidation mechanism based on the analysis of oxidation by-products. It would be of very high interest to continue this kind of research in order to better understand plasma technology. The development of ASPDE sampling procedure might prove to be an effective tool for further research here. In general, plasma oxidation can be assumed as an "accelerated" atmospheric chemistry.

Chapter 6 reports how plasma discharges in combination with heterogeneous catalysts, both in-plasma and post-plasma, strongly improve energy efficiency and reduce by-product formation. A negative influence of humidity was found on the hybrid plasma catalytic technology. Introducing semiconductors in the plasma zone remains very promising and requires further research. As it was also reviewed in Chapter 2, many of the hybrid plasma catalyst papers report on IPC. However, little information is available on the exact working principle of these in-plasma processes. Generally it is assumed that UV radiation is emitted by excited nitrogen molecules. However, since there are no indications of UV production in our experiments, is claimed that also other processes may be able to generate reactive electron-hole pairs. Similar conclusions have been observed by other researchers. Therefore, we highly recommend further research on the investigation of the relative importance of both semiconductor activation theories in order to better understand and optimize IPC technology.

In this work it was chosen to continue research using post-plasma catalysis (**Chapter 6** and Chapter 7). Since a negative affect of humidity was observed earlier, six catalyst types were tested for toluene oxidation using PPC (**Chapter 7**). Although ozone removal is influenced to a lower degree, each tested catalyst showed different toluene reduction performances at elevated water molecule concentrations. Based on sorption experiments it was concluded that corresponding VOC equilibrium sorption constants are correlated with the obtained toluene removal efficiency. This partitioning coefficient is mainly determined by Van der Waals interactions and is different for each catalyst. Therefore, it is suggested that further research on producing, selecting and testing new catalysts should focus on the sorption characteristic.

8.1 Critical analysis of hybrid plasma catalyst technology using S.W.O.T. approach

In this work it was proven that hybrid plasma catalyst technology has great potential to treat polluted indoor air. However, to determine whether it is useful to continue further research, a S.W.O.T. analysis has been applied. This is an often used strategic planning tool that evaluates the Strengths, Weaknesses, Opportunities, and Threats involved in a project or business venture. In Table 8.1., a modest S.W.O.T. analysis of hybrid plasma catalyst technology for indoor air treatment is given. This table will be used as a guideline for further discussion of perspectives and conclusions.

Table 8.1. S.W.O.T. analysis of hybrid plasma catalyst technology for the treatment of indoor air

STRENGHTS	WEAKNESSES

- **Reactor design**:
   - Compact
   - Modular (beneficial for upscaling)
   - No rotating parts
   - Low pressure drop
 	
- Wide **application range** (VOC, biological pollutants, PM)
 	
- **Technology**:
   - Innovation
   - Flexibility
   - Adaptability
 	
- Improvement of **human health** (ethical and market advantage)
 	
- **Economics**
 	
- **Market size**
	- **Reactor design**:
	   - high voltage
	   - mechanical reliability (catalyst deactivation, electrode aging)
	
	- Decreased performances at high **humidities** (e.g. swimming pool, bathrooms,…)
	
	- **Technology**:
	   - Process reliability
	   - In some cases possible necessity of filter media (increase of pressure drop and maintenance)
	
	- **Uncertainty** about by-product formation and mineralization rates

OPPORTUNITIES	THREATS

- increasing **market size**:
     - growing awareness of importance of IAQ
     - increasing fuel costs might result in inadequate ventilation of buildings
 	
 - **Operation cost** can be reduced by further developing IPC technology
 	
 - **Legislative initiatives**
	- Risk for **ozone** emission
	
	 - Lack of **customer's knowledge** and high number of **competitors** on market

For the *strengths* of hybrid NTP technology, its flexibility, adaptability, economics and market size will be discussed in more detail. The innovation and potential of the reactor design has is already been discussed in Chapter 4, while the application range and capabilities for improving human comfort has been thoroughly described in Chapter 1 and Chapter 2.

As *opportunity* the increasing market size is shortly discussed, it is clear that a correlation exists with growing legislation concerning indoor air quality (Chapter 1.6). It is also straightforward that further research (e.g. IPC) may result in a further increase of hybrid NTP performance. *Weaknesses* as the uncertainty of by-product formation (Chapter 5.3.2), high voltage (Chapter 4.1.1) and catalyst deactivation (Chapter 6.3.1.4) are mentioned earlier in this work. However, the mechanical and process reliability of the hybrid NTP technology will be discussed in this chapter. The *threats* as represented in Table 8.1 can be considered as straightforward and will not be discussed in more detail.

8.1.1 Strengths - Flexibility and adaptability

Flexibility and adaptability can be defined as the ability of a technology to handle wide fluctuations in the problem stream. The physical and chemical characteristics of indoor air strongly fluctuate. Plasma (catalytic) technology scores very high on flexibility since the produced radicals (e.g. hydroxyl radicals) are very reactive for a wide range of VOCs (non-

selectivity). Next, electric power applied to plasma sources can be easily adapted in order to respond to changing properties. As it will be discussed in Section 8.1.2.2., flexible technologies can be scaled up with little or no difficulty.

8.1.2 Strengths - Economic approach of hybrid plasma catalyst technology

Table 8.1. mentions that from an economic point of view, plasma catalysis scores high in a S.W.O.T. analysis. The following section is dedicated to the economics of our indoor air cleaning technology.

8.1.2.1   Comparing plasma technology with other advanced oxidation processes: energy requirements and economics

Several advanced oxidation processes can be selected, each of them sharing a common denominator of hydroxyl radical chemistry for VOC oxidation. Industrial applications of non-thermal plasma for gas treatment are slowly growing (Aerox NV, PLASMACAT, AAP, etc.). Important parameters influencing the selection of this technology include economics, economy of scale, regulations, effluent quality goals, operation (maintenance, control, safety) and robustness (flexibility to change). Although all these parameters are equally important, economics usually dominate. Therefore, an attempt has been made to compare NTP and hybrid plasma-catalyst technology with more accepted advanced oxidation processes. For gas treatment applications, possible AOP include homogeneous ultraviolet irradiation, ultraviolet irradiation mediated by ozone (UV/O$_3$) or H$_2$O$_2$ (UV/H$_2$O$_2$), heterogeneous photocatalysis using semiconductor catalysts (e.g. UV/TiO$_2$), electron beam irradiation, X-ray or gamma-ray radiolysis and non-thermal plasmas (Bolton et al., 2001). It is very difficult to compare different techniques by a common denominator since pollutant concentrations and/or

treatment goals strongly differ in the reported works. Indeed, for odor treatment a complete mineralization is not requested, a chemical conversion or partial oxidation can be sufficient to solve the problem. On the other hand, to meet emission standards, higher energies are necessary since an actual degradation (mineralization) is obligatory.

Bolton et al. (2001) also reported that a simple understanding of the overall kinetic behavior of VOC removal (whether zero or first order) is necessary for describing meaningful energy efficiencies. Rosenfeldt et al. (2006) calculated the amount of required energy to produce OH radicals available for VOC oxidation in water matrices. It is clear that this is the most promising tool for AOP screening. However, very detailed studies are required before this parameter can be applied to compare AOPs due to a high complexity and the non-complete understanding of their chemical and physical behavior. It is for example very critical to include hydroxyl radical scavenging in this kind of calculations, and today knowledge is inadequate to fulfill this, so further research on radical concentration quantification would be highly useful.

As an alternative, it was chosen to compare AOPs using the E_{EO} value, defined as the electric energy per concentration order (kWh m^{-3} order^{-1}). This tool was proposed the first time by Bolton et al. (2001), and is applied frequently in recent research papers (Lizama et al., 2002; Stefan and Bolton, 2005; Chen et al., 2007). The E_{EO} parameter gives a realistic estimation of energy requirements for electric-driven systems (AOP) and implies that it takes the same amount of energy to reduce the contaminant concentration for 100 ppb$_v$ to 10 ppb$_v$ in contaminated gas streams as it would to reduce it from 10 ppb$_v$ to 1 ppb$_v$. This E_{EO} parameter is based on the same idea as the characteristic energy ε_o in Chapter 5; however the latter energy parameter is usually used to compare plasma sources rather than different AOPs. E_{EO} is based on a simple mechanism that is applicable to most AOPs in air:

$$removal\ rate = -\frac{d\,[\overline{C}]}{dt} = \frac{\xi P k_C\,[\overline{C}]/V}{k_C\,[\overline{C}] + \sum_i k_{Si}\,[\overline{S}_i]} \tag{8.1}$$

With   P   electric power (W)

        V   treated volume (m³)

        k_C 2th order rate constant of active radical and VOC (M s^{-1})

        k_{Si} 2th order rate constant of active radical and scavenger i (M s^{-1})

        $[C_i]$ concentration of VOC (M)

        $[S_i]$ concentration of radical scavengers (M)

        ξ constant related to system and type of technology (mol s^{-1} W^{-1})

This means that for low concentrations (indoor levels) the conversion rate can be assumed as first order since $k_C[C] \ll \Sigma\ k_{Si}[S_i]$ and the removal rate equation can be written

as: $rate = -\dfrac{d\,[\overline{C}]}{dt} = \dfrac{\xi P k_C}{V\left(\sum_i k_{Si}\,[\overline{S}_i]\right)}[\overline{C}]$ $\tag{8.2}$

After integration, equation 8.2 can be rewritten as:

$$\ln\left(\frac{C_{in}}{C_{out}}\right) = \frac{\xi P k_C \tau}{V\left(\sum_i k_{Si}\,[\overline{S}_i]\right)} \tag{8.3}$$

with τ the residence time (s) in the AOT reaction zone. This parameter is inversely correlated with the gas flow rate Q which is defined as treated volume that is treated per second V τ^{-1} (m³ h^{-1}). Including this, together with a conversion factor of 0.435, equation 8.3. can be converted into a logarithmic equation as:

$$\log\left(\frac{C_{in}}{C_{out}}\right) = \frac{0.435\,\xi P k_C}{Q\left(\sum_i k_{Si}\,[\overline{S}_i]\right)} \tag{8.4}$$

Generally, E_{EO} values (kWh m^{-3} order^{-1}) for AOP flow-through operations can be calculated as:

$$E_{EO} = \frac{P}{Q\log(C_{in}/C_{out})} = \frac{\sum_i k_{Si}\,[\overline{S}_i]}{\xi k_c} \tag{8.5}$$

Like other gaseous advanced oxidation processes, non-thermal plasmas can also be monitored using this E_{EO} approach. To prove this, obtained toluene oxidation data using plasma alone or hybrid plasma catalyst technology (both in dry and humid conditions) were plotted as function of energy density ($= P \, Q^{-1}$) as represented in Figure 8.1.:
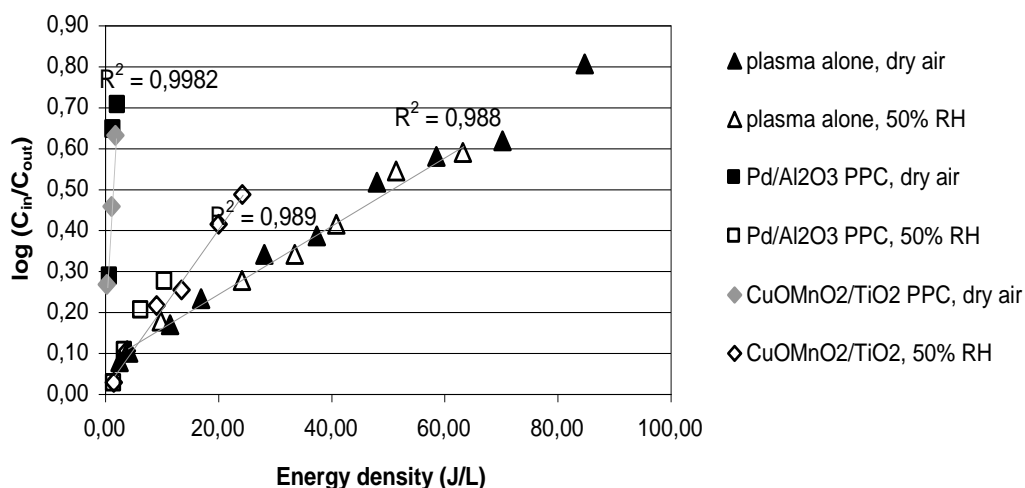
Figure 8.1. Linear relationship between energy density (J L^{-1}) and logarithm of ratio between inlet and outlet VOC concentration indicating first-order kinetics (Q = 10 L min^{-1}, p = 101.3 kPa, T = 298.15 K)

Figure 8.1. shows a first order relationship between $\log(C_{in}/C_{out})$ as function of energy density. Therefore electric energy per order (E_{EO}) (kWh m^{-3} order^{-1}) can be perfectly applied on plasma related experiments.

In Table 8.2, plasma alone and hybrid plasma catalyst technologies are compared with other AOP, such as UV, ozone/UV, ozone/UV/TiO$_2$ and UV/TiO$_2$. E_{EO} calculations are based on toluene oxidation results for flow-through reactor concepts. Toluene concentrations of all these techniques varied between 0 and 5 ppm$_v$.

Table 8.2. Comparison between AOP technologies applicable for indoor air cleaning purposes based on E_{EO} (kWh m^{-3} order^{-1}) concept.

AOP	$C_{in,tol}$ (ppb$_v$)	P (W)	Q (m³ s^{-1})	$C_{out,tol}$ (ppb$_v$)	E_{EO} (kWh m^{-3} order^{-1})	Reference
Plasma alone (dry air)	500,0	2,9	1,670E-04	290,0	2,650E-02	This work
Plasma alone (50% RH)	500,0	4,1	1,670E-04	270,0	2,720E-02	This work
Plasma Pd/Al$_2$O$_3$ (dry air)	500,0	0,4	1,670E-04	100,0	8,560E-04	This work
Plasma Pd/Al$_2$O$_3$ (50% RH)	500,0	1,8	1,670E-04	270,0	9,870E-03	This work
Ozone/UV (35% RH)	5000,0	18,2	5,000E-05	1600,0	1,218E-01	Pengyi et al. (2003)
Ozone/UV/TiO$_2$ (35% RH)	5000,0	18,2	5,000E-05	645,0	6,814E-02	Pengyi et al. (2003)
UV/TiO$_2$ (dry air)	250,0	75,0	3,780E-01	230,0	1,522E-03	Chen and Zhang (2008)
UV/TiO$_2$ (47% RH)	26,0	18,0	5,000E-07	9,6	2,311E+01	Demeestere et al. (2008)
UV (dry air)	600,0	4,0	6,670E-05	230,0	4,000E-02	Jeong et al. (2005)

It is clear that plasma related technologies prove to be cost efficient for the abatement of low concentrations toluene when compared with other techniques. It has to be remarked that this statement is especially true for low contaminated streams.

8.1.2.2 Upscaling and cost estimation

As already discussed in Chapter 1 indoor air VOC concentrations strongly fluctuate for each building. Measured indoor levels are the result of a steady-state between VOC emission by multiple indoor sources (Chapter 1) and VOC removal as a result of mechanical or natural ventilation. Especially in new or renovated buildings mechanical ventilation systems are often installed to guarantee a good IAQ. A study by Chao and Chan (2001) revealed that even for high ventilated buildings (air exchange rate > 1 h^{-1}) toluene and TVOC concentrations are quantified (Table 8.3.). As already mentioned in Chapter 1 officially recommended indoor air concentration guidelines are not translated yet in international legislation. Tentative levels of concern for TVOC amount of $200 - 300$ µg m^{-3} have been suggested by Guo et al. (2003). Table 8.3 shows that in both office as non-office buildings average TVOC values exceeded this guideline.

Table 8.3. Toluene and TVOC concentrations (µg m^{-3}) in well ventilated office and non-office buildings (Chao and Chan, 2001).

Room type	air exchange rate (h^{-1})	Concentration range (µg m^{-3})	TOLUENE Mean concentration (µg m^{-3}) (n=10)	TVOC Mean concentration (µg m^{-3}) (n=10)
Office	1.7 ± 0.9 (n = 10)	10.6 – 214.8	52.8	316.4
non-office	1.9 ± 0.8 (n = 10)	12.8 – 678.4	206.3	518.2

In Flanders the indoor air quality guideline for toluene was set at 260 µg m^{-3} (Stranger et al., 2007). Table 8.3 again shows that at least one non-office building exceeds this guideline by a factor of almost three. It has to be mentioned that the largest fraction of non-office buildings has no mechanical ventilation system; resulting TVOC (and thus toluene) concentrations can be very high. In table 1.1. it is shown that a maximum indoor toluene concentration of 36,970 µg m^{-3} has been measured.

In this work the reactor was designed to treat gas flow rates of 10 L min^{-1} (0,6 m³ h^{-1}). To estimate the operation costs of the hybrid plasma catalytst technology for indoor air cleaning, a well ventilated room with a volume of 200 m³ (length 10 m, width 10 m, height 2 m) was used as a standard room. This building is supposed to be contaminated with a toluene air concentration of 678.4 µg m^{-3}. Based on results as represented in Table 8.3, it can be carefully assumed that these conditions are valid for at least 10% of present mechanically ventilated buildings. To meet indoor quality guidelines for toluene concentration (260 µg m^{-3}), a toluene reduction with of 0.38 concentration order has to be achieved. Since it is advisable to have one air exchange each hour; consequently the lab setup should be scaled-up in order to handle gas flow rates of 200 m³ h^{-1}. Assuming 12 hours of operation per day, 350 workings days per year and an average energy cost of 0.06 € kWh^{-1} for industry (Electrabel, 2008), the calculated total cost for electricity based on the E_{EO} value for the PPC reactor concept (data from 50% RH, Table 8.2) would be:

$$\text{Annual operation cost} \left(\frac{euro}{year}\right) = 9.870 \text{ x}10^{-3} \frac{kWh}{m^3 order} \text{ x } 0,38 \text{ } order \text{ x } 200 \frac{m^3}{hour} \text{ x } 12 \frac{hour}{day} \text{ x } 350 \frac{day}{year} \text{ x } 0.06 \frac{euro}{kWh}$$

$$= 189 \frac{euro}{year}$$

When the standard office is occupied by ten people, this would mean an energy cost of 19 € person^{-1} year^{-1} to guarantee good indoor air quality.

As mentioned during the S.W.O.T. analysis, plasma catalyst hybrid technology is a flexible AOP and can be scaled-up easily. To upscale the lab reactor so that the flow rate of 200 m³ h^{-1} can be treated the mesh radius would be multiplied by a factor 7 (resulting diameter 28 cm) and keeping an identical pin number/mesh area ratio, gas flow rates of 29.4 m³ h^{-1} can be treated. Next, by placing 8 reactor modules in series (instead of 2), gas flow rates of 120 m³ h^{-1} can be treated. With these adaptations the residence time in the plasma zone does not change. Increasing gas flow rates by a factor 2 is possible when the applied energy density is equally increased so that the plasma reactivity remains constant (see Chapter 4; effect of gas flow rate). In conclusion, by increasing the reactor dimensions, increasing the number of pins, placing more modules in series, increasing gas velocity through the reactor, and simultaneously increasing the applied energy density, gas flow rates of 200 m³ h^{-1} can eventually be treated with a reactor that remains considerably compact. Since the plasma section is upscaled, the amount of inserted post-plasma catalysts have to be increased accordingly. Literature reveals that this should not be a problem; Jeong et al. (2005) reported that despite a reduced contact time in the gas phase when increasing flow rate, the same level of VOC conversion could be maintained for (photo)catalytic oxidation processes. This can be explained by an increased contact time between reactants and catalysts due to creating a turbulent flow regime in the catalyst bed.

8.1.3 Strenghts - Market size

Experts predict that the overall US indoor air quality market alone, worth US$ 5.6 billion in 2003, will rise at an average annual growth rate of 11.1% to US$ 9.4 billion by 2008 (BBC, 2006). Currently, the end-use markets with the largest potential include residential dwellings, commercial buildings, schools and health care facilities. Next, also during industrial production processes highly clean air is often required (e.g. clean rooms) (BBC, 2005). Research revealed that the commercial segment was the largest market for IAQ equipment and services, accounting for 26% of the US market in 2005.

The most recent series of indoor air cleaners is mostly based on photocatalysis using TiO_2 irradiated by UV light. Recently Daikin develops, manufactures and markets indoor air purifiers and sold more than 300,000 units in Japan during 2004 (Daikin, 2008).

8.1.4 Opportunities - Market size

Although today, national legislation to control and improve indoor air quality has not matured yet to garantee a healthy indoor air. It can be highly expected that the number of regulatory initiatives for indoor air quality guidelines is increasing (Chapter 1.6). Consequently, a growing market size can be expected in near future.

8.2 Perspectives and future research – Handling opportunities, weaknesses and threats

In order to improve our reactor concept, weaknesses and opportunities (Table 8.1.) should be converted into strengths by doing further research and development. Threats however, are negative properties of a technology that can not be avoided. However, choosing the right safety measures, good engineering and commercial style, these threats should not be considered as risks to commercialize hybrid plasma catalyst technology for indoor air cleaning. In this section some weaknesses will be highlighted and perspectives and future research will be formulated. It has to be noted that several of the weaknesses and opportunities have been discussed in this chapter earlier (e.g. need for further research on IPC, problem of humidity, economics, market size, etc.)

8.2.1 Weakness – Mechanical reliability

Reliability of AOP technologies can be measured by the frequency of technical failure. This parameter can be considered as a weakness for plasma technology since the specialty parts and equipment requires experts for maintenance. Further work has to be conducted to improve this weakness, both on catalyst deactivation and on electrode sputtering (Figure 8.2.).
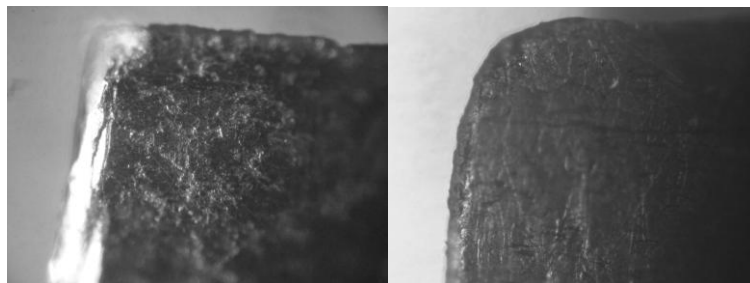

Figure 8.2. Electrode sputtering; comparison between new (left) and used (right) pin electrode

In Chapter 6 some conclusions have been made on catalyst deactivation by nitrate deposition. However, until now there was no knowledge on how PPC catalysts would behave during long-term experiments. Secondly, the lifetime of the electrodes may be a critical parameter since it is known that impact-reactions of highly energetic electrons might cause sputtering of the metal material used (Soldera et al., 2005) (Figure 8.2.). A sharp cathode electrode is needed to create a sufficiently strong electric field. Pin erosion and flattening might eventually stop plasma generation. This effect has been observed using copper pin electrodes on a relatively small time scale. For stainless steel electrodes no short-term effects are observed, effects on long-term should be investigated.

8.2.2 Weakness - Process reliability

Process reliability can be defined as the ability of a given technology to consistently meet effluent goals. Today, insufficient research of the PPC technology has been done to guarantee a high process reliability since it has not been investigated whether also particulate matter, micro organisms, viruses,… are efficiently removed from indoor air. Expectations are positive since plasma sterilization has been reported earlier as a simple and efficient way of killing bacteria (Ekem et al., 2006; Choi et al., 2006; Xu et al., 2006). Next, the charge transfers between the plasma reactor electrodes will also function as a small electrostatic precipitator. This means that particulate matter and aerosol probably will be withdrawn and precipitate on the electrodes. Whether the particulate matter will be collected until problems occur, or they are collected and oxidized due to the extremely high concentrations of reactive species at the electrode surface, remains a question that should be answerd by further research. Recently Chen and Zhang (2008) also reported negative interferences when tests were conducted using a multiple VOC mixture. Further research on these topics could be of high importance.

To conclude, a study of Howard-Reed et al. (2005) made clear that factors such as air cleaner location, status of the heating and air conditioning system, relative humidity and temperature affect the air cleaner performance. Real-life measurements and/or the development and evaluation of models (such as CONTAM (Howard-Reed et al., 2007) might be effective tools for predicting and improving indoor air cleaner performances (Rifat and Zhao, 2007). Accordingly, Ao and Lee (2005) dedicate their research to investigate whether the enhancement effect of the TiO_2/AC shown in the laboratory experiments is also verified by installing it into a commercial indoor air cleaner. Sun et al. (2008) concluded that there is an urgent need for defining parameters and establishing correlations between subjective assessments and objective concentrations.

Summary

Summary

Indoor air is often of poor quality due to the construction of airtight buildings and an increasing amount of indoor pollution sources. Since people spend around 85% of their time in enclosed environments, health effects caused by an inadequate indoor air quality have been proven. A summary of relevant indoor air pollutants and their sources is provided in Chapter 1. Indoor air quality is determined by physical (temperature, light, relative humidity) and chemical parameters (organic and inorganic pollutants, particulate matter, biological pollutants). This work, however, focuses on the presence of VOC in indoor air. Literature reviews revealed that up to 900 indoor VOC can be detected of which more than 350 compounds have concentrations exceeding 1 ppb_v.

Non-destructive techniques such as mechanical and electronic filtration or chemisorption, are not efficient for treating indoor air quality. Therefore, in recent years, advanced oxidation processes receive growing attention due to their potential for degrading a wide range of VOC at mild conditions. In Chapter 2, non-thermal plasma technology is defined as a promising technology to clean indoor air. However, a more effective use of plasma is possible by exploiting its inherent synergetic potential through combination with heterogeneous catalysts. In a second part, Chapter 2 reviews the state-of-the-art of this hybrid plasma catalyst technology. This review focuses on changes of plasma properties caused by the insertion of catalyst material. These changing plasma characteristics eventually enhance the production of new active species, and thus increase the oxidation power of the plasma discharge. Similar, it is also discussed how plasma discharges on their turn affect catalyst properties. Finally, an overview of recent (2004-2007) published hybrid plasma catalyst configurations for VOC and nitrogen oxide abatement is given in this chapter.

In Chapter 3, solid-phase dynamic extraction (SPDE) is investigated for the first time as an innovative technology for VOC sample preparation and enrichment technique. A home made sampling device is constructed to make a detailed study of SPDE kinetics for toluene extraction. It is proven that multiple aspirating and dispensing cycles were necessary to obtain toluene equilibrium between gas and coating phase. A mechanistic model is proposed to explain that in every dispensing step during SPDE, significant losses of retained analytes occur due to desorption processes. A new accelerated solid-phase dynamic extraction procedure (ASPDE) has been developed, which proved to have high potential in ambient/indoor air monitoring, being a factor of 6 and 35 more sensitive than SPME and conventional gas syringe sampling.

In Chapter 4 it is chosen to operate a discharge in a positive streamer regime using a 4-pins-to-mesh plasma reactor. It is concluded that particularly humidity affected the plasma discharge characteristics. For an applied voltage of 18,4 kV, a current of 0,6 mA is measured in dry air, while this was only 0,3 mA for 60% relative humidity. It is also revealed that nitrogen monoxide is almost instantaneously converted in nitrogen dioxide. For an energy density of 10 J L^{-1}, NO_2 outlet concentrations are 1500 ppb$_v$ and 500 ppb$_v$ at dry air and 50% RH, respectively.

In Chapter 5, the plasma reactor is tested for toluene oxidation, toluene removal efficiencies prove most optimal at a relative humidity of 26%. A further increase of the humidity proves to result in an adverse effect. Two phenomena explain this behavior; while water is partially dissociated in the plasma discharge producing more hydroxyl radicals, high water concentrations reduce electron concentrations by an increased amount of electron attachment processes. During toluene oxidation experiments, reaction products such as formic acid, benzaldehyde, benzyl alcohol, nitrophenols,… were identified. Based on this information, a

plasma toluene degradation mechanism is proposed for the first time, with hydroxyl radicals playing a major role in initiating H-abstraction and OH-addition.

In Chapter 6, in-plasma (IPC) and post-plasma (PPC) catalysis is investigated for two reasons; reducing the amount of by-products (e.g. ozone, nitrogen oxides, partially oxidized hydrocarbons) and improving the VOC abatement efficiency. Introducing a TiO_2 catalyst in-plasma is not effective in ozone reduction, while adding only 10g of $CuOMnO_2/TiO_2$ in post-plasma position results in a reduction of the ozone outlet concentration by a factor 7. Both heterogeneous catalysts (TiO_2 and $CuOMnO_2/TiO_2$) prove capable to reduce NO_x levels in the outlet gas stream by up to 90%. Compared with plasma alone and for dry air, toluene (C_{in} = 0.5 ppm_v) is removed more efficiently by introducing Aerolyst 7706 TiO_2 (IPC). However, best results are obtained by inserting 10 g $CuOMnO_2/TiO_2$ down flow the plasma reactor modules (PPC): resulting toluene removal efficiencies range up to 40 times higher. In humid gas streams, PPC toluene removal efficiency decreases by competitive adsorption. In Chapter 6 it is explained that deactivation of the catalyst material is the result of the formation of HNO_3 in the plasma discharge. These molecules adsorb on the catalyst, surface nitrate ion concentrations were 0.184 mg/m² and 0.143 mg/m² for TiO_2 and MnO_2-CuO/TiO_2 catalysts respectively.

In Chapter 7, six catalysts are tested downstream a DC corona discharge. Their chemical composition proved to have a strong impact on the PPC ozone removal performance. Despite the effect of humidity proves to be moderate for ozone degradation (Chapter 6 and Chapter 7), a more pronounced limiting effect is observed on post-plasma catalytic toluene removal. Sorption measurements using EPICS methodology revealed that toluene equilibrium constants and corresponding removal efficiencies are logarithmically correlated (R^2= 0.966 ±0.012 (n=4)). Based on sorption data, Van der Waals and electron-donor/acceptor interactions are calculated, both proved to be strongly affected by humidity. For Pd/Al_2O_3

catalyst, Van der Waals values are 7.4, 6.2, 5.6, 5.4 and 4 $(mJ/m^2)^{0.5}$ for relative humidities of respectively 8, 17, 31, 37 and 55%.

Chapter 8 includes the general discussion, conclusions and perspectives. Based on a S.W.O.T. analysis the strengths, weaknesses, opportunities and threats of hybrid plasma catalyst technology is discussed.

Samenvatting

Samenvatting

Onvoldoende ventilatie en het stijgend aantal emissiebronnen binnenshuis resulteren in een slechte binnenluchtkwaliteit. Aangezien mensen ongeveer 85% van hun tijd binnenskamers doorbrengen, kunnen gezondheidseffecten gecorreleerd worden aan deze onvoldoende binnenluchtkwaliteit. In Hoofdstuk 1 worden de meest relevante binnenluchtpolluenten en hun respectievelijke bronnen samengevat. Binnenluchtkwaliteit wordt bepaald door fysische (temperatuur, licht, relatieve luchtvochtigheid) en chemische parameters (organisch en anorganische polluenten, particulair materiaal, biologische polluenten). In dit werk wordt de focus echter gelegd op de aanwezigheid van VOC in binnenlucht. Literatuuronderzoek toonde immers aan dat tot 900 verschillende VOC in binnenlucht kunnen gedetecteerd worden, waarvan meer dan 350 verbindingen met concentraties hoger dan 1 ppb$_v$.

Niet-destructieve technieken zoals mechanische en elektrische filtratietechnieken of chemisorptie, blijken niet efficient voor het behandelen van binnenlucht. Daarom wordt de laatste jaren steeds meer aandacht gegeven aan onderzoek op geavanceerde oxidatie processen. Deze technologie is namelijk in staat een groot gamma VOC af te breken in atmosferische omstandigheden. In Hoofdstuk 2, wordt niet-thermisch plasma beschreven als een veelbelovende technologie om binnenlucht te zuiveren. Een efficiëntere toepassing van plasma is realiseerbaar wanneer gecombineerd met heterogene katalysatoren. In een tweede deel van Hoofdstuk 2 wordt de stand-van-zaken van deze hybride plasma katalysator technologie beschreven. Deze review focust zich onder andere op de invloed van katalysatoren op de plasma karakteristieken. De gewijzigde plasma eigenschappen kunnen de vorming van nieuwe reactieve species positief beïnvloeden, en bijgevolg het totale oxidatieve vermogen van een plasma-ontlading aanzienlijk verhogen. Er wordt echter ook besproken hoe plasma-ontladingen op hun beurt katalysator eigenschappen kunnen veranderen. Tot slot

wordt in dit hoofdstuk een overzicht gegeven van recente (2004-2007) publicaties omtrent hybride plasma katalysator technologie toegepast voor VOC en stikstofoxide verwijdering.

In Hoofdstuk 3, wordt Solid-Phase Dynamic Extraction (SPDE) voor de eerste keer onderzocht als een opconcentrerende VOC bemonsteringstechniek. Een home-made bemonsteringstoestel werd ontworpen om de SPDE kinetiek tijdens tolueen extractie te kunnen bestuderen. Er is aangetoond dat meerdere opzuigende en uitblazende stappen nodig zijn voordat tolueenconcentraties tussen gas- en coatingfase in evenwicht zijn. Door middel van een mechanistisch model is aangetoond dat tijdens elke uitblazende stap, desorptieprocessen resulteren in een significante verlies aan gesorbeerde massa. Uiteindelijk is een versnelde Solid-Phase Dynamic Extraction (ASPDE) ontwikkeld: uit metingen blijkt ASPDE een factor 6 en 35 efficiënter te zijn dan SPME en conventionele gasspuit monstername.

In Hoofdstuk 4 is gekozen om met een positieve streamer ontlading te werken die gegenereerd wordt door middel van een 4-pins-rooster plasma reactor. Er is waargenomen dat vooral luchtvochtigheid een sterke invloed heeft op de plasma-karakteristieken. Bij een spanning van 18,4 kV, wordt een stroomsterkte van 0,6 mA gemeten in droge lucht, terwijl dit slechts 0,3 mA blijkt wanneer de relatieve luchtvochtigheid 60% bedraagt. Uit metingen blijkt dat stikstofmonoxide nagenoeg ogenblikkelijk wordt omgezet in stikstofdioxide. Voor een energiedensiteit van 10 J L^{-1}, bedragen NO_2 uitlaatconcentraties respectievelijk 1500 ppb$_v$ en 500 ppb$_v$ in droge en 60% RV lucht.

In Hoofdstuk 5 is de plasmareactor getest voor tolueenoxidatie. Tolueenafbraak blijkt het meest optimaal in lucht met een relatieve luchtvochtigheid van 26%. Het verder opdrijven van de luchtvochtigheid blijkt echter tot een omgekeerde effect te leiden. Twee processen kunnen dit verklaren; enerzijds wordt water deels gedissocieerd in de plasma-ontlading met vorming van hydroxylradicalen, anderzijds reduceren hoge concentraties watermoleculen de totale

elektronenconcentratie door frequentere elektronenaanklampingsprocessen. Tijdens tolueenoxidatie-experimenten zijn de belangrijkste reactieproducten geïdencifeerd waaronder azijnzuur, benzaldehyde, benzylalcohol, nitrofenolen,... Op basis van deze informatie, is voor de eerste keer het reactiemechanisme voorgesteld waarop tolueen door een niet-thermisch plasma afgebroken wordt. Hydroxylradicalen blijken een belangrijke rol te spelen via H-abstractie en OH-additie processen.

In Hoofdstuk 6, is in-plasma (IPC) en post-plasma (PPC) katalyse onderzocht om twee redenen: het reduceren van bijproducten (bv. ozon, stikstofoxides, VOC oxidatieproducten) en een verbetering van de VOC afbraak-efficiëntie. Er is aangetoond dat het introduceren van TiO_2 in de plasmazone niet resulteert in ozonreductie. Het toevoegen van slechts 10g $CuOMnO_2/TiO_2$ in post-plasma positie doet de ozon uitlaatconcentratie weliswaar met een factor 7 dalen. Beide heterogene katalysatoren (TiO_2 en $CuOMnO_2/TiO_2$) blijken in staat te zijn NO_x af te breken met een verwijderingsefficiëntie tot 90%. In droge lucht kan tolueen (C_{in} = 0,5 ppm_v) efficiënt verwijderd worden door het introduceren van de Aerolyst 7706 TiO_2 (IPC). De beste resultaten zijn weliswaar opgemeten na het toevoegen van 10 g $CuOMnO_2/TiO_2$ in post-plasma positie (PPC). De tolueenverwijderingsefficientie van de PPC configuratie blijkt tot 40 keer hoger te zijn dan met plasma alleen. In vochtige gasstromen, daalt de PPC tolueenverwijdering echter door competitieve adsorptie. In Hoofdstuk 6 wordt ook beschreven dat de desactivatie van katalysatoren veroorzaakt kan zijn door de vorming van HNO_3 in de plasma-ontlading. Deze molecules blijken immers op het katalysator-oppervlak te adsorberen, gemeten nitraation-concentraties op TiO_2 en MnO_2-CuO/TiO_2 katalysatoren zijn bijvoorbeeld 0.184 mg/m² en 0.143 mg/m².

In Hoofdstuk 7 zijn zes katalysatoren getest stroomafwaarts de DC corona ontlading (PPC). Er is aangetoond dat de chemische samenstelling van deze katalysatoren de PPC ozon verwijderingefficiëntie sterk beïnvloeden. Terwijl het effect van vocht niet belangrijk blijkt

voor ozondegradatie (Hoofdstuk 6 en Hoofdstuk 7), is een limiterend effect waargenomen op PPC tolueenverwijdering. Sorptiemetingen gebaseerd op de EPICS methodologie toonden aan dat tolueenevenwichtsconstanten en corresponderende tolueenverwijderingefficiënties logaritmisch gecorreleerd zijn ($R^2= 0.966 \pm 0.012$ (n=4)). Op basis van sorptiemetingen, zijn Van der Waals en electron-donor/acceptor interacties berekend. Beide parameters worden sterk beïnvloed door de luchtvochtigheid. Voor een Pd/Al_2O_3 katalysator blijken Van der Waals waarden bijvoorbeeld 7.4, 6.2, 5.6, 5.4 and 4 $(mJ/m^2)^{0.5}$ bij luchtvochtigheden van respectievelijk 8, 17, 31, 37 and 55%.

Hoofdstuk 8 bevat de algemene discussie, conclusies en toekomstperspectieven. Op basis van een S.W.O.T. analyse worden de sterktes, zwaktes, mogelijkheden en bedreigingen van hybride plasma katalyse technologie besproken.

Bibliography

Bibliography

Abraham M.H, Andonianhaftvan J., Whiting G.S., Leo A. and Taft R.S. (1994). Hydrogen-bonding, the factors that influence the solubility of gases and vapors in water at 298-K, and a new method for its determination, Journal of the Chemical Society-Perkin Transactions, 2(8), 1777-1791.

AERIAS (2008) Data supplied by Air Quality Sciences from more than 3000 indoor locations, analyzed by mass spectrometry, URL: http://www.aerias.org

Akyuz M., Cortet P.P. and Cooray V. (2005). Positive streamer discharges along liquid dielectric sufraces: effect of dielectric constant and surface properties, IEEE Transaction on Dielectrics and Electrical Insulation, 12(3), 579-585.

Albering H.J., Hoogewerff J.A. and Kleinjans J.C.S. (1996). Survey of Rn-222 concentrations in dwellings and soils in the Dutch Belgian border region, Health Physics, 70(1), 64-69.

Ao C.H. and Lee S.C. (2005). Indoor air purification by photocatalyst TiO_2 immobilized on an activated carbon filter installed in an air cleaner, Chemical Engineering ScienceVolume 60 (1), 103-109.

Ao C.H., Lee S.C., Mak C.L. and Chan L.Y. (2003). Photodegradation of volatile organic compounds (VOCs) and NO for indoor air purification using TiO_2: promotion versus inhibition effect of NO, Applied catalysis B: environmental, 42, 119-129.

Ao C.H., Lee S.C., Yu J.Z. and Xu J.H. (2004). Photodegradation of formaldehyde by photocatalyst TiO_2: effects on the presences of NO, SO_2 and VOCs, Applied catalysis B: environmental, 54, 41-50.

Atkinson R, Aschmann S.M. and Pitts J.N. (1988). Rate Constants for the Gas-Phase Reactions of the NO_3 Radical with a Series of Organic-Compounds at 296 ± 2 K, Journal of Physical Chemistry, 92(12), 3454-3457.

Atkinson R, Baulch D.L., Cox R.A., Crowley J.N., Hampson R.F., Hynes R.G., Jenkin M.E., Rossi M.J. and Troe J. (2004). Evaluated kinetic and photochemical data for atmospheric

chemistry: Volume I - gas phase reactions of O_x, HO_x, NO_x and SO_x species, Atmospheric Chemistry and Physics, 4, 1461-1738.

Atkinson R, Baulch D.L., Cox R.A., Hampson R.F., Kerr J.A., Rossi M.J. and Troe J. (2000). Evaluated kinetic and photochemical data for atmospheric chemistry: Supplement VIII, halogen species - IUPAC Subcommittee on Gas Kinetic Data Evaluation for Atmospheric Chemistry, Journal of Physical and Chemical Reference Data, 29(2), 167-266.

Atkinson R. and Arey J. (2003). Gas-phase tropospheric chemistry of biogenic volatile organic compounds: a review, Atmospheric Environment, 37(2), 197-219.

Atkinson R. and Arey J. (2007). Mechanisms of the gas-phase reactions of aromatic hydrocarbons and PAHs with OH and NO_3 radicals, Polycyclic Aromatic Compounds, 27(1), 15-40.

Baltussen E., Cramers C.A. and Sandra P.J.F. (2002). Sorptive sample preparation - a review, Analytical and Bioanalytical Chemistry, 373(1-2), 3-22.

Bartolotti L.J. and Edney E.O. (1995). Density functional theory derived intermediates from the OH initiated atmospheric oxidation of toluene, Chemical Physics Letters, 245, 119-122.

BBC Report (2005). U.S. Indoor Air Quality Market and Trends, p. 189.

Berry D., Mainelis G. and Fennell, D. (2007). Effect of an ionic air cleaner on indoor/outdoor particle ratios in a residential environment, Aerosol Science and Technology, 41(3), 315-328.

Bicchi C., Cordero C., Liberto E., Rubiolo P., Sgorbini B. (2004). Automated headspace solid-phase dynamic extraction to analyse the volatile fraction of food matrices, Journal of Chromatography A, 1024(1-2), 217-226.

Blin-Simiand N., Tardiveau P., Risacher A., Jorand F. and Pasquiers S. (2005). Removal of 2-heptanone by dielectric barrier discharges - The effect of a catalyst support, Plasma Processes and Polymers, 2(3), 256-262.

Boeniger M.F. (1995). Use of Ozone Generating Devices to Improve Indoor Air-Quality, American Industrial Hygiene Association Journal, 56(6), 590-598.

Bolton J.R., Bircher K.G., Tumas W. and Tolman C.A. (2001). Figures-of-merit for the technical development and application of advanced oxidation technologies for both electric- and solar-driven systems, Pure and Applied Chemistry, 73, 627-637.

Brown S.K., Sim M.R., Abramson M.J. and Gray C.N. (1994). Concentrations of Volatile Organic-Compounds in Indoor Air - a Review, Indoor Air, 4(2), 123-134.

Brownson R.C., Figgs L.W. and Caisley L.E. (2002). Epidemiology of environmental tobacco smoke exposure, Oncogene, 21(48), 7341-7348.

Carrer P., Maroni M., Alcini D. and Cavallo D. (2001). Allergens in indoor air: environmental assessment and health effects, Science of the Total Environment, 270 (1-3), 33-42.

CEC (Commission of the European Communities) (1999). Council Directive 1999/13/EC on the limitation of emissions of volatile organic compounds due to the use of organic solvents in certain activities and installations, Official Journal of the European Communities L85/1–L85/25, 29.03.1999.

Chae C.Y. and Chan G.Y. (2001). Quantification of indoor VOC in twenty mechanically ventilated buildings in Hong Kong, Atmospheric Environment, 35, 5895-5913.

Chae J., Demidiouk, V., Yeulash M., Choi I.C. and Jung T.G. (2004). Experimental study for indoor air control by plasma-catalyst hybrid system, IEEE Transaction on plasma science, 32(2), 493-497.

Chang M.B. and Lee H.M. (2004). Abatement of perfluorocarbons with combined plasma catalysis in atmospheric-pressure environment, Catalysis Today, 89(1-2), 109-115.

Chavadej S., Kiatubolpaiboon W., Rangsunvigit P. and Sreethawong T. (2007). A combined multistage corona discharge and catalytic system for gaseous benzene removal, Journal of Molecular Catalysis A: Chemical, 263(1-2), 128-136.

Chen H.W., Ku Y., Irawan A. (2007). Photodecomposition of o-cresol by UV-LED/TiO$_2$ process with controlled periodic illumination, Chemosphere, 69, 184-190.

Chen J. and Wang P. (2005). Effect of relative humidity on electron distribution and ozone production by DC coronas in air, IEEE Transaction on plasma science, 33(2), 808-812.

Chen J.H. and Davidson J.H. (2002). Ozone production in the positive DC corona discharge: Model and comparison to experiments, Plasma Chemistry and Plasma Processing, 22(4), 495-522.

Chen W. and Zhang J.S. (2008). UV-PCO device for indoor VOCs removal: Investigation on multiple compounds effect, Building and Environment, 43(3), 246-252.

Choi J.H., Han I., Baik H.K., Lee M.H., Han D.W., Park J.C., Lee I.S., Song K.M. and Lim Y.S. (2006). Analysis of sterilization effect by pulsed dielectric barrier discharge, Journal of Electrostatics, 64 (1), 17-22.

Cooray V. and Rahman M. (2005). Efficiencies for production of NO_x and O_3 by streamer discharges in air at atmospheric pressure, Journal of Electrostatics, 63, 977-983.

Daikin (2008). URL: http://www.daikin.be (21/01/2008)

Delagrange S., Pinard L. and Tatibouet J.M. (2006). Combination of a non-thermal plasma and a catalyst for toluene removal from air: Manganese based oxide catalysts, Applied Catalysis B: Environmental, 68(3-4), 92-98.

Demeestere K., Dewulf J. and Van Langenhove H. (2003). Gas-solid adsorption of selected volatile organic compounds on titanium dioxide Degussa P25, Chemical Engineering Science, 58, 2255-2267.

Demeestere K., Dewulf J., De Witte B. and Van Langenhove H. (2007). Sample preparation for the analysis of volatile organic compounds in air and water matrices, Journal of Chromatography A, 1153(1-2), 130-144.

[a]Demeestere K., Dewulf J., De Witte B. and Van Langenhove H. (2005). Titanium dioxide mediated heterogeneous photocatalytic degradation of gaseous dimethyl sulfide: Parameter study and reaction pathways, Applied Catalysis B-Environmental, 60(1-2), 93-106.

Demeestere K., Dewulf J., De Witte B., Beeldens A. and Van langenhove H. (2008). Heterogeneous photocatalytic removal of toluene from air on building materials enriched with TiO_2, Building and Environment, 43(4), 406-414.

[b]Demeestere K., Dewulf J., Ohno T., Salgado P.H. and Van Langenhove H. (2005). Visible light mediated photocatalytic degradation of gaseous trichloroethylene and dimethyl sulfide on modified titanium dioxide, Applied Catalysis B-Environmental, 61(1-2), 140-149.

Demeestere K., Dewulf J., Van Langenhove H. and Sercu B. (2003). Gas-solid adsorption of selected volatile organic compounds on titanium dioxide Degussa P25, Chemical Engineering Science, 58(11), 2255-2267.

De Souza A.R. and Touzeau M. (1983). Quenching reaction of metastable nitrogen molecules N_2 (A^3 Sigma; v=0, 1, 2) by O and O_2. Conference proceeding XVI International Conference on Phenomena in ionized gases, 546-457.

Devahasdin S., Fan C., Li J.K. and Chen D.H. (2003). TiO_2 photocatalytic oxidation of nitric oxide: transient behavior and reaction kinetics, Journal of Photochemistry and Photobiology A: Chemistry, 156, 161-170.

Devins, J.C. (1956). Mechanism of ozone formation in the silent electric discharge, Journal of Electrochemical Society, 103(8), 460-466.

De Visscher A., Dewulf J., Van Durme J., Leys C., Morent R. and Van Langenhove H. (2008). Non-thermal plasma destruction of allyl alcohol in waste gas: kinetics and modelling, Plasma Sources Science and Technology, 17, 11p. (doi: 10.1088/0963-0252/17/1/015004)

Dewulf J., Van Langenhove H. and Everaert P. (1999). Determination of Henry's law coefficients by combination of the equilibrium partitioning in closed systems and solid-phase microextraction techniques, Journal of Chromatography A, 830, 353-363.

d'Hennezel O., Pichat P. and Ollis D.F. (1998). Benzene and toluene gas-phase photocatalytic degradation over H_2O and HCL pretreated TiO_2: by-products and mechanisms, Journal of Photochemistry and Photobiology A: Chemistry, 118, 197-204.

Dhoot S.N. and Freeman B.D. (2003). Kinetic gravimetric sorption of low volatility gases and vapors in polymers, Review of Scientific Instruments, 74(12), 5173-5178.

Diaz E., Ordonez S., Vega A. and Coca J. (2005). Influence of catalyst treatments on the adsorption properties of gamma-Al_2O_3 supported Pt, Rh and Ru catalysts, Microporous and Mesoporous Materials, 77(2-3), 245-255.

Ding H.X., Zhu A.M., Lu F.G., Xu Y., Zhang J. and Yang X.F. (2006). Low-temperature plasma-catalytic oxidation of formaldehyde in atmospheric pressure gas streams, Journal of Physics D-Applied Physics, 39(16), 3603-3608.

Duten X., Packan D., Yu L., Laux C.O. and Kruger C.H. (2002). DC and pulsed glow discharges in atmospheric pressure air and nitrogen, IEEE Transactions on Plasma Science, 30(1), 178-179.

Einaga H., Harada M. and Futamura S. (2005). Structural changes in alumina-supported manganese oxides during ozone decomposition, Chemical Physics Letters, 408, 377-380.

Ekem N., Akan T., Akgun Y., Kiremitci A., Pat S. and Musa G. (2006). Sterilization of Staphylococcus aureus by atmospheric pressure pulsed plasma, Surface and Coatings Technology, 201 (3-4), 993-997.

Electrabel (2008). Bijlage bij de bijzondere voorwaarden, Electrabel electriciteit-laagspanning, p.2.

EPA US Environmental Protection Agency (1991). Indoor Air Quality and Work Environment Study, Volume IV. Research Triangle Park, NC. June.

EPA US Environmental Protection Agency (2007). URL:
http://www.epa.gov/appcdwww/iemb/sources.htm

Fanger P.O. (2000). Good air quality in offices improves productivity, Journal of Mechanical Engineering, 46(7), 408-412.

Fanger O. (2006). What is IAQ? Indoor Air, 16(5), 328-334.

Flavornet (2006). URL: http://www.flavornet.org

Foest R., Kindel E., Ohl A., Stieber M. and Weltmann K.D. (2005). Non-thermal atmospheric pressure discharges for surface modification, Plasma Physics and Controlled Fusion, 47, 525-536.

Fouad L. and Elhazek S. (1995). Effect of humidity on positive corona discharge in a three electrode system, Journal of Electrostatics, Selected Papers from the 1994 Joint ESA/IEJ Symposium on Electrostatics, 35(1), 21-30.

Futamura S., Zhang A., Einaga H. and Kabashima H. (2002). Involvement of catalyst materials in nonthermal plasma chemical processing of hazardous air pollutants, Catalysis Today, 72, 259-265.

Girard B. (1996). Retention index calculation using Kovats constant model for linear temperature-programmed gas chromatography, Journal of Chromatography A, 721, 279-288.

Goodman A.L., Bernard E.T. and Grassian V.H. (2001). Spectroscopic Study of nitric acid and water adsorption on oxide particles: Enhanced nitric acid uptake kinetics in the presence of adsorbed water, Journal of Physical Chemistry, 105, 6443-6457.

Gordiets B.F., Ferreira C.M., Guerra, Loureiro J.M.A.H., Nathorny J., Pagnon D., Touzeau M. and Vialle M. (1997). Kinetic model of a low-pressure N_2-O_2 flowing glow discharge, IEEE Transaction on Plasma Science, 23, 750-768.

Gorgenyi M., Dewulf J. and Van Langenhove H. (2006). Temperature dependence of the Kovats retention index - The entropy index, Journal of Chromatography A, 1137(1), 84-90.

Goss K.U. (1994). Adsorption of organic vapors on polar mineral surface and on a bulk water surface: development of an empirical predictive model. Environmental science & technology, 28, 640-645.

Goss K.U. (2004). The air/surface adsorption equilibrium of organic compounds under ambient conditions, Critical Reviews in Environmental Science and Technology, 34(4), 339-389.

Goss K.U. and Schwarzenbach R.P. (2002). Adsorption of a diverse set of organic vapors on quartz, $CaCO_3$, and alpha-Al_2O_3 at different relative humidities, Journal of Colloid and Interface Science, 252(1), 31-41.

Goss K.U. (1997). Conceptual model for the adsorption of organic compounds from the gas phase to liquid and solid surfaces, Environmental Science & Technology, 31(12), 3600-3605.

Grinshpun S.A., Mainelis G., Trunov M., Adhikari A., Reponent T. and Willeke K. (2005). Evaluation of ionic air purifiers for reducing aerosol exposure in confined indoor spaces, Indoor Air, 15, 235-245.

Grossmannova H., Neirynck D. and Leys C. (2006). Atmospheric discharge combined with Cu-Mn/Al$_2$O$_3$ catalyst unit for the removal of toluene, Czechoslovak Journal of Physics, 56, 1156-1161.

Groves-Kirkby C.J., Denman A.R., Phillips P.S., Tornberg R., Woolridge A.C. and Crockett R.G.M. (2007). Domestic radon remediation of U.K. dwellings by sub-slab depressurisation: Evidence for a baseline contribution from constructional materials, Environment International In Press, Corrected Proof.

Guo Y.F., Ye D.Q., Chen K.F., He J.C. and Chen W.L. (2006). Toluene decomposition using a wire-plate dielectric barrier discharge reactor with manganese oxide catalyst in situ, Journal of Molecular Catalysis A: Chemical, 245(1-2), 93-100.

Hackam R. and Akiyama H. (2000). Air pollution control by electrical discharges, IEEE Transactions on Dielectrics and Electrical Insulation, 7(5), 654-683.

Halios C.H., Assimakopoulos V.D., Helmis C.G. and Flocas H.A. (2005). Investigating cigarette-smoke indoor pollution in a controlled environment, Science of the Total Environment, 337(1-3), 183-190.

Hamilton J.F., Webb P.J., Lewis A.C. and Reviejo M.M. (2005). Quantifying small molecules in secondary organic aerosol formed during the foto-oxidation of toluene with hydroxyl radicals, Atmopheric Environment, 39, 7263-7275.

Hammer T., Kappes T. and Baldauf M. (2004). Plasma catalytic hybrid processes: gas discharge initiation and plasma activation of catalytic processes, Catalysis Today, 89, 5-14.

Han S.B. and Oda T. (2007). Decomposition mechanism of trichloroethylene based on by-product distribution in the hybrid barrier discharge plasma process, Plasma Sources Science & Technology, 16(2), 413-421.

Hatsukami D., Mooney M., Murphy S., LeSage M., Babb D. and Hecht S. (2007). Effects of high dose transdermal nicotine replacement in cigarette smokers, Pharmacology Biochemistry and Behavior, 86(1), 132-139.

He Z., Liu J. and Cai W. (2005). The important role of the hydroxy ion in phenol removal using pulsed corona discharge, Journal of Electrostatics, 63, 371-386.

Heisig C., Zhang W. and Oyama S.T. (1997). Decomposition of ozone using carbon-supported metal oxide catalysts, Applied catalysis B: environmental, 14, 117-129.

Hensel K., Katsura S. and Mizuno A. (2005). DC microdischarges inside porous ceramics, IEEE Transactions on Plasma Science, 33(2), 574-575.

Higashi M. and Fuji K. (1997). Treatment of exhaust gas from vehicles by discharge plasma reactors, Electrical Engineering in Japan, 120(2), 1-7.

Holzer F., Kopinke F.D. and Roland, U. (2005). Influence of ferroelectric materials and catalysts on the performance of non-thermal plasma (NTP) for the removal of air pollutants, Plasma Chemistry and Plasma Processing, 25(6), 595-611.

Howard P.H and Meylan W.M. (1997). Handbook of physical properties of organic chemicals, Boca Raton, CRC Press, Inc., 1585 p.

Howard-Reed C., Nabinger, S.J. and Emmerich, S.J. (2005). Predicting gaseous air cleaner performance in the field, Proceedings indoor air, 1335-1339.

Hu X.D., Nicholas J., Zhang J.J., Linjewile T.M., de Filippis P. and Agarwal P.K. (2002). The destruction of N_2O in a pulsed corona discharge reactor, Fuel, 81(10), 1259-1268.

Hubbard H.F., Coleman B.K., Sarwar G. and Corsi R.L. (2005). Effects of an ozone-generating air purifier on indoor secondary particles in three residential dwellings, Indoor Air, 15, 432-444.

Hueso J.L., Caballero A., Cotrino J. and Gonzalez-Elipe A.R. (2007). Plasma catalysis over lanthanum substituted perovskites, Catalysis Communications, 8(11), 1739-1742.

IEH (Institute for Envrionment and Health) (1996). Assessment on indoor air quality in the home. Institute for Environment and Health, Leicester, UK.

Intriago L., Diaz E., Ordonez S. and Vega A. (2006). Combustion of trichloroethylene and dichloromethane over protonic zeolites: Influence of adsorption properties on the catalytic performance, Microporous and Mesoporous Materials, 91(1-3), 161-169.

Ionikh Y., Meshchanov A.V., Röpcke J. and Rousseau A. (2006). A diode laser study and modeling of NO and NO_2 formation in a pulsed DC air discharge, Chemical Physics, 322, 411-422.

Jaakkola J.J.K., Tuomaala P. and Seppanen O. (1994). Air Recirculation and Sick Building Syndrome - a Blinded Crossover Trial, American Journal of Public Health, 84(3), 422-428.

Jarnstrom H., Saarela K., Kalliokoski P., Pasanen A.L. (2006). Reference values for indoor air pollutant concentrations in new, residential buildings in Finland, Atmospheric Environment, 40(37), 7178-7191.

Jeong J., Sekiguchi K., Lee W. and Sakamoto K. (2005). Photodegradation of gaseous volatile organic compounds (VOCs) using TiO_2 photoirradiated by an ozone-producing UV lamp: decomposition characteristics, identification of by-products and water-soluble organic intermediates, Journal of Photochemistry and Photobiology A: Chemistry, 169 (3-5), 279-287.

Jochmann M.A., Kmiecik M.P., Torsten C.S. (2006). Solid-phase dynamic extraction for the enrichment of polar volatile organic compounds from water, Journal of Chromatography A, 1115, 208-216.

Jochmann M.A., Yuan X. and Schmidt T.C. (2007). Determination of volatile organic hydrocarbons in water samples by solid-phase dynamic extraction, Analytical and Bioanalytical Chemistry, 387(6), 2163-2174.

Jones A.P. (1999). Indoor air quality and health, Atmopheric Environment, 33, 4535-4564.

Jun J., Kim J.C., Shin J.H., Lee K.W. and Baek Y.S. (2004). Effect of electron beam irradiation on CO_2 reforming of methane over Ni/Al_2O_3 catalysts, Radiation Physics and Chemistry, 71(6), 1095-1101.

Kang M., Ko Y.R., Jeon M.K., Lee S.C., Choung S.J., Park J.Y., Kim S. and Choi S.H. (2005). Characterization of Bi/TiO_2 nanometer sized particle synthesized by solvothermal method and CH_3CHO decomposition in a plasma-photocatalytic system, Journal of Photochemistry and Photobiology A-Chemistry, 173(2), 128-136.

Kim F.H., Ogata A. and Futamura S. (2006). Effect of different catalysts on the decomposition of VOCS using flow-type plasma-driven catalysis, IEEE Transactions on Plasma Science, 34(3), 984-995.

[a]Kim H.H., Kobara H., Ogata A. and Futamura S. (2005). comparative assessment of different nonthermal plasma reactors on energy efficiency and aerosol formation from the decomposition of gas-phase benzene, IEEE transactions on industry applications, 41(1), 206-214.

[b]Kim H.H., Ogata A. and Futamura S. (2005). Atmospheric plasma-driven catalysis for the low temperature decomposition of dilute aromatic compounds, Journal of Physics D-Applied Physics, 38(8), 1292-1300.

[c]Kim H.H., Oh S.M., Ogata A. and Futamura S. (2005). Decomposition of gas-phase benzene using plasma-driven catalyst (PDC) reactor packed with Ag/TiO_2 catalyst, Applied Catalysis B: Environmental, 56(3), 213-220.

Kim H.H., Prieto G., Takashima K., Katsura S. and Mizuno A. (2002). Performance evaluation of discharge plasma process for gaseous pollutant removal, Journal of Electrostatics, 55(1), 25-41.

Kim S.B. and Hong S.C. (2002). Kinetic study for photocatalytic degradation of volatile organic compounds in air using thin film TiO_2 photocatalyst, Applied Catalysis B-Environmental, 35(4), 305-315.

Kolobov V.I. and Arslanbekov R.R. (2006). Simulation of electron kinetics in gas discharges, IEEE Transactions on Plasma Science, 34(3), 895-909.

Koutsospyros A.D., Yin S.M., Christodoulatos C. and Becker K. (2005). Plasmochemical degradation of volatile organic compounds (VOC) in a capillary discharge plasma reactor, IEEE Transactions on Plasma Science, 33(1), 42-49.

Kwak J.H., Peden C.H.F. and Szanyi J. (2006). Non-thermal plasma-assisted NO_x reduction over Na-Y zeolites: the promotional effect of acid sites, Catalysis Letters, 109(1-2), 1-6.

Lachenmeier D.W., Kroener L., Musshoff F., Madea B. (2003). Application of tandem mass spectrometry combined with gas chromatography and headspace solid-phase dynamic

extraction for the determination of drugs of abuse in hair samples, Rapid Communications in Mass Spectrometry, 17(5), 472-478.

Lai H.K., Bayer-Oglesby L., Colvile R., Götschi T., Jantunen M.J., Künzli N., Kulinskaya E., Schweizer C. and Nieuwenhuijsen M.J. (2006). Determinants of indoor air concentrations of $PM_{2.5}$, black smoke and NO_2 in six European cities (EXPOLIS study), Atmospheric Environment, 40, 1299-1313.

Lee H.M., Chang M.B. and Yang S.C. (2003). Plasma-assisted process for removing NO/NO_x from gas streams with C_2H_4 as additive, Journal of Environmental Engineering, 129(9), 800-810.

Li D., Yakushiji D., Kanazawa S., Ohkubo T. and Nomoto Y. (2002). Decomposition of toluene by streamer corona discharge with catalyst, Journal of Electrostatics, 55, 311-319.

Lin H., Huang Z., Shangguan W. and Peng X. (2007). Temperature-programmed oxidation of diesel particulate matter in a hybrid catalysis-plasma reactor, Proceedings of the Combustion Institute, 31(2), 3335-3342.

Lipinski J. (2001). Automated solid phase dynamic extraction - Extraction of organics using a wall coated syringe needle, Fresenius Journal of Analytical Chemistry, 369(1), 57-62.

Liu C.J., Wang J.X., Yu K.L., Eliasson B., Xia Q., Xue B. and Zhang Y.H. (2002). Floating double probe characteristics of non-thermal plasmas in the presence of zeolite, Journal of Electrostatics, 54(2), 149-158.

Lizama C., Freer J., Baeza J. and Mansilla H.D. (2002). Optimizad photodegradation of Reactive Blue 19 on TiO_2 and ZnO suspensions, Catalysis Today, 76, 235-246.

Loh M.M., Levy J.I., Spengler J.D., Houseman E.A. and Bennett D.H. (2007). Ranking cancer risks of organic hazardous air pollutants in the United States, Environmental Health Perspectives, 115(8), 1160-1168.

Lu B., Zhang X., Yu X., Feng T. and Yao S. (2006). Catalytic oxidation of benzene using DBD corona discharges, Journal of Hazardous Materials, 137(1), 633-637.

Luczynska C.M. (1994). Risk-Factors for Indoor Allergen Exposure, Respiratory Medicine 88(10), 723-729.

Luo R.X., Yi Y.N., Huang Z.W. and Lin R.T. (1996). Indoor burning coal air pollution and lung cancer - a case-control study in Fuzhou, China, Lung cancer, 14, 113-119.

Magureanu M., Mandache N.B., Eloy P., Gaigneaux E.M. and Parvulescu V.I. (2005). Plasma-assisted catalysis for volatile organic compounds abatement, Applied catalysis B: environmental, 61, 12-20.

[a]Magureanu M., Mandache N.B., Hu J., Richards R., Florea M. and Parvulescu V.I. (2007). Plasma-assisted catalysis total oxidation of trichloroethylene over gold nano-particles embedded in SBA-15 catalysts, Applied Catalysis B: Environmental, 76(3-4), 275-281.

[b]Magureanu M., Mandache N.B., Parvulescu V.I., Subrahmanyam C., Renken A. and Kiwi-Minsker L. (2007). Improved performance of non-thermal plasma reactor during decomposition of trichloroethylene: Optimization of the reactor geometry and introduction of catalytic electrode, Applied Catalysis B: Environmental, 74(3-4), 270-277.

Maki F. and Aoki T. (2006). Changes of indoor humidity in various living spaces, Mokuzai Gakkaishi, 52(1), 37-43.

Malik M.A., Minamitani Y. and Schoenbach K.H. (2005). Comparison of catalytic activity of aluminum oxide and silica gel for decomposition of volatile organic compounds (VOCs) in a plasmacatalytic reactor, IEEE Transactions on Plasma Science, 33(1), 50-56.

Maroni M., Axelrad R. and Bacaloni A. (1995). NATO Efforts to Set Indoor Air Quality Guidelines and Standards, American Industrial Hygiene Association Journal, 56(5), 499-508.

Martos P. and Pawliszyn J. (1999). Time-weighted average sampling with solid phase micro-extraction device: implications for enhanced personal exposure monitoring to airborne pollutants, Analytic chemistry, 71, 1513.

Miranda B., Diaz E., Ordonez S., Vega A. and Dieze F.V. (2007). Oxidation of TCE over metal oxide catalysts: kinetic studies and correlation with adsorption properties, Chemosphere, 66, 1706-1715.

Miranda B., Diaz E., Ordonez S., Vega A., Diez F.V. (2007). Oxidation of TCE over metal oxide catalysts: kinetic studies and correlation with adsorption properties, Chemosphere, 66, 1706-1715.

Mok Y.S. and Ham S.W. (1998). Conversion of NO to NO_2 in air by a pulsed corona discharge process, Chemical Engineering Science, 53(9), 1667-1678.

Mok Y.S., Nam C.M., Cho M.H. and Nam I.S. (2002). Decomposition of volatile organic compounds and nitric oxide by nonthermal plasma discharge processes, IEEE Transactions on Plasma Science, 30(1), 408-416.

Molhave L. and Krzyzanowski M. (2000). The right to healthy indoor air, Indoor Air-International Journal of Indoor Air Quality and Climate, 10(4), 211-211.

Morent R. and Leys C. (2005). Ozone generation in air by a DC-excited multi-pin-to-plane plasma source, Ozone Science and Engineering, 27(3), 239-245.

Morent R., Dewulf J., Steenhaut N., Leys C. and Van Langenhove H. (2006). Hybrid plasma-catalyst system for the removal of trichloroethylene in air, Journal of Advanced Oxidation Technologies, 9(1), 53-58.

Morent R., Dewulf J., Steenhaut N., Leys C. and Van Langenhove H. (2004). Catalyst assisted abatement of trichloroethylene in air by a positive DC corona discharge, Proceedings of XV International Conference on Gas Discharges and their Applications GD2004, Toulouse, September 5-10.

Morent R., Leys C., Dewulf J., Neirynck D., Van Durme J. and Van Langenhove H. (2007). DC-excited non-thermal plasmas for VOC abatement, Journal of Advanced Oxidation Technologies, 10, 127-136.

Morrison G.C. and Nazaroff W.W. (2002). Ozone interactions with carpet: Secondary emissions of aldehydes, Environmental Science & Technology, 36(10), 2185-2192.

Musshoff F., Lachenmeier D.W., Kroener L. and Madea B. (2003). Automated headspace solid-phase dynamic extraction for the determination of cannabinoids in hair samples, Forensic Science International, 133(1-2), 32-38.

Musshoff F., Lachenmeier D.W., Kroener L. and Madea B. (2002). Automated headspace solid-phase dynamic extraction for the determination of amphetamines and synthetic designer drugs in hair samples, Journal of Chromatography A, 958(1-2), 231-238.

Narula C.K., Daw C.S., Hoard J.W. and Hammer T. (2005). Materials issues related to catalysts for treatment of diesel exhaust, International Journal of Applied Ceramic Technology, 2(6), 452-466.

NIST (2007). Chemical Kinetics Database on the Web, Standard Reference Database 17, version 7.0, Release 1.3, http://kinetics.nist.gov.

Niu J.H., Zhu A.M., Shi C., Shi L.L., Song Z.M. and Xu Y. (2005). NO_x removal in catalyst-pellet-filled dielectric barrier discharge plasma with methane additive, Chinese Journal of Catalysis, 26(9), 803-808.

Nojgaard J.K., Bilde M., Stenby C., Nielsen O.J. and Wolkoff P. (2006). The effect of nitrogen dioxide on particle formation during ozonolysis of two abundant monoterpenes indoors, Atmospheric Environment, 40(6), 1030-1042.

Oda T., Yamashita Y., Takezawa K. and Ono R. (2006). Oxygen atom behaviour in the nonthermal plasma, Thin Solid Films, 506-507, 669-673.

Ogata A., Ito D., Mizuno K., Kushiyama S. and Yamamoto T. (1999). Removal of dilute benzene using zeolite-hybrid plasma reactor, in Conference Record of the IEEE-IAS Annual Meeting (Oct. 3-7), Phoenix, AZ, 1467-1472.

Oh S.M., Kim H.H., Ogata A., Einaga H., Futamura S. and Park D.W. (2005). Effect of zeolite in surface discharge plasma on the decomposition of toluene, Catalysis Letters, 99(1-2), 101-104.

Okubo M., Inoue M., Kuroki T. and Yamamoto T. (2005). NO_x reduction after treatment system using nitrogen nonthermal plasma desorption, IEEE Transactions on Industry Applications, 41(4), 891-899.

Ono R. and Oda T. (2002). Measurement of hydroxyl radicals in pulsed corona discharge, Journal of Electrostatics, 55, 333-342.

Pekarek S., Pospisil M. and Krysa J. (2006). Non-thermal plasma and TiO_2-assisted n-heptane decomposition, Plasma Processes and Polymers, 3(3), 308-315.

Penetrante B.M. (1998). Simultaneous removal of NO_x and SO_2 from combustion flue gas by pulsed electron beams, Combustion Science and Technology, 133(1-3), 135-150.

[a]Penetrante B.M., Brusasco R.M., Merritt B.T. and Vogtlin G.E. (1999). Environmental applications of low-temperature plasmas, Pure and Applied Chemistry, 71(10), 1829-1835.

Penetrante B.M., Hsiao M.C., Bardsley J.N., Merritt B.T., Vogtlin G.E., Kuthi A., Burkhart C.P. and Bayless J.R. (1997). Identification of mechanisms for decomposition of air pollutants by non-thermal plasma processing, Plasma sources science and technology, 6, 251-259.

[b]Penetrante B.M., Pitz W.J., Brusasco R.M., Merritt B.T. and Vogtlin G.E. (1999). Plasma processing of hydrocarbons and NO_x in lean-burn engine exhaust, Abstracts of Papers of the American Chemical Society, 217, 930.

Pengyi Z., Fuyan L., Gang Y., Qing C. and Wanpeng Z. (2003). A comparative study on decomposition of gaseous toluene by O_3/UV, TiO_2/UV and $O_3/TiO_2/UV$, Journal of Photochemistry and Photobiology A: Chemistry, 156(1-3), 189-194.

Pichat P., Disdier J., Hoang V.C., Mas D., Goutailler G. and Gaysse C. (2000). Purification/deodorization of indoor air and gaseous effluents by TiO_2 photocatalysis, Catalysis Today, 63, 363-369.

Pinard L., Mijoin J., Ayrault P., Canaff C. and Magnoux P. (2004). On the mechanism of the catalytic destruction of dichloromethane over Pt zeolite catalysts, Applied Catalysis B-Environmental, 51(1), 1-8.

Pommer L., Fick J., Andersson B. and Nilsson C. (2004). The influence of O_3, relative humidity, NO and NO_2 on the oxidation of alpha-pinene and Delta(3)-carene, Journal of Atmospheric Chemistry, 48(2), 173-189.

Pribytkov A.S., Baeva G.N., Telegina N.S., Tarasov A.L., Stakheev A.Y., Tel'nov A.V. and Golubeva V.N. (2006). Effect of electron irradiation on the catalytic properties of supported Pd catalysts, Kinetics and Catalysis, 47(5), 765-769.

Puerta L., Fernandez-Caldas E. and Lockey R.F. (1997). Indoor allergens: detection and environmental control measures. In: Bardana, E.J., Montanaro, A. (Eds.), Indoor Air Pollution and Health. Marcel Dekker, New York, pp.215-229.

Radhakrishnan R., Oyama S.T., Ohminami Y. and Asakura K. (2001). Structure of MnO_x/Al_2O_3 catalyst: A study using EXAFS, in situ laser raman spectroscopy and ab initio calculations, Journal of Physical Chemistry B, 105(38), 9067-9070.

Rajch E., Jaworek A., Sobczyk A.T. and Krupa A. (2006). Comparative studies of dc corona and back discharges in different gases, Czechoslovak Journal of Physics, 56, 803-814.

Rakitskaya T.L., Ennan A.A., Granatyuk I.V., Bandurko A.Y., Balavoine G.G.A., Geletii Y.V. and Paina V.Y. (1999). Kinetics and mechanism of low-temperature ozone decomposition by Co-ions adsorbed on silica, Catalysis Today, 53(4), 715-723.

Raoof A., Guilbaud J.P., Van Damme H., Porion P. and Levitz P. (1998). Analysis of the multilayer thickness relationship for water vapor and nitrogen adsorption, Journal of Colloid and Interface Science, 206(1), 1-9.

Rappe K.G., Hoard J.W., Aardahl C.L., Park P.W., Peden C.H.F. and Tran D.N. (2004). Combination of low and high temperature catalytic materials to obtain broad temperature coverage for plasma-facilitated NO_x reduction, Catalysis Today, 89(1-2), 143-150.

Rehfuess E., Corvalan C. and Neira M. (2006). Indoor air pollution: 4000 deaths a day must no longer be ignored, Bulletin of the World Health Organization, 84(7), 508-508.

Ridgway K., Lalljie S.P.D. and Smith R.M. (2006). Comparison of in-tube sorptive extraction techniques for non-polar volatile organic compounds by gas chromatography with mass spectrometric detection, Journal of Chromatography A, 1124(1-2), 181-186.

Riffat S.B. and Zhao X. (2007). Preliminary study of the performance and operating characteristics of a mop-fan air cleaning system for buildings, Building and Environment, 42 (9), 3241-3252.

Rodrigo H., Tan B.H., Allen N.L. (2005). Negative and positive impulse corona development along cylindrical insulator surfaces, IEEE Proceedings-Science Measurement and Technology, 152(5), 201-206.

Roland U., Holzer F. and Kopinke F.D. (2005). Combination of non-thermal plasma and heterogeneous catalysis for oxidation of volatile organic compounds Part2. Ozone decomposition and deactivation of γ-Al_2O_3. Applied catalysis B: environmental, 58(3-4), 217-226.

Roland U., Holzer F. and Kopinke F.D. (2002). Improved oxidation of air pollutants in a non-thermal plasma, Catalysis Today, 73, 315-323.

Rosenfeldt E.J., Linden K.G., Canonica S. and Von Gunten U. (2006). Comparison of the efficiency of OH radical formation during ozonation and the advanced oxidation processes O_3/H_2O_2 and UV/H_2O_2, Water Research, 40, 3695-3704.

Rudolph R., Francke K.P. and Miessner H. (2003). OH radicals as oxidizing agent for the abatement of organic pollutants in gas flows by dielectric barrier discharges, Plasmas and Polymers, 8(2), 153-161.

Rudolph R., Francke K.P. and Miessner H. (2002). Concentration dependence of VOC decomposition by dielectric barrier discharges, Plasma Chemistry and Plasma Processing, 22(3), 401-412.

Saito Y., Ueta I., Ogawa M., Hayashida M. and Jinno K. (2007). Miniaturized sample preparation needle: A versatile design for the rapid analysis of smoking-related compounds in hair and air samples, Journal of Pharmaceutical and Biomedical Analysis, 44(1), 1-7.

Sano T., Negishi N., Sakai E. and Matsuzawa S. (2006). Contributions of photocatalytic/catalytic activities of TiO_2 and [gamma]-Al_2O_3 in nonthermal plasma on oxidation of acetaldehyde and CO, Journal of Molecular Catalysis A: Chemical, 245(1-2), 235-241.

Schieweck A., Lohrengel B., Siwinski N., Genning C. and Salthammer T. (2005). Organic and inorganic pollutants in storage rooms of the Lower Saxony State Museum Hanover, Germany, Atmospheric Environment, 39(33), 6098-6108.

Schleibinger H. and Rüden H. (1999). Air filters from HVAC systems as possible source of volatile organic compounds (VOC) - laboratory and field assays, Atmopheric Environment, 33, 4571-4577.

Sekiguchi H., Sanada A. and Sakamoto K. (2003). Degradation of toluene with an ozone-decomposition catalyst in the presence of ozone, and the combined effect of TiO_2 addition, Catalysis Communications, 4, 247-252.

Seppanen O.A. and Fisk W. (2006). Some quantitative relations between indoor environmental quality and work performance or health, HVAC&R Research, 12(4), 957-973.

Seuwen R. and Warneck P. (1996). Oxidation of toluene in NO free air: Product distribution and mechanism, International Journal of Chemical Kinetics, 28(5), 315-332.

Shih Y.H. and Wu S.C. (2002). Sorption kinetics of toluene in humin under two different levels of relative humidity, Journal of Environmental Quality, 31(3), 970-978.

Singer B.C., Coleman B.K., Destaillats H., Hodgson A.T., Lunden M.M., Weschler C.J. and Nazaroff W.W. (2006). Indoor secondary pollutants from cleaning product and air freshener use in the presence of ozone, Atmospheric Environment, 40(35), 6696-6710.

Sobacchi M.G., Saveliev A.V., Fridman A.A., Gutsol A.F. and Kennedy L.A. (2003). Experimental assessment of pulsed corona discharge for treatment of VOC emissions, Plasma Chemistry and Plasma Processing, 23(2), 347-370.

Soldera F., Lasagni A., Mucklich F., Kaiser T. and Hrastnik K. (2005). Determination of the cathode erosion and temperature for the phases of high voltage discharges using FEM simulations, Computational Materials Science, 32(1), 123-139.

Staack D., Farouk B., Gutsol A.F. and Fridman A.A. (2006). Spectroscopic studies and rotational and vibrational temperature measurements of atmospheric pressure normal glow plasma discharges in air, Plasma Sources Science & Technology, 15(4), 818-827.

Stefan M.I. and Bolton J.R. (2005). Fundamental approach to the fluence-based kinetics and electrical energy efficiency parameters in photochemical degradation reaction: polychromatic light, Journal of Environmental Engineering and Science, 4, 13-18.

Stranger M., Potgieter-Vermaak S.S. and Van Grieken R. (2007). Comparative overview of indoor air quality in Antwerp, Belgium, Environment International, 33(6), 789-797.

[a]Subrahmanyam C., Magureanu M., Renken A. and Minsker-Kiwi L. (2006). Catalytic abatement of volatile organic compounds assisted by non-thermal plasma Part 1. A novel dielectric barrier discharge reactor containing catalytic electrode, Applied catalysis B: environmental, 65, 150-156.

[b]Subrahmanyam C., Magureanu M., Renken A. and Minsker-Kiwi L. (2006). Catalytic abatement of volatile organic compounds assisted by non-thermal plasma Part II. Optimized catalytic electrode and operating conditions, Applied Catalysis B-Environmental, 65, 157-162.

Subrahmanyam C., Renken A. and Kiwi-Minsker L. (2007). Novel catalytic dielectric barrier discharge reactor for gas-phase abatement of isopropanol, Plasma Chemistry and Plasma Processing, 27(1), 13-22.

Sullivan R.C., Thornberry T. and Abbatt J.P.D. (2004). Ozone decomposition kinetics on alumina: effects of ozone partial pressure, relative humidity and state of film oxidation, Atmospheric Chemistry and Physics Discussions, 4, 1977-2002.

Sun Q., Zhu A.M., Yang X.F., Niu J.H., Xu Y., Song Z.M. and Liu J. (2005). Plasma-catalytic selective reduction of NO with C_2H_4 in the presence of excess oxygen, Chinese Chemical Letters, 16(6), 839-842.

Sun Y., Fang L., Wyon D.P., Wisthaler A., Lagercrantz L. and Strom-Tejsen P. (2008). Experimental research on photocatalytic oxidation air purification technology applied to aircraft cabins, Building and Environment, 43(3), 258-268.

Sundell J. (2004). On the history of indoor air quality and health, Indoor Air, 14, 51-58.

Tidahy H.L., Siffert S., Wyrwalski F., Lamonier J.F. and Aboukais A. (2007). Catalytic activity of copper and palladium based catalysts for toluene total oxidation, Catalysis Today, 119(1-4), 317-320.

Tillborgs G., Wildemeersch D. and De Schrijver K. (2005). Wonen en gezondheid. Ministerie van de vlaamse gemeeschap, nr 3241/292, 176p
http://wwwwvcvlaanderenbe/gezondheidsmilieu/wonen/wonen_en_gezondheidpdf.

Tran D.N., Aardahl C.L., Rappe K.G., Park P.W. and Boyer C.L. (2004). Reduction of NO_x by plasma-facilitated catalysis over In-doped gamma-alumina, Applied Catalysis B-Environmental, 48(2), 155-164.

Urashima K. and Chang J.S. (2000). Removal of volatile organic compounds from air streams and industrial flue gases by non-thermal plasma technology, IEEE Transactions on Dielectrics and Electrical Insulation, 7(5), 602-614.

Van Durme J. (2006). Monitoring campaign of indoor air quality in some indoor environments in Flanders. unpublished results.

Van Winkle M.R. and Scheff P.A. (2001). Volatile organic compounds, polycyclic aromatic hydrocarbons and elements in the air of ten urban homes, Indoor Air-International Journal of Indoor Air Quality and Climate, 11(1), 49-64.

Vertriest R., Morent R., Dewulf J., Leys C. and Van Langenhove H. (2003). Multi-pin-to-plate atmospheric glow discharge for the removal of volatile organic compounds in waste air, Plasma Sources Science and Technology, 12, 412-416.

VITO (2008). Comparison of four commercial indoor air cleaners based on removal efficiency of particulate matter and VOC, non published results (confidential).

Wagner V., Jenkin M.E., Saunders S.M., Stanton J., Wirtz K. and Ping M.J. (2003). Modelling of the photooxidation of toluene: conceptual ideas for validating detailed mechanisms, Atmospheric Chemistry and Physics, 3, 89-106.

Wallace L.A. (1997). Sick building syndrome. Bardana, EJ, Montanaro, A (Eds), Indoor Air Pollution and Health Marcel Dekker, New York, pp 83-103.

Wallis A.E., Whitehead J.C. and Zhang K. (2007). Plasma-assisted catalysis for the destruction of CFC-12 in atmospheric pressure gas streams using TiO_2, Catalysis Letters, 113(1-2), 29-33.

Wang Y.F., Lee W.J., Chen C.Y., Hsieh L.T. (1999). Decomposition of dichlorodifluoromethane by adding hydrogen in a cold plasma system, Environmental Science & Technology, 33(13), 2234-2240.

Wang Z., Bai Z., Yu H., Zhang J. and Zhu T. (2004). Regulatory standards related to building energy conservation and indoor-air-quality during rapid urbanisation in China, Energy and buildings, 36, 1299-1308.

Weschler J.C. (2004). New Directions: Ozone-initiated reaction products indoors may be more harmful than ozone itself, Atmospheric Environment, 38(33), 5715-5716.

Weschler C.J. (2000). Ozone in indoor environments: Concentration and chemistry, Indoor Air, 10(4), 269-288.

Wittmann G., Demeestere K., Dombi A., Dewulf J. and Van Langenhove H. (2005). Preparation, structural characterization and photocatalytic activity of mesoporous Ti-silicates, Applied Catalysis B: Environmental, 61(1-2), 47-57.

Wolkoff P. (2003). Trends in Europe to reduce the indoor air pollution of VOCs, Indoor Air, 13(6), 5-11.

Wolkoff P., Clausen P.A., Wilkins C.K., Hougaard K.S. and Nielsen G.D. (1999). Formation of strong airway irritants in a model mixture of (+)-alpha-pinene/ozone, Atmospheric Environment, 33(5), 693-698.

World Health Organization (WHO) (2000). Indoor Air Quality: Organic Pollutants, EURO Report and Studies, Copenhagen.

Wu X., Ding X., Qin W., He W. and Jiang Z. (2006). Enhanced photo-catalytic activity of TiO_2 films with doped La prepared by micro-plasma oxidation method, Journal of Hazardous Materials, 137(1), 192-197.

Xiong G., Koziel J.A. and Pawliszyn J. (2004). Air sampling of aromatic hydrocarbons in the presence of ozone by solid-phase microextraction, Journal of Chromatography A, 1025, 57-62.

Xu L., Liu P., Zhan R.J., Wen X.H., Ding L.L. and Nagatsu M. (2006). Experimental study and sterilizing application of atmospheric pressure plasmas, Thin Solid Films, 506-507, 400-403.

Yoshida H. (2004). Survey of chemicals emission factors from building materials for interiors, RILEM international Symposium on Environment-Conscious Materials and Systems for Sustainable Development (proceedings), 251-259.

Zhang J. and Adamiak K. (2007). A multi-species DC stationary model for negative corona discharge in oxygen; pint-plane configuration, Journal of Electrostatics, 65, 459-464.

Zhang L.F., Anderson W.A., Sawell S. and Moralejo C. (2007). Mechanistic analysis on the influence of humidity on photocatalytic decomposition of gas-phase chlorobenzene, Chemosphere, 68(3), 546-553.

Zhao J. and Yang X. (2003). Photocatalytic oxidation for indoor air purification: a literature review, Building and Environment, 38, 645-654.

Zhu C., Li N., Re D. and Guan J. (2007). Uncertainty in indoor air quality and grey system method, Building and Environment, 42(4), 1711-1717.

Curriculum Vitae

Curriculum Vitae

Personalia

Last name:	Van Durme
First name:	Jim
Date of birth:	4 December 1981
Place of birth:	Eeklo
Adress:	Oostveld 48, 9940 Sleidinge (Evergem)
Civil status	Unmarried
Telephone:	+32 473 839434
Email:	Jim.Vandurme@ugent.be

Education

2004-2008:   PhD training, Faculty of Bioscience Engineering, Ghent University

Promotor: prof.dr.ir. Jo Dewulf

1999-2004:   Bio-engineer in Environmental Technology, Faculty of Bioscience Engineering, Ghent University

Master thesis: Atmospheric glow discharge for the treatment of waste gases pollutated with oxygenated and chlorinated volatile organic compounds

Promotors: Prof.dr.ir. Jo Dewulf and Prof.dr.ir. C. Leys

1993-1999:   Science – mathematics (8 hours/week), Sint-Vincentiuscollege, Eeklo

Professional experiences

2004-2008: Ghent University, Faculty of Bioscience Engineering, Environmental Organic Chemistry and Technology Research Group and Laboratory for Microbial Ecology and Technology: Doctoral research in Applied Biological Sciences.

> <u>Title</u>: Development of heterogeneous plasma catalysis for the abatement of health damaging organic micropollutants in indoor environments
>
> <u>Promotors</u>: prof. dr. ir. Jo Dewulf and Prof.dr.ir. C. Leys

1997-2004: Summer work at Campina (Sleidinge), Oleon (Ertvelde) and Volvo Cars (Ghent)

Teaching and tutoring experience

Teaching (theory), practical lessons, updating course notes for;

2004-2008 : Environmental chemistry for masters GAS environmental sanitation

2005-2008 : Environmental Chemistry (organic) for master in Bioscience Engineering (Chemistry and Environmental Technology)

2005-2008: Environmental Technology: physical and chemical processes for masters in Bioscience Engineering (Chemistry and Environmental Technology)

2004-2008: Tutor of 3 Master students Bio-engineering, 1Master student Environmental Sanitation, 2 Master students involved in bilateral project with Ghent University (Hungary and Czech), and 1 Bachelor student Chemistry and Environment (Sint-Lieven high school, Departement Ghent)

Scientific publications

Peer-reviewed publications in international journals

- Jim Van Durme, Jo Dewulf, Wouter Sysmans, Christophe Leys and Herman Van Langenhove (2007). Abatement and degradation pathways of toluene in indoor air by positive corona discharge. Chemosphere 68(10), 1821-1829.

- Jim Van Durme, Jo Dewulf, Wouter Sysmans, Christophe Leys and Herman Van Langenhove (2007). Efficient toluene abatement in indoor air by a plasma catalytic hybrid system. Applied Catalysis B: Environmental 74(1-2), 161-169.

- Rino Morent, Christophe Leys, Jo Dewulf, Dieter Neirynck, Jim Van Durme and Herman Van Langenhove (2007). DC-excited non-thermal plasmas for VOC abatement. Journal of Advanced Oxidation Technologies, 10(1), 127-136.

- Jim Van Durme, Kristof Demeestere, Jo Dewulf, Frederik Ronsse, Leentje Braeckman, Jan Pieters and Herman Van Langenhove (2007). Accelerated solid-phase dynamic extraction of toluene from air. Journal of Chromatography A, 1175, 145-153.

- Jim Van Durme, Jo Dewulf, C. Leys and Herman Van Langenhove (2008). Combining non-thermal plasma with heterogeneous catalysis in waste gas treatment: A review. Applied Catalysis B: Environmental 78(3-4), 324-333.

- Alex De Visscher, Jo Dewulf, Jim Van Durme, Christophe Leys, Rino Morent and Herman Van Langenhove (2008). Non-thermal plasma destruction of allyl alcohol in waste gas: kinetics and modeling, Plasma Sources Science and Technology, 17, doi:10.1088/0963-0252/17/1/015004

- Jim Van Durme, Jo Dewulf, Kristof Demeestere, Christophe Leys and Herman Van Langenhove (2008). Post-plasma catalytic technology for the removal of toluene from indoor air. Applied Catalysis B: Environmental, submission.

Publications as abstract/proceeding for congresses and seminars

- Jim Van Durme, Jo Dewulf, Roeland Vertriest, Christophe Leys and Herman Van Langenhove. Non-thermal atmospheric pressure plasma discharges for the oxidation of volatile organic compounds in air. In Proceedings of The Second European Conference on Oxidation and Reduction Technologies for In-Situ and Ex-Situ Treatment of Water, Soil and Air (ECOR-2), 12 jun 2005 – 15 jun 2005, Göttingen, Germany, 2p.

- Eszter Horváth, Jim Van Durme, Jo Dewulf and Herman Van Langenhove. Solid-phase microextraction and on-fiber derivatization for the assessment of indoor air treatment technology. In Proceedings of the 12th symposium on analytical and environmental problems, 26 sept 2005, Szeged (Hungary), 114-118.

- Jim Van Durme, Jo Dewulf, Christophe Leys, Rino Morent and Herman Van Langenhove (2005). Destruction of limonene in a non-thermal DC plasma discharge. In Proceedings of the 2nd International Workshop on Cold Atmospheric Pressure Plasma: Sources and Applications (CAPPSA 2005), 30 aug 2005 – 2 sep 2005, Brugge (België), 123-126.

- Jim Van Durme, Jo Dewulf, Wouter Sysmans, Christophe Leys, Rino Morent and Herman Van Langenhove (2006). Indoor air purification by non-thermal plasma catalysis. In Book of abstracts and e-proceedings of the Environmental Applications of Advanced Oxidation Processes (EAAOP-1), 7 sep 2006 – 9 sep 2006, Chania-Creta (Griekenland), 310.

- Jim Van Durme, Jo Dewulf, Wouter Sysmans, Christophe Leys and Herman Van Langenhove (2007). Plasma based toluene abatement in indoor air: removal efficiency and degradation pathways. In book of abstracts of the XXVIII International

Conference on Phenomena in Ionized Gases (ICPIG), 15 jul 2007 – 20 jul 2007, Praha (Czech Republic), 151.

- Jim Van Durme, Jo Dewulf, Olivier Mare, Christophe Leys and Herman Van Langenhove (2007). Indoor Air Purification: Effect of Humidity on Plasma Catalytic Removal of Volatile Organic Compounds. In Proceedings of the 13th International Conference on Advanced Oxidation Technologies for Treatment of Water, Air and Soil (AOTs-13), 24 sep 2007 – 27 sep 2007, Niagara Falls(New York, VS), 2 p.

- Kristof Demeestere, Jim Van Durme, Jo Dewulf and Herman Van Langenhove (2008). Innovative solid-phase dynamic extraction of volatile organic compounds from air: a mechanistic study leading to improved extraction kinetics. In Proceedings of The 10th International Symposium on Advances in Extraction Techniques (ExTech-10), 28 jan 2008 – 30 jan 2008, Brugge (Ghent).

Participipiation to international conferences, symposia and study stages abroad

Oral presentations

- Jim Van Durme, Jo Dewulf, Christophe Leys, Rino Morent and Herman Van Langenhove. Destruction of limonene in a non-thermal DC plasma discharge, 2d International Workshop on Cold Atmospheric Pressure Plasma: Sources and Applications (CAPPSA 2005), Brugge, België, 30 aug 2005 – 2 sep 2005.

- Jim Van Durme, Jo Dewulf, Wouter Sysmans, Christophe Leys, Rino Morent and Herman Van Langenhove. Indoor air purification by non-thermal plasma catalysis, Environmental Applications of Advanced Oxidation Processes (EAAOP-1), Chania-Creta (Griekenland), 7 sep 2006 – 9 sep 2006.

- Jim Van Durme, Jo Dewulf, Olivier Maere, Christophe Leys and Herman Van Langenhove. Indoor air purification: effect of humidity on plasma catalytic removal of volatile organic compounds, Workshop on bilateral project between Ghent and Prague University, Antwerp (Belgium), 21 sep 2007.

- Jim Van Durme, Jo Dewulf, Olivier Maere, Christophe Leys and Herman Van Langenhove. Indoor Air Purification: Effect of Humidity on Plasma Catalytic Removal of Volatile Organic Compounds, The 13th International Conference on Advanced Oxidation Technologies for Treatment of Water, Air and Soil (AOTs-13), Niagara Falls, New York, VS, 24 sep 2007 – 27 sep 2007

Poster presentations

- Jim Van Durme, Jo Dewulf, Roeland Vertriest, Christophe Leys and Herman Van Langenhove (2005). Non-thermal atmospheric pressure plasma discharges for the oxidation of volatile organic compounds in air. The Second European Conference on Oxidation and Reduction Technologies for In-Situ and Ex-Situ Treatment of Water, Soil and Air (ECOR-2), Göttingen, Germany, 12 jun 2005 – 15 jun 2005.

- Jim Van Durme, Jo Dewulf, Wouter Sysmans, Christophe Leys and Herman Van Langenhove (2007). Plasma based toluene abatement in indoor air: removal efficiency and degradation pathways. XXVIII International Conference on Phenomena in Ionized Gases (ICPIG), Praha, Czech Republic, 15 jul 2007 – 20 jul 2007.

- Kristof Demeestere, Jim Van Durme, Jo Dewulf and Herman Van Langenhove (2008). Innovative solid-phase dynamic extraction of volatile organic compounds from air: a mechanistic study leading to improved extraction kinetics. The 10th International Symposium on Advances in Extraction Techniques (ExTech-10), Brugge, Gent, 28 jan 2008 – 30 jan 2008.

Passive participation

"Bouwen en Binnenmilieu", 12 dec 2007, KVIV-Ingenieurshuis, Antwerp (Belgium).

Study stages abroad

14/01/2008-26/01/2008: Stay at 'Czech Technical University' in bilateral project